NTNU – Trondheim
Norwegian University of
Science and Technology

Experimental Investigations of Freeze-Bonds between Saline Ice-Blocks

Ice-Properties and Reproducibility

Henning Helgøy

Civil and Environmental Engineering
Submission date: June 2012
Supervisor: Knut Vilhelm Høyland, BAT

Norwegian University of Science and Technology
Department of Civil and Transport Engineering

Master's thesis project description

Background

As offshore oil- and gas-exploration enters arctic areas an increased knowledge about the action from special ice-features as ice-ridges are required. Studies of freeze-bonds are considered important in order to gain a better understanding of the failure mechanisms in an ice-ridge. Research on the topic of freeze-bonds has been performed at NTNU recently, and two projects on this topic were delivered at NTNU during autumn 2011. This master thesis is a continuation of the project work *"Study of freeze-bond strength in relation to the contact surfaces for small-scale experiments"* by Helgøy (2011). Considerably higher freeze-bond strengths were measured during these measurements, compared to what has been reported by Repetto-Llamazares et al. (2011a) *"Experimental studies on shear failure of freeze-bonds in saline ice: Part I. Set-up, failure mode and freeze-bond strength"* and Repetto-Llamazares and Høyland (2011a) *"Experiments on the relation between freeze-bonds and ice rubble strength Part II: Freeze-bond experiments and comparison with numerical simulations"*. The reproducibility of these investigations should be assessed as part of this master thesis.

Task description

1. Develop a experimental procedure for evaluating the reproducibility of the work from Repetto-Llamazares et al. (2011a) and Repetto-Llamazares and Høyland (2011a). The set-up should be designed taking into consideration and trying to avoid the challenge experienced by Helgøy (2011) with collision between the force applying piston and the test frame. The experimental procedure should particularly consider the differences in results reported by Helgøy (2011) and the results reported by Repetto-Llamazares and Høyland (2011a), i.e. differences in the ambient air temperature of the submersion basin, the contact surface properties (natural and sawn), the time - temperature history of the ice-blocks and the ice crystal size and orientation.

2. Experimental investigations should be carried out in the ice laboratory at the Department of Civil and Transport Engineering at NTNU and at Hamburg Ship Model Basin (HSVA). These experiments should have a special attention to the physical properties of the ice used to form freeze-bonds.

3. The experimental results should be evaluated in relation to how the different parameters in the experimental set-up have affected the freeze-bond strength, and a special consideration should be made to the reproducibility of the measurements of Repetto-Llamazares et al. (2011a) and Repetto-Llamazares and Høyland (2011a).

Abstract

This thesis presents and analyse laboratory investigations of the shear strength of freeze-bonds created between two saline ice-blocks. One hundred and eighty one experiments were conducted during spring 2012 in the ice laboratory at NTNU and at Hamburg Ship Model Basin (HSVA). The applied experimental setup is similar to the set-up used by Repetto-Llamazares et al. (2011a) and Repetto-Llamazares and Høyland (2011a). The reproducibility of the measurements from these articles and how the freeze-bond strength varies with the physical properties of the ice used to form freeze-bonds were investigated. Investigating the physical properties of the ice involved temperature, salinity and density measurements, thin section analysis and characterisation of the visual appearance of the ice. We consider our results to be important knowledge for future work to perform more accurate small-scale experiments on freeze-bonds. The measured freeze-bond strengths had a range of 1.9 to 94.9 kPa.

The following factors were varied during the experiments: *a*) Two sample dimensions were used: small ice-blocks with dimensions of $60 \cdot 40 \cdot 22$ [mm] and $90 \cdot 40 \cdot 22$ [mm], with a nominal contact area between the ice-blocks of $60 \cdot 40$ [mm], and large ice-blocks with dimensions of $140 \cdot 140 \cdot 27$ [mm] and $180 \cdot 140 \cdot 27$ [mm], and a nominal contact area between the ice blocks of $140 \cdot 140$ [mm]; *b*) Four contact surfaces were used: artificially produced and the natural top or bottom of the ice-sheet. Groves made during sawing of the artificially prepared surfaces were either normal to or parallel with the longitudinal ice-block direction; *c*) Two ice-blocks directions were made by having the longitudinal ice-block direction normal to or parallel with the ice-growth direction; *d*) Assembling the freeze-bond was made by placing the ice-blocks in contact with each other in water or in air; *e*) The water temperature in the submersion basin was either on, or slightly above the freezing point; *f*) Changing the time - temperature historie of the ice-blocks were done by either storing the ice at -7 °C at all time, or for a defined period of time cooling the ice-blocks down to -20 °C. The initial ice-block temperature of -7 °C, submersion time of 10 min, confinement pressure during submersion of 1.9 kPa and velocity of the force applying piston of 2 mm/s were kept constant, and are equal to Repetto-Llamazares and Høyland (2011a).

Physical properties of the freeze-bonding ice-blocks affected the freeze-bond strength. Weak freeze-bonds were obtained for ice-blocks with a low initial salinity ($S < \sim 1$ ppt), and strong freeze-bonds were obtained if the ice-blocks had a

high initial salinity ($S > \sim 2$ ppt). The low salinity ice-blocks were in addition seen to have a transparent look and few brine channels and voids. High salinity ice-blocks had an opaque look and contained many brine channels and voids. Keeping the longitudinal ice-block direction normal to the ice-growth direction, and assembling the samples in water gave stronger freeze-bonds. Freeze-bonds created between two natural bottom surfaces gave the strongest freeze-bonds, while the weakest freeze-bonds were obtained for the artificially prepared surfaces. Surfaces with an initially high surface roughness gave weaker freeze-bonds. The grove direction of the artificially prepared surfaces, the water temperature in the submersion basin, the sample size and the time - temperature history of the ice-blocks did not affect the freeze-bond strength.

We did not manage to reproduce the results of Repetto-Llamazares et al. (2011a). Different submersion time (5 vs. 10 min) and confinement pressure (0.66 vs. 1.9 kPa) in the experiments of Repetto-Llamazares et al. (2011a) and us are probably the main reasons for the observed differences. We believe that comparable freeze-bond strengths would be obtained if identical test parameters had been applied. We do from this consider the experiments of Repetto-Llamazares et al. (2011a) to be reproducible.

Repetto-Llamazares and Høyland (2011a) reports a very low average freeze-bond strength, 3.6 kPa, for the submersion time, confinement pressure, initial ice-block temperature and piston velocity applied in our thesis. We have not been able to obtain such low average freeze-bond strengths. We believe that the low freeze-bond strengths obtained by Repetto-Llamazares and Høyland (2011a) is an effect of the physical properties of the ice-blocks applied in their experiments, i.e. transparent ice-blocks with a low salinity. Based on the assumption that they were using low salinity ice-blocks, the experiments of Repetto-Llamazares and Høyland (2011a) are considered to be reproducible.

Sammendrag

Denne oppgaven omhandler laboratorieundersøkelser av skjærstyrken til frysebånd dannet mellom to saltvannsisblokker. Hundreogåttien forsøk ble gjennomført i løpet av våren 2012 i islaboratoriet ved NTNU og ved Hamburg Ship Model Basin (HSVA). Det anvendte forsøksoppsettet er tilsvarende til forsøksoppsettet brukt av Repetto-Llamazares et al. (2011a) og Repetto-Llamazares og Høyland (2011a). Repeterbarheten til resultatene i disse to artiklene, samt hvordan frysebåndstyrken varierer med de fysiske egenskapene til isen som er brukt til å danne frysebånd er undersøkt. Isens fysiske egenskaper er undersøkt gjennom saltinnhold, temperatur og tetthetsmålinger, undersøkelser av tynnslip og ved å beskrive utseende på isen. Vi anser resultatene fra forsøkene våre å være viktige i forhold til å utvikle og gjennomføre nøyaktige fremtidige frysebåndundersøkelser i liten skala. Frysebåndstyrker fra 1.9 til 94.9 kPa ble målt i forsøkene.

Følgende faktorer ble undersøkt: *a*) To størrelser prøvestykker ble benyttet: Små prøvestykker med utvendige dimensjoner $60 \cdot 40 \cdot 22$ [mm] og $90 \cdot 40 \cdot 22$ [mm], og en nominell kontaktflate på $60 \cdot 40$ [mm], og store prøvestykker med utvendige dimensjoner $140 \cdot 140 \cdot 27$ [mm] og $180 \cdot 140 \cdot 27$ [mm] med en nominell kontaktflate på $140 \cdot 140$ [mm]; *b*) Fire kontaktoverflater ble benyttet: kunstige overflater og isens naturlige bunn og topp overflate. De kunstige overflatene ble fremstilt ved saging. Saging av isen ga rette riller i overflaten på isen, rillene var enten orientert langsmed eller normalt til isblokkenes lengderetning; *c*) Lengderetningen til isblokkene var enten orientert parallelt med, eller normalt til isens vekstretning; *d*) Isblokkene ble enten satt sammen under vann eller i luft; *e*) Vanntemperaturen i neddykkingsbassenget var enten på eller rett over frysepunktet; *f*) Tids - temperaturhistorien til isblokkene ble endret ved enten å lagre isblokkene ved -7 °C hele tiden, eller ved å lagre isen på -20 °C i en bestemt periode. Den initiale istemperaturen på -7 °C, neddykkingstiden på 10 min, overlagringstrykket under neddykking på 1.9 kPa og pålastingshastigheten på 2 mm/s ble holdt konstant, og er tilsvarende til Repetto-Llamazares og Høyland (2011a).

Isens fysiske egenskaper ble i stor grad funnet til å påvirke frysebåndstryken. Dersom isen hadde et lavt saltinnhold ($S < \sim 1$ ppt) før neddykking ble svake frysebånd dannet. Sterke frysebånd ble dannet dersom isen hadde et høyt saltinnhold ($S > \sim 2$ ppt) før neddykking. Et transparent utseende samt få saltlakekanaler og porer ble observert for isblokker med et lavt saltinnhold. Isblokker med et høyt saltinnhold hadde et hvitaktig utseende samt mange salt-

lakekanaler og porer. Sterkere frysebånd ble dannet vist lenderetningen til isblokkene var normalt til isens vekstretning. Sterkere frysebånd ble også dannet vist isblokkene ble satt sammen under vann. Frysebånd dannet mellom to naturlige bunnoverflater var sterkest, mens de svakeste frysebåndene ble dannet mellom to kunstige overflater. En høy overflateruhet før neddykking ga svakere frysebånd. Frysebåndstryken ble ikke påvirket av rilleretningen til de kunstig fremstilte overflatene, tids - temperaturhistorien til isblokkene eller størrelsen på prøvestykkene.

Vi klarte ikke å reprodusere resultatene til Repetto-Llamazares et al. (2011a). Forskjellig neddykkingstid (5 kontra 10 min) og overlagringstrykk (0.66 kontra 1.9 kPa) i forsøkene til Repetto-Llamazares et al. (2011a) og oss er trolig hovedårsaken til de målte forskjellene. Vi tror at tilsvarende frysebåndstyrker ville ha blitt dannet vist vi hadde brukt like parametre. Fra dette anses forsøkene til Repetto-Llamazares et al. (2011a) som reproduserbare.

En veldig lav gjennomsnittlig frysebåndstyrke, 3.6 kPa, for den neddykkingstiden, overlagringstrykket, initiale istemperaturen og pålastingshastigheten som vi benyttet er rapportert av Repetto-Llamazares og Høyland (2011a). Vi har ikke i snitt klart å fremstille tilsvarende svake frysebånd, men foreslår at de lave frysebåndstyrkene rapportert av Repetto-Llamazares og Høyland (2011a) er en effekt av type is benyttet deres forsøk, m.a.o. transparent is med et lavt saltinnhold. Basert på antagelsen om at de har benyttet is med et lavt saltinnhold, anser vi forsøkene til Repetto-Llamazares og Høyland (2011a) som reproduserbare.

Preface

This thesis is submitted in fulfilment of my master's degree in Civil and Environmental Engineering at the Norwegian University of Science and Technology (NTNU), under supervision of Professor Knut Vilhelm Høyland. The specialisation topic of my master's degree has been Marine Civil Engineering.

The experiments discussed in this thesis have been performed in the ice laboratory of the Department of Civil and Transport Engineering at NTNU and in the ice tank at Hamburg Ship Model Basin (HSVA). The experiments at NTNU were performed together with Oda Skog Astrup, which at the same time performed experiments for her master thesis. These experiments were supported by the Sustainable Arctic Marine and Coastal Technology (SAMCoT) Centre for Research-based Innovation (CRI) through the Research Council of Norway and all the SAMCoT partners. The experiments at HSVA were performed as a part of the project Rubble Ice Transport on Arctic Offshore Structures (RITAS), and were supported by the European Community's 7^{th} Framework Programme through the grant to the budget of the Integrated Infrastructure Initiative HYDRALAB-IV, Contract no. 261520[1].

[1]This document reflects only the authors' views and not those of the European Community. This work may rely on data from sources external to the HYDRALAB project Consortium. Members of the Consortium do not accept liability for loss or damage suffered by any third party as a result of errors or inaccuracies in such data. The information in this document is provided "as is" and no guarantee or warranty is given that the information is fit for any particular purpose. The user thereof uses the information at its sole risk and neither the European Community nor any member of the HYDRALAB Consortium is liable for any use that may be made of the information.

Acknowledgements

First of all I would like to thank Knut for being my supervisor during my work with this thesis. He has been an inspiring supervisor and has been giving me a lot of useful feedback and guidance. I would also like to express my thankfulness for his believe in me as a master student, had for giving me the opportunity to perform laboratory work both at NTNU and at HSVA.

The second person which has been of great importance for this thesis is Oda. She has been my lab partner through many long working days in the lab, both at NTNU and at HSVA. Her help has been invaluable, and I would also like to thank her for useful discussions during the lab work.

For the experiments performed at NTNU I would like to thank Johan for his help with equipment in the lab. Frank and Tage at NTNU "Fellesverkstedet" for doing a great job helping me manufacturing the test frame for the NTNU-experiments. At HSVA I would specially thank Kalle and the ice-tank crew for their hospitality, technical and scientific support. I would also like to thank the rest of the RITAS team for their social gathering during our weeks in Hamburg.

At last I would like to thank all my good friends through my years at the university and all those who have supported me on the way from being a carpenter and to become an engineer.

I would also like to acknowledge the support from the SAMCoT CRI and HYDRALAB-IV.

Trondheim, June 2012

Henning Helgøy

Contents

List of Figures

List of Tables

List of Symbols

Greek letters

Δt	[s]	Submersion time
ρ_i	[kg/m^3]	Ice density
σ	[Pa]	Confinement pressure
σ_{sub}	[Pa]	Confinement pressure during submersion
σ_{test}	[Pa]	Confinement pressure during freeze-bond strength testing
τ_{nom}	[Pa]	Nominal shear stress
τ_{fb}	[Pa]	Freeze-bond strength
$\tau_{fb,nom}$	[Pa]	Nominal freeze-bond strength
$\tau_{fb,real}$	[Pa]	Real freeze-bond strength
ϕ	[°]	Angle of internal friction
ϕ_τ	[°]	Angle of internal friction for the freeze-bond strength

Latin letters

A_{fb}	[m^2]	Nominal contact area of the freeze-bonding ice-blocks
A_{ub}	[%]	Unbounded area of the freeze-bonding surface in percent of A_{fb}
C_i	[J/K]	Heat capacity of the ice
c	[Pa]	Cohesion
c_τ	[Pa]	Cohesion for the freeze-bond strength

F	[N]	Piston force
H	[m]	Height
h_b	[m]	Ice-block thickness
k_i	[W/(m · K)]	Thermal conductivity of the ice
L	[m]	Length
l_i	[J/g]	Latent heat of the ice
m	[g]	Mass
T	[°C]	Temperature
T_{air}	[°C]	Ambient air temperature of the submersion basin
T_i	[°C]	Initial ice-block temperature
T_{water}	[°C]	Submersion basin water temperature
S	[ppt]	Salinity
S_l	[ppt]	Lower ice-block salinity
S_{sb}	[ppt]	Submersion basin salinity
S_{tot}	[ppt]	Combined salinity of both the upper and lower ice-block
S_u	[ppt]	Upper ice-block salinity
V	[m/s]	Piston velocity
W	[m]	Width

Chapter 1

Introduction

1.1 Background

Increased knowledge of the failure processes in an ice-ridge is required as oil- and gas-exploration enters ice-infested areas. Failure of freeze-bonds developed as a part of an ice-ridge is considered to be associated with the initial loads. Increased knowledge of this phenomenon is thus needed to obtain more reliable calculations of loads exerted during failure of an ice-ridge, and further to design safe and reliable structures. Loads from ice-ridges are considered as a challenge for the design of offshore structures, ice-breaking vessels and subsea pipelines.

Scientific articles on the topic of experimental investigations of freeze-bonds between saline ice-blocks have recently been published by Repetto-Llamazares et al. (2011a) and (2011b), Repetto-Llamazares and Høyland (2011a) and Serré et al. (2011). The three first articles deal with investigations of single freeze-bonds, while the last treats freeze-bonds as a part of the failure process in two dimensional shear-box experiments on ice-rubble. Two projects on the topic of single freeze-bonds were also delivered at NTNU during autumn 2011, namely Astrup (2011) and Helgøy (2011). The experimental set-up used in this thesis is based on differences between their results and the results of Repetto-Llamazares and Høyland (2011a), as described by Helgøy (2011).

The development of a material model for the freeze-bond failure is a long-term

goal for the freeze-bond investigations. A further development is to embed this material model in a general numerical model for the failure of an ice-ridge, including all the failure mechanisms in an ice-ridge.

1.2 Objective

The objective of this thesis is to highlight the importance of how physical properties (salinity, density, crystal structure and orientation) and the contact surface properties of the ice-blocks used to form freeze-bonds affect the freeze-bond strength.

1.3 Research question

The freeze-bond strengths measured by Helgøy (2011) were considerably stronger than the freeze-bond strengths measured by Repetto-Llamazares and Høyland (2011a). These experiments used equal sample dimensions, confinement pressures, submersion time and initial ice-block temperature. Our research question has been to investigate the reproducibility of the results from Repetto-Llamazares et al. (2011a) and Repetto-Llamazares and Høyland (2011a) by keeping a constant confinement pressure, submersion time and initial ice-block temperature, and investigate how the two ice-blocks forming the freeze-bond affect the freeze-bond strength. The differences described by Helgøy (2011) between their results and the results of Repetto-Llamazares and Høyland (2011a) were the starting point of the investigations:

- Different ambient room temperature of the submersion basin (-1 and -7 °C).
- Different contact surfaces; Natural top and bottom of the ice-sheet and artificially prepared surfaces by sawing.
- Time - temperature history of the ice-blocks used to form freeze-bonds; Constantly stored at -7 °C, or for a defined period of time exposed to -20 °C, and then heated to and tested at -7 °C.
- Crystal size and orientation of the ice-blocks used to form freeze-bonds.

1.4 Methods

The investigations in this thesis have been performed through experimental laboratory investigations of small-scale freeze-bonds. Experiments have been performed in the ice laboratory of the Department of Civil and Transport Engineering at NTNU and at Hamburg Ship Model Basin (HSVA), and included 136 freeze-bond strength tests at NTNU, divided into 10 test configurations, and 45 freeze-bond strength tests at HSVA, divided into 4 test configurations. Physical properties of the ice were determined through temperature, salinity and density measurements, and through investigations of thin sections. A visual characterisation of the ice has in addition been important.

The experimental set-up used during the NTNU-experiments was an improved version of the set-up used by Repetto-Llamazares and Høyland (2011a). Equal sample dimensions were applied in these experiments. At HSVA both the test frame and sample dimensions used during the NTNU-experiments, and the test frame and sample dimensions used by Repetto-Llamazares et al. (2011a) were applied. Except for changing the ice-properties and sample dimensions an equal initial ice-block temperature ($-7\,^{\circ}\mathrm{C}$), submersion time (10 min), confinement pressure (1.9 kPa) and piston velocity (2 mm/s) were used in all experiments. These parameters are equal to the experimental parameters used by Repetto-Llamazares and Høyland (2011a).

The experiments at NTNU were carried out together with Oda Skog Astrup, who at the same time performed two dimensional shear-box experiments on ice-rubble for her master thesis, see Astrup (2012). Equal types of ice were used in the experiments of Astrup (2012) and in our experiments. The effect of changing the longitudinal direction of the ice-blocks ("Horizontal" and "Vertical", see section 3.4.2) and keeping the ambient temperature of the submersion basin at two levels (-1 and $-7\,^{\circ}\mathrm{C}$) were investigated in both our single freeze-bond experiments and in the shear-box experiments of Astrup (2012). Similarities were found between the first peak strength of the ice-rubble, i.e. freeze-bond failure, and the freeze-bond strengths measured in the single freeze-bond experiments. A discussion of the coherence between the results from the single freeze-bond experiments and the shear-box experiments is presented by Astrup (2012).

1.5 Limitations

The aim of our experiments has been to investigate the peak stress during a shear test of a freeze-bond (= freeze-bond strength, τ_{fb}), and to relate this to the test variables. Some general comments have been given to the material behaviour, but it has not been analysed or discussed in detail. Stress - time or stress - displacement diagrams of each test are presented in appendix D.

1.6 Accuracy

Density measurements presented in this thesis are based on dimensional measurements of relatively small samples. The surfaces of the measured samples were not completely even, and some uncertainty must be added to these results.

An unbounded area between the two freeze-bonding surfaces was seen for some samples. Determination of this area was sometimes difficult due to a soft transition between the bounded and unbounded areas. The accuracy level of these measurements is in spite of this considered to be sufficient.

1.7 Layout

This thesis is divided into to six chapters. A review of the main theory on the topic of freeze-bonding between saline ice-blocks is presented in chapter 2. Chapter 3 presents the experimental method, while results are given in chapter 4. Both these chapter handles the NTNU- and HSVA-experiments separately. Comments on the experimental methods used by Repetto-Llamazares et al. (2011a) and Repetto-Llamazares and Høyland (2011a) are given through chapter 3. Chapter 5 presents a discussion of the obtained measurements. The chapter starts with an assessment of the results from the different test configurations, both the NTNU- and the HSVA-experiments. Our results are further compared to the results of Repetto-Llamazares et al. (2011a) and Repetto-Llamazares and Høyland (2011a), and the reproducibility of these investigations is discussed. The last section of this chapter evaluates the applied experimental method. Conclusions and recommendations for further work are presented in chapter 6.

Extensive appendixes are enclosed. A table chronologically presenting results for each sample is presented in appendix A. Vertical cross-sectional thin sections of freeze-bonds are found in appendix B. Appendix C presents cross-sectional thin sections of the applied ice-sheets. Stress - time or stress - displacement diagrams for each test is presented in appendix D. Two test-frames were used in the experiments, appendix E contains a principle drawing of each of these.

Chapter 2

Theory

2.1 Ice-ridges

Ice-ridges are created by environmental action on level-ice, usually in the areas between landfast- and drifting-ice. The ice-ridge is a line-like feature, and is considered to have cross section as illustrated in figure 2.1. Submerged parts of the ice-ridge is named the ice-keel, while the parts above water is named the sail. Dependent on the age of the ice-ridge a consolidated layer is formed in the upper parts of the ice-keel. The voids between the ice-blocks are refrozen in the consolidated layer. In the remaining parts of the ice-keel, named the unconsolidated layer, the voids between the ice-blocks are filled with water or slush. The ice-blocks in this unconsolidated part of the ice-keel may be partly frozen to each other. This connection between the ice-blocks is termed freeze-bond. Freeze-bonds are mainly considered of interest for young, first-year ice-ridges. Freeze-bonds may also be formed between contacting ice-blocks in the sail. Typical figures of first-year ice-ridges are a total porosity of 25 to 40%, a salinity of 4 to 8 ppt and a keel to sail ratio of 4-5 (Løset et al., 2006). The size of the ice-blocks in the sail and keel varies. Høyland (2007) reports an average ice-block dimension of 0.38 m thick, 0.86 m wide and 1.3 m, measured in the Barents Sea.

Actions excreted by an ice-ridge may according to the ISO-19906 (2010) be divided in to two parts, namely from the consolidated and unconsolidated layer

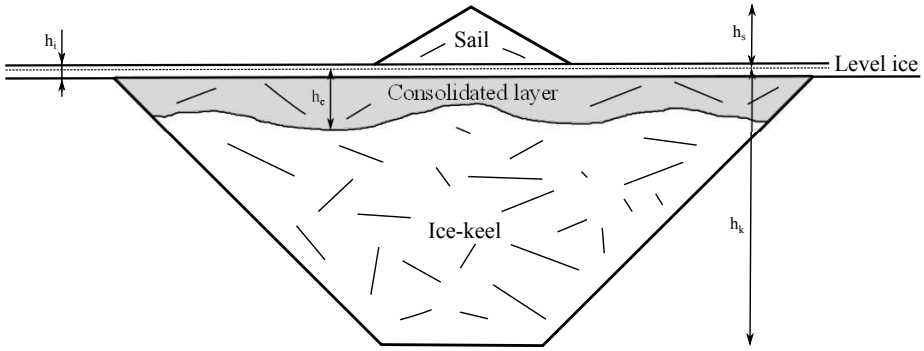

Figure 2.1: Ice-ridge cross section. h_s = sail height, h_k = ice-keel thickness, h_c = consolidated layer thickness and h_i = level ice thickness.

in the ice-keel. Due to the small area of the sail compared to the remaining parts of the ice-ridge actions from the sail may be disregarded. It is today most common to use a Mohr-Coulomb failure criterion to describe loads from an ice-ridge. This failure criterion applies an internal friction angle (ϕ) and cohesion (c). No well-defined order of these parameters is known today. Due to the large particle size, it has also been discussed how reliable it is to consider the ice-ridge as a continuum (Løset et al., 2006, Serré, 2011).

The following three mechanisms are suggested by Shafrova and Høyland (2008) to govern the failure of the unconsolidated part of the ice-keel:

- Strength of freeze-bonds between ice-blocks.
- Dimension and orientation of ice-blocks.
- Strength of submerged ice in the ice-keel.

These three mechanisms would further lead to at least three physical mechanisms:

- Failure of freeze-bonds.
- Rotation and rearrangement of the ice-blocks.
- Internal failure of ice-blocks.

The strength of ice-rubble have by Liferov and Bonnemaire (2005) been discussed to depend upon the confinement pressure, strain-rate, size of ice-blocks,

void ratio and time history. Høyland (2010) has further elaborated the effects of the ice-block size and time history, and presents these as dependent on size of the ice-blocks, initial ice-block temperature, consolidation time and the surrounding oceanic flux.

2.2 Former freeze-bond investigations

All known literature on the topic of experimental work on freeze-bonds handles artificially created freeze-bonds, and not freeze-bonds created as a part of an ice-ridge. Experimental investigations have been performed in the field, but the majority of the literature is describing laboratory investigations. A general investigation topic has been freeze-bond strength measurements. Some investigations of the freeze-bond growth and thermal development have also been performed. The main method used to form freeze-bonds applies two ice-blocks which is separated with a known distance, or pushed together with a predefined pressure. These ice-blocks are then left for a certain time in air, or submerged in water, for creation of the freeze-bond. Fresh and saline water have been used for submersion of the ice-block, in addition to in situ submersion in sea water.

Investigating the relation between the freeze-bond strength (τ_{fb}) and the submersion time (Δt), confinement pressure (σ), initial ice-block temperature (T_i), contact surface and velocity (V) of the force applying piston have been the main focus in the previous investigations. The freeze-bond strength, in our case a shear strength, is defined from the Mohr-Coulomb failure criterion, see equation 2.1. This criterion applies the cohesion (c_τ) and the angle of internal friction (ϕ_τ) as material properties, while the normal stress (σ) is defined from the boundary conditions. The two material properties c_τ and ϕ_τ define a yield surface or failure surface in the τ-σ space, so that for a given sigma a shear strength τ_{fb} is defined.

Three methods have been applied for measuring the freeze-bond strength. A conceptual sketch of these methods can be seen in figure 2.2. Ettema and Schaefer (1986), Repetto-Llamazares et al. (2011a) and Repetto-Llamazares et al. (2011b), Repetto-Llamazares and Høyland (2011a), Astrup (2011) and Helgøy (2011) applied a test set-up with two ice-blocks laying on top of each other, with a horizontally aligned freeze-bond. In this set-up the lower ice-block is kept in a fixed position, while a horizontal force is applied to the upper ice-block. All these investigations were performed as laboratorial investigations.

Combined field and laboratory investigations was performed by Shafrova and Høyland (2008) and Marchenko and Chenot (2009). Shafrova and Høyland (2008) used a set-up where the freeze-bond was aligned at 45° as a part of a sample tested in uniaxial compression. Marchenko and Chenot (2009) applied a set up with two ice-blocks in contact with each other, with a vertically aligned freeze-bond when measuring the freeze-bond strength. In their experiments the force was applied vertically downwards. Repetto-Llamazares and Høyland (2011b) have also presented a review of the experimental work of Ettema and Schaefer (1986), Shafrova and Høyland (2008), Marchenko and Chenot (2009) and Repetto-Llamazares et al. (2011a).

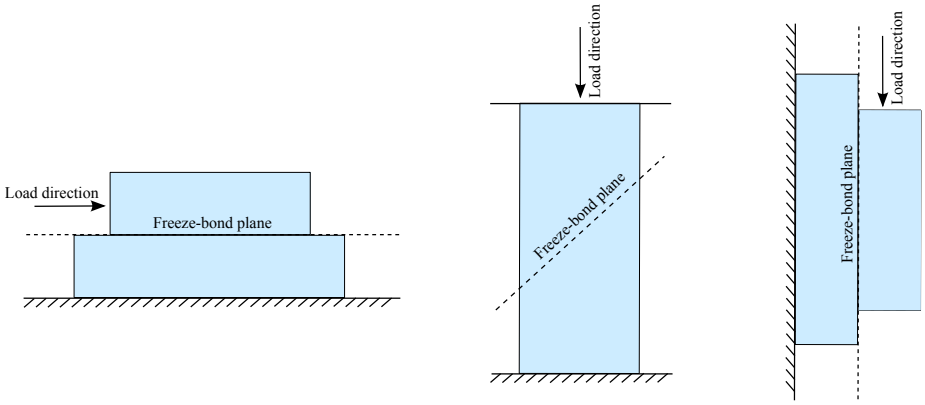

Figure 2.2: Principle sketch of three formerly applied freeze-bond strength test set-ups.

$$\tau_{fb} = c_\tau + tan(\phi_\tau)\sigma \tag{2.1}$$

Common for all the above motioned investigations was that they applied a set-up with direct contact between the two freeze-bonding ice-blocks. Bailey (2011) applied a set-up where the two freeze-bonding surfaces were separated with a distance of 5 to 20 mm, this gap was then refrozen with new ice during submersion. A four-point shear strength test was used to measure the freeze-bond strength in their experiments.

The freeze-bond experiments performed in this thesis have been made from samples submerged in water, with an initial contact between the freeze-bonding

surfaces. A summary of the experimental method and results from the authors which have performed experiments on freeze-bonds created in water is presented in table 2.1. It should be noted that Astrup (2011) and Helgøy (2011) applied the same set of experiments in their investigations.

Table 2.1: Experimental method, main test parameters and results from the experiments of Ettema and Schaefer (1986) (-E&S (1986)-), Shafrova and Høyland (2008) (-S&H (2008)-), Repetto-Llamazares et al. (2011a) (-RLetal (2011a)-), Repetto-Llamazares and Høyland (2011a) (-RL&H (2011a)-), Astrup (2011) and Helgøy (2011).

Experimenter	Method, Test parameters and Results
E&S (1986)	Horizontal freeze-bond, Freshwater ice $\Delta t = 0$ to 4 min, $\sigma = 0$ to 4 kPa, $T_i = -10$ °C $\tau_{fb} = 0.5$ to 6 kPa
S&H (2008)	Uniaxial compression, Freeze-bond at 45°, Sea ice $\Delta t = 24$ to 60 h, $T_i = -5.6$ to -19.9 °C $\tau_{fb,mean} = 15$ to 53 kPa for level ice $\tau_{fb,mean} = 54$ to 195 kPa for ice-foot ice[a]
RLetal (2011a)	Horizontal freeze-bond, Saline HSVA-model ice $\Delta t = 1$ min to 20 h, $\sigma = 0.125$ to 2.04 kPa, $T_i = -1.2$ to -14 °C $\tau_{fb} = 0.8$ to 29.5 kPa
RL&H (2011a)	Horizontal freeze-bond, Laboratory made saline ice $\Delta t = 10$ min to 20 h, $\sigma = 0.35$ to 2.04 kPa, $T_i = -7$ °C $\tau_{fb,mean} = 0.48$ to 3.95 kPa
Astrup (2011) & Helgøy (2011)	Horizontal freeze-bond, Laboratory made saline ice with small crystals $\Delta t = 10$ min, $\sigma = 2.04$ kPa, $T_i = -7.5$ °C $\tau_{fb} = 9.5$ to 114.8 kPa

[a] See details in section 2.3.3

2.3 Freeze-bond strength vs. test parameter

The majority of the experimental investigations on freeze-bonds have investigated how the freeze-bond strength (τ_{fb}) varies with the submersion time (Δt), confinement pressure (σ), initial ice-block temperature (T_i), contact surface and velocity (V) of the force applying piston. A summary of the effects of each of these parameters follows for the experiments performed with freeze-bonds created in water.

2.3.1 Submersion time

A bell-shaped relationship curve between the freeze-bond strength and the submersion time was predicted by Shafrova and Høyland (2008). This curve is presented in figure 2.3. This relation was further investigated by Repetto-Llamazares et al. (2011a). They applied submersion times of 1, 5 and 20 min and 1, 4.5, 9.5 and 20 h, and established a bell-shaped curve showing the submersion time - freeze-bond strength relationship. They found increasing freeze-bond strengths up to 5 min submersion, followed by decreasing freeze-bond strengths for increasing submersion times. They suggest that three phases may be applied to characterise this relationship. Each phase relates the freeze-bond strength to the freeze-bond porosity.

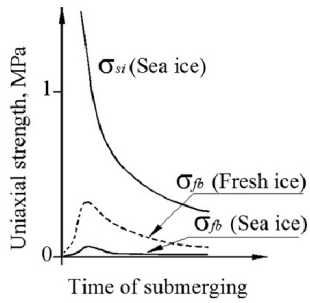

Figure 2.3: Bell-shaped curve form Shafrova and Høyland (2008). σ_{si} = strength of sea ice. σ_{fb} = strength of freeze-bonds.

At the initial phase the freeze-bond strength increases towards a maximum, and is governed by the freezing process. This phase ends when the brine salinity and temperature of the freeze-bond are in equilibrium. This corresponds to the point where the freeze-bond temperature and porosity have reached their minimum values. In the second phase the freeze-bond temperatures increase and brine drains. Both these effects are assumed to affect the freeze-bond porosity. Increasing temperatures would lead to increasing porosity, while brine drainage would lead to decreasing porosity. It is assumed that heating occurs faster than brine is drained. This would further lead to a total increase in the freeze-bond porosity, and hence a reduction of the freeze-bond strength. In the third phase the freeze-bond temperature and salinity are in equilibrium with the surrounding water. Without gradients processes develop slower, and the freeze-bond strength stabilizes.

Increasing freeze-bond strengths with increasing submersion times were also observed by Ettema and Schaefer (1986). They applied a short submersion time of 10 s to 4 min. For samples submerged in fresh-water the freeze-bond strengths were clearly increasing with the submersion time. Less increase in the freeze-bond strengths was found for samples submerged in 3% saline water. Samples submerged in water with a high salinity, 12.5 and 25%, showed no increase in the freeze-bond strength with increasing submersion times.

2.3.2 Confinement pressure

Increasing freeze-bond strengths with increasing confinement pressure was measured by Ettema and Schaefer (1986). The effect on the freeze-bond strength from increasing the confinement pressure was in the range of 6 to 10 times larger if the samples had been submerged in distilled water, compared to 12.5 to 25% saline water. All these tests were performed with a submersion time of 10 s. Shafrova and Høyland (2008) did not manage to extract any clear trends regarding the confinement pressure from their measurements.

Repetto-Llamazares et al. (2011a) measured increasing freeze-bond strengths with increasing confinement pressures. They applied a Mohr-Coulomb failure criterion, and used this to describe the relation between the confinement pressure and freeze-bond strength, see equation 2.1. All these measurements were performed with a submersion time of 20 h. From these measurements sets of material parameters, cohesion (c_τ) and friction angle (ϕ_τ), have been reported. By extrapolation of their results Repetto-Llamazares et al. (2011a) showed that their measurements and the measurements of Shafrova and Høyland (2008) were corresponding.

Two confinement pressure configurations were applied by Repetto-Llamazares and Høyland (2011a). Firstly they used a "Classical" configuration, applying an equal confinement pressure during submersion and strength testing. This "Classical" configuration has been applied during all the other freeze-bond experiments. In addition they used an "Inverse" configuration. In the "Inverse" configuration a high confinement pressure was applied during submersion, and a low confinement pressure during strength testing, and vice versa. Two levels of confinement pressures were applied for the "Classical" configuration. Both of these showed increasing freeze-bond strengths with increasing confinement pressure. No clear trends were found for the "Inverse" configuration.

2.3.3 Initial ice-block temperature

A thorough discussion of the effects from the initial ice-block temperature on the freeze-bond strength have been presented by Repetto-Llamazares et al. (2011a). They suggest that the width and height of the bell-shaped submersion time - freeze-bond strength relationship, figure 2.3, is governed by the initial ice-block temperature together with the thermal properties and the size of the ice-blocks. They also state that the thermal properties (C_i, k_i, l_i, ρ_i) of the ice-blocks introduce a complicating factor to the relationship between the initial ice-block temperature, submersion time and the freeze-bond strength.

Shafrova and Høyland (2008) compared the initial ice-block volume and the ice-block volume at the time of freeze-bond strength testing. The results showed that the weakest freeze-bonds were found for the samples with the largest volume reduction. The complicating influence of the thermal properties of the ice-blocks have also been illustrated by Shafrova and Høyland (2008). In general they obtained the highest freeze-bond strengths for the ice-blocks with the lowest porosity. This was assumed to be an effect of the higher potential of cold in less porous ice-blocks. However, some of the samples tested by Shafrova and Høyland (2008) were made out of ice-foot ice. This ice had a total porosity of 25%, with an gas fraction of 20%. In contrary to the remaining samples a high freeze-bond strength, but a low compression strength were obtained for these samples. They state that the physical properties of this porous ice, a combination of a low thermal conductivity and a high mass diffusion, is the main contribution to this phenomenon.

The effect of the initial ice-block temperature was also investigated by Repetto-Llamazares et al. (2011a), for a submersion time of 20 h. They only found a clear trend for the tests applying a low confinement pressure (0.13 kPa). The trend from these measurements was opposite to the results from Shafrova and Høyland (2008), and showed increasing freeze-bond strengths for increasing initial temperatures. They explain this trend by a faster freeze-bond formation for initially colder ice-blocks. A fast freeze-bond formation would look in more brine, resulting in increasing freeze-bond porosities, and further reduced freeze-bond strengths. They suggests that the effect of the initial ice-block temperature is suppressed by the effect of the confinement pressure for confinement pressures higher than 0.13 kPa.

2.3.4 Contact surface

The relation between the contact surface properties and the freeze-bond strength was investigated by Helgøy (2011). They applied four surface configurations created from different combinations of the natural top and bottom surface of the ice-sheet. The surface combinations were made by bringing the top surface in contact with the top surface, the bottom surface in contact with the bottom surface, the top surface in contact with the bottom surface and vice versa. The location of the two contact surfaces, the upper or the lower ice-block, separated the two last configurations. They report that freeze-bonds created between two bottom surfaces in average were 2.2 times stronger than freeze-bonds created between two top surfaces. The two other configurations were measured to have freeze-bond strengths in the intermediate range of the "Top - Top" and "Bottom - Bottom" samples. S2 model ice with small crystals was applied in these experiments.

Bailey (2011) applied the natural top surface of the ice, and a sawn bottom surface as the surfaces facing the freeze-bonding gap. A granular ice-texture was present at the top surface, while the sawn bottom surface had columnar crystals aligned perpendicular to the freeze-bond. During strength testing it was seen that the fracture tended to follow the interface of the top surface ice-block.

Repetto-Llamazares et al. (2011a) used HSVA-model ice in their experiments. Random combinations of the top and bottom surfaces of the ice-sheet were in their experiments used to form freeze-bonds. Repetto-Llamazares and Høyland (2011a) and Serré et al. (2011) cut their final ice-block dimensions with a band-saw, and were by this applying an artificially prepared sawn contact surface. Repetto-Llamazares and Høyland (2011a) informed that their contact surface from a visual inspection was smoother than the contact surfaces applied by Repetto-Llamazares et al. (2011a). Sawn contact surfaces were also used by Shafrova and Høyland (2008). Ettema and Schaefer (1986) produced ice in aluminium containers, and used a heated plate to smooth the surfaces.

2.3.5 Piston velocity

The effect from the velocity of the force applying piston on the measured freeze-bond strength have been investigated by Ettema and Schaefer (1986) and Astrup (2011). Ettema and Schaefer (1986) applied piston velocities of 0.44 and 0.84 mm/s, while Astrup (2011) applied piston velocities of 1 and 10 mm/s.

None of these experiments showed any dependence between the piston velocity and measured freeze-bond strengths. Equivalent freeze-bond strengths were measured for both the high and the low piston velocities.

2.4 Freeze-bond texture

Investigations of the freeze-bond texture were performed by Helgøy (2011). The investigations were performed through analysis of thin sections. The thin sections showed that the freeze-bond may be considered as a surface feature if the ice-blocks have an initial good contact between the surfaces. Gaps with a thickness of 0.4 mm and up to 1 mm were found to be present inside the freeze-bonds. Ice-blocks with a nominal contact area of $40 \cdot 60$ [mm] were used in their experiments. The thin sections also showed that the freeze-bond consisted of ice with a granular ice-texture.

2.5 Ice growth properties and crystal structure

Sea-ice is a crystalline multiphase material consisting of pure ice, brine and gas-pockets. At the initial growth stage ice-platelets, less than 0.5 mm thick, are formed. These are randomly oriented, and grows horizontally on the water surface. If undisturbed a thin cover of randomly oriented crystals is formed. Underneath the initial skin a transition zone is developed, this is due to a higher heat transport parallel with the basal plane. An effect of this is that a prevailing vertical ice-growth occurs. The grain size is rapidly increasing in the transition zone. Below the transition zone a columnar zone is created. This is extending to the bottom of the ice-sheet, with a columnar crystal structure and horizontal c-axis (Weeks, 2010).

At the interface between water and ice a skeleton layer is developed during ice-growth. It is from the process which occurs in this layer that brine entrapment originates. Ice-platelets, normally less than 0.25 mm thick and more than 10 mm wide, grows into the water as fingers. The platelet thickness is governed by the ice-growth velocity (Harrison and Tiller (1963) referred in Løset et al. (2006)). When the ice-growth ends, the skeleton layer erodes, this creates a smoother bottom surface of the ice-sheet.

Chapter 3

Experimental method

3.1 Introduction

Shear strength measurements of freeze-bonds created between two saline ice-blocks have been investigated in the ice laboratory at NTNU and at HSVA. At NTNU 136 samples distributed on 10 test configurations were tested. The set-up used for these experiments were an improved version of the set-up used by Repetto-Llamazares and Høyland (2011a). The experiments at HSVA included 45 samples distributed on 4 test configurations. Both the test frame used by Repetto-Llamazares et al. (2011a) and the test frame used in the NTNU-experiments were used at HSVA. Comments on the methods used by Repetto-Llamazares et al. (2011a), Repetto-Llamazares and Høyland (2011a) and Helgøy (2011) are given through the presentation of the experimental set-up. Common for both the NTNU and HSVA set-ups is that they are based on the experimental set-up suggested by Ettema and Schaefer (1986). The NTNU-experiments were conducted in February 2012 while the HSVA-experiments were conducted during the last weeks of April 2012.

Astrup (2012) performed 2D shear-box experiments at the same time as the freeze-bond tests at NTNU were conducted. Equal ice-block dimensions, ice properties and test environment were used for the shear-box and freeze-bond experiments.

3.2 Freeze-bond test procedure

Figure 3.1 illustrates the main procedure of shear strength testing of freeze-bonds. Firstly two ice-blocks were cut to predefined dimensions from a larger ice sheet. The lower ice-block was longer than the upper. This was done in order to fix the freeze-bonded sample in the vertical direction during strength testing. The initial ice-block temperature, T_i, and the sample dimensions were used as test parameters at this stage. The nominal contact area between the ice-blocks, A_{fb}, and the ice-block thickness, h_b, are used as parameters to describe the ice-block dimensions.

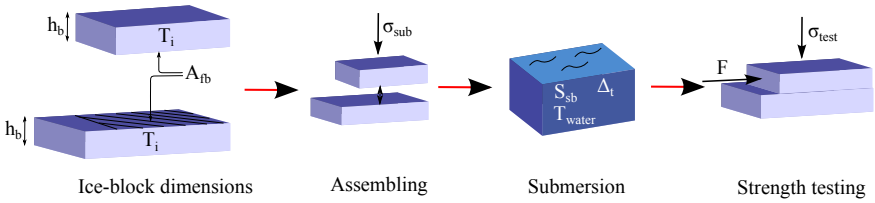

Figure 3.1: Flow-chart of the freeze-bond test procedure.

Secondly the two ice-blocks were assembled. Assembling was either done by putting the ice-blocks in contact with each other in water or in air. This was followed by applying a confinement pressure, σ_{sub}. Metal weights, with a wooden plate to distribute the load, were used to apply the confinement pressure. The sample was then directly submerged into a basin with a given salinity, S_{sb}, and water temperature, T_w, for a fixed time, Δt. The freeze-bond strength was measured subsequently, one to three minutes, after submersion by pushing or pulling the upper block with a fixed velocity, V, until fracture occurred. Force, F, exerted by the piston and the piston displacement was recorded during the experiments. Equal weights were used during submerging and strength testing, resulting in a somewhat higher confinement pressure during testing, σ_{test}.

The freeze-bond strength in relation to the ice salinity, density and the crystal structure and orientation and the comparability to previous studies has been the main focus of this study. The test parameters and set-up are thus chosen to be equal or close to the studies by Repetto-Llamazares et al. (2011a) and Repetto-Llamazares and Høyland (2011a). These studies applied a wide range of the above mentioned test parameters (T_i, σ_{sub}, σ_{test}, Δt, S_{sb}, V, A_{fb}, h_b). A selection of these parameters were chosen since we aimed at investigating the

freeze-bond strength - ice-property relation. The former investigations which aimed at testing a range of these parameters had less focus on the ice properties. Test parameters used in our experiments compared with the parameters used by Repetto-Llamazares et al. (2011a), Repetto-Llamazares and Høyland (2011a) and Helgøy (2011) is found in table 3.1.

Table 3.1: Comparison of test parameters in the present experiments at NTNU and HSVA to the work of Repetto-Llamazares et al. (2011a) (-RLetal (2011a)-), Repetto-Llamazares and Høyland (2011a) (-RL&H (2011a)-) and Helgøy (2011).

	NTNU	HSVA	RLetal (2011a)	RL&H (2011a)	Helgøy (2011)
T_i	−7 °C	−7 °C	−14 to −1.2 °C	−7 °C	−7.5 °C
Δt	10 min	10 min	1 min to 20 h	10 min and 20 h	10 min
σ_{sub}	1.9 kPa	1.9 kPa	0.125 to 2.04 kPa	0.35 and 1.9 kPa	1.9 kPa
σ_{test}	2.04 kPa	2.2 kPa	0.125 to 2.04 kPa	0.48 and 2.04 kPa	2.04 kPa
V	2 mm/s	2.1 mm/s	0.7 and 0.78 mm/s	2.1 mm/s	0.94 mm/s
S_{sb}	8 to 9.1 ppt	6.7 to 7.3 ppt	7 to 13 ppt	8 ppt	8 ppt
A_{fb}	$40 \cdot 60$ [mm]	$40 \cdot 60$ [mm] and $140 \cdot 140$ [mm]	$140 \cdot 140$ [mm]	$40 \cdot 60$ [mm]	$40 \cdot 60$ [mm]
h_b	22 mm	22 and 27 mm	25 to 35 mm	22 mm	22 mm

3.3 Thin sections

Thin sections were prepared both at NTNU and at HSVA. A microtome was used to plane the samples down to a thickness of 0.2 to 0.4 mm. Polarized pictures of the crystal structure were then taken through a polaroscope, in addition to non-polarized pictures. The thin sections were used to study the ice-texture and the void distribution.

3.4 NTNU-experiments

At NTNU freeze-bond shear strength tests were performed with the test rig used by Repetto-Llamazares and Høyland (2011a) and Helgøy (2011). Figure 3.2a shows an overview picture of this test rig. The freeze-bonded sample was fixed in the test rig by an aluminium frame. This frame was designed for our

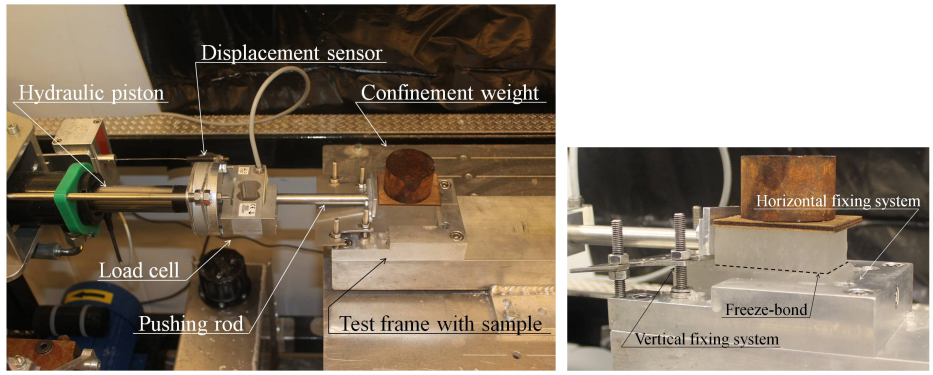

(a) Overview picture of the test rig. **(b)** Test frame.

Figure 3.2: Test rig and frame used in the NTNU-experiments.

experiments, and is an improved version of the plastic frame used by Repetto-Llamazares and Høyland (2011a) and Helgøy (2011). Increasing the system stiffness, reduced the bending moment in the freeze-bond and eliminating the collision, which Helgøy (2011) experienced between the piston and plastic frame, was the objective for designing the aluminium frame. A picture of the test frame is shown in figure 3.2b, while a principle drawing is found in appendix E.

Ice-blocks with dimensions $90 \cdot 40 \cdot 22$ [mm] (lower block) and $60 \cdot 40 \cdot 22$ [mm] (upper block) were used to form the freeze-bonded sample. A band-saw was used to cut the samples. Shear force was applied to the freeze-bond by pushing the upper block with a hydraulic piston. A 1 kN load cell was connected between the hydraulic piston and the rod pushing the upper ice-block to measure the freeze-bond strength. The displacement sensor was connected at the fixing point of the load cell. Force and displacement were recorded with 100 Hz frequency and 16-bit resolution. The piston had a fixed velocity of (mean, standard deviation, max, min) 2.03, 0.05, 2.18, 1.85 mm/s.

3.4.1 Ice properties

Saline ice produced in the ice production basin "Frysis II" was used in the experiments. This production basin is equipped with heated walls and bottom to induce ice-growth from above, has a surface area of $1200 \cdot 800$ [mm] and a depth

of 1300 mm. Three ice sheets ("Ice 1", "Ice 2" and "Ice 3") were produced for the experiments, all from water with a salinity of 8 ppt. Ice growth started from a free water surface, without seeding. Produced ice sheet thickness varied between the different ice sheets, ranging from 110 to 188 mm. Production temperature for Ice 1 was −20 °C. Fluctuating temperatures between −20 °C and −7 °C were used during the production of Ice 2 and Ice 3. Table 3.2 contains production data of the three ice sheets.

Table 3.2: Production data of the ice produced at NTNU. Ice thickness was measured in the centre and at the edge of the basin. Salinity of an ice-core of the full ice-sheet thickness was also measured.

	Ice 1	Ice 2	Ice 3
Centre thickness [mm]	165	140	110
Edge thickness [mm]	188	140	110
Core salinity [ppt]	2.28	1.52	1.37

This sections were used to study the ice texture of the three ice-sheets. Ice 1 may be classified as S2 ice with a columnar crystal structure below an approximately 40 mm thick transition zone. The columnar grains had a diameter of roughly 10 mm. Such a classification was not possible to do for Ice 2 and 3. The crystal structure may seem to be columnar with very large grains, but a full determination of the crystal structure is not possible to obtain from the thin sections. Pictures of vertical cross-sectional thin sections of each ice sheet are located in appendix C.

The ice was stored in larger blocks at −7 °C in sealed plastic bags, after extraction from the production basin. Storing time varied from 1 to 15 days before testing, see details in table 3.3. Except for the "Vertical, Cut-Parallel, −1 °C, Stored" configuration the final ice-block dimensions were cut at the day of testing.

Table 3.3: Storage time between removal of ice from the production basin and until preparation of final ice-block dimension.

Series	1000	2000	3000	4000	5000	6000	6000 "Stored"	7000
Storage time	1 day	4 days	8 days	9 days	4 days	15 days	8 days	1 day
Ice number	1	1	1	1	2	1	1	3

3.4.2 Test configurations

Seven test series were conducted, denoted series 1000 to 7000. Each series lasted from three to ten hours. The tests were divided into ten test configurations. Figure 3.3 illustrates the procedure of preparing the test configurations. Table 3.4 gives the complete test matrix, and states the number of tests per configuration. The actual number of samples the different statistical parameters are based on is presented in chapter 4. The tests were performed with as large spread as possible in the sequence the different test configurations were tested. A chronological list of the tests is found in appendix A.

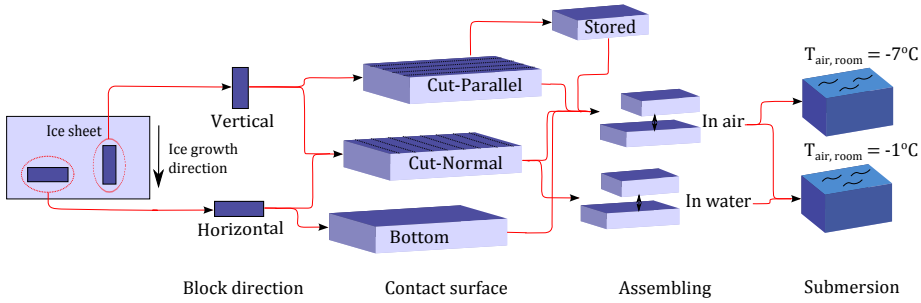

Figure 3.3: Flow-chart of the test configurations used in the NTNU-experiments.

The use of two different ice-block directions, horizontal and vertical ice-blocks, formed the basis of the test configurations. Horizontal ice-blocks had the longitudinal direction normal to the ice growth, while vertical ice-blocks had the longitudinal direction parallel with the ice growth. Secondly three different contact surfaces were applied. The natural bottom of the ice sheet was one of the contact surfaces, while the two others were artificially made by sawing. Sawing the ice blocks made straight groves in the surface. The two surfaces were made by either arranging these groves parallel or normal to the longitudinal ice-block direction, shown in figure 3.4. Only equal surfaces were placed in contact with each other, e.g. bottom in contact with bottom, normal groves in contact with normal groves and parallel groves in contact with parallel groves.

The ice-blocks used for the "Vertical, Cut-Parallel, $-1\,^{\circ}C$, Stored" configuration were stored for seven days in sealed plastic boxes after cutting the final ice-block dimensions. Six of the days were at $-7\,^{\circ}C$, while one day in the middle of the storing period was at $-20\,^{\circ}C$. The ice used in the remaining

Table 3.4: Test matrix for the NTNU-experiments.

Block orientation	Surface	Ambient air temprature	Additional	Number of test per series: 1000 *Ice 1*	2000 *Ice 1*	3000 *Ice 1*	4000 *Ice 1*	5000 *Ice 2*	6000 *Ice 1*	7000 *Ice 3*	Total number of tests
Vertical	Cut - Parallel	-1°C	Stored						13		13
		-1°C		6	2		3			5	16
		-7°C		5		5					10
	Cut - Normal	-1°C		6	2		3	6	1	5	22
		-1°C	In water				5		7		12
		-7°C		5		5					10
Horizontal	Cut - Normal	-1°C			8		3	6		5	22
		-1°C	In water				5		7		12
	Bottom	-1°C					6			7	13
		-7°C		5							5

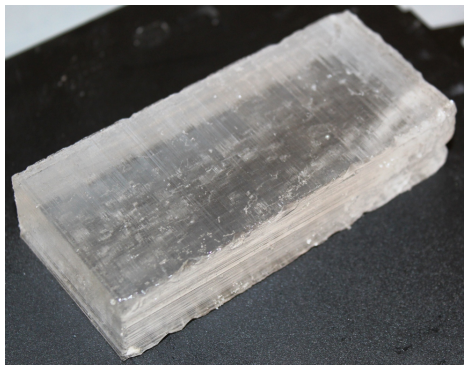

(a) Normal groves - "Cut-Normal", Ice 3, $(90 \cdot 40 \cdot 22$ mm)

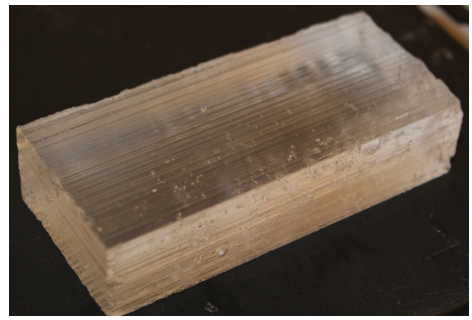

(b) Parallel groves - "Cut-Parallel", Ice 3, $(90 \cdot 40 \cdot 22$ mm)

Figure 3.4: Pictures of the two different sawn contact surfaces.

configurations was kept at -7 °C at all time. Repetto-Llamazares and Høyland (2011a) exposed the ice-blocks to temperatures of -20 °C, but stored them at -7 °C. Repetto-Llamazares and Høyland (2011a) also prepared the final block dimensions shortly after the ice was removed from the production basin, and stored the samples pre-cut.

Freeze-bonds were either assembled "In air" or "In water". For assembling "In air" the two ice-blocks were placed on top of each other in air, as seen in figure 3.5, and subsequently submerged in water. Repetto-Llamazares et al. (2011a), Repetto-Llamazares and Høyland (2011a) and Helgøy (2011) assembled the samples "In air". Assembling "In water" was made by placing the blocks in contact with each other in water by hand, lift them up in air, applying the confinement pressure and subsequently submerging the sample in water.

The ambient air temperature of the submersion basin was kept at two levels, -1 °C and -7 °C. Repetto-Llamazares and Høyland (2011a) used a ambient air temperature of -1 °C, while Helgøy (2011) used -7.5 °C. With an ambient air temperature of -7 °C ice was continuously formed in the basin, but ice was not formed during sample submersion if the ambient air temperature was -1 °C. A thin ice-layer was formed on the water surface if the basin was left untouched for some days with a ambient air temperature of -1 °C. The water temperature in the basin was continuously measured during the experiments. Mean water temperature during each test series is presented in table 3.5. We tried to keep

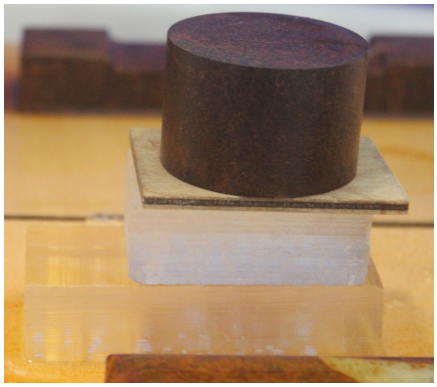

Figure 3.5: Assembling of a freeze-bonded sample in air (Ice 3).

the salinity in the basin at 8 ppt, but it was measured to be in the range of 8 and 9.01 ppt during the tests. The ambient air temperature during freeze-bond testing was equal to the initial ice-block temperature, -7 °C.

Table 3.5: Mean water temperature in the submersion basin and ambient air temperature during each test series.

Series	1000 - "−1 °C"	1000 - "−7 °C"	2000	3000	4000	5000	6000	7000
Mean water temprature [°C]	−0.43	−0.54	−0.49	−0.56	−0.49	−0.48	−0.40	−0.51
Ambient air temprature [°C]	−1	−7	−1	−7	−1	−1	−1	−1

3.4.3 Measured variables

Additional measurements were performed in connection with the freeze-bond strength tests. The submersion basin salinity was measured one to two times per test series, preferably in the beginning and end of each series. Physical properties were measured in identical ice-blocks to the ones used to form freeze-bonds. These measurements included measuring the ice-block dimensions, weight, core temperature, and salinity. The ice-block dimensions and weight were used to calculate the ice-block density.

Pictures of the fractured surfaces were taken shortly after the freeze-bond strength were measured. Both the upper and lower contact surfaces were photographed.

The pictures were used to estimate the freeze-bonded area between the two ice-blocks. Salinity of the separate ice-blocks and the joint salinity of both ice-blocks were measured. Surface pictures were made of all samples, while six samples lack complete salinity measurements, details are found in appendix A.

Water temperature in the submersion basin was recorded continuously during each test series. Two equal sensors were connected to a PT-100 data logger which recorded the temperature. One of these sensors had a malfunction during the last test series. For this reason only measurements from the sensor functioning all along were used.

3.4.4 Thin sections

Totally 15 freeze-bond thin sections were prepared for all test configurations. Pictures of these are found in appendix B. A summary of the number of thin sections prepared for each test configuration is found in table 3.6. The thin sections prepared for samples with equal ice-block direction and contact surface, but with different ambient air temperature of the submersion basin, are placed in one group. As illustrated in figure 3.6, the thin sections were prepared in the middle of the freeze-bonded sample.

Table 3.6: Number of thin sections prepared for the different test-configurations.

	Ice 1	Ice 2	Ice 3
Vertical, Cut-Parallel, Stored			
Vertical, Cut-Parallel	2		
Vertical, Cut-Normal	1	2	1
Vertical, Cut-Normal, In water	1		
Horizontal, Cut-Normal	2	2	1
Horizontal, Cut-Noraml, In water	1		
Horizontal, Bottom	1		1

In addition to thin sections of freeze-bond samples, vertical cross sectional thin sections of each ice-sheet were produced. One cross section was made for Ice 1 and 2, while two cross sections were made for Ice 3. Before production, the samples were precooled to a temperature of $-15\,^{\circ}\mathrm{C}$ to $-20\,^{\circ}\mathrm{C}$, and the production temperature was kept in the same range.

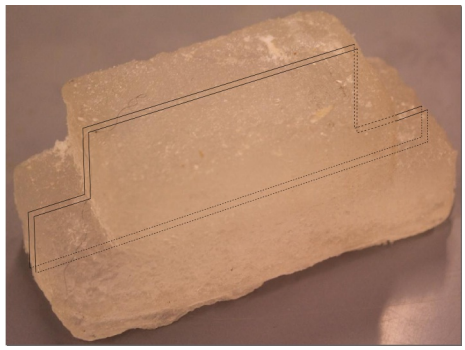

Figure 3.6: Location of freeze-bond thin sections.

3.5 HSVA-experiments

Two test frames were used in the HSVA-experiments. With the test frame designed for the NTNU-experiments 25 samples were tested, whereas 20 samples were tested with the test frame used by Repetto-Llamazares et al. (2011a). Figure 3.7a shows an overview picture of the test rig with the test frame used by Repetto-Llamazares et al. (2011a), through this thesis named the HSVA-frame. An overview picture of the test rig with the NTNU-frame is seen in figure 3.7c. There were two principal differences between the NTNU and HSVA-frame. The HSVA-frame applied larger ice-blocks to form the freeze-bond, and shear force was applied to the freeze-bond by pulling a lid connected to the upper ice-block. In addition was the HSVA-frame, seen in figure 3.7b, made of plastic, while the NTNU-frame was made of aluminium. A principle drawing of the HSVA-frame is found in appendix E.

Ice-blocks with dimensions $180 \cdot 140 \cdot 27$ [mm] (lower block) and $140 \cdot 140 \cdot 27$ [mm] (upper block) were used with the HSVA-frame. This yield an 8.17 times larger nominal contact area between the ice-blocks compared to the ice-blocks used with the NTNU-frame. Repetto-Llamazares et al. (2011a) used equal width and length of the ice-blocks, but left the ice thickness untouched. Since the ice produced for our experiments was around 40 mm thick, the samples were cut to a fixed thickness of 27 mm. Repetto-Llamazares et al. (2011a) used ice-blocks with a thickness varying between 25 and 35 mm. All sample dimensions were cut by a band-saw.

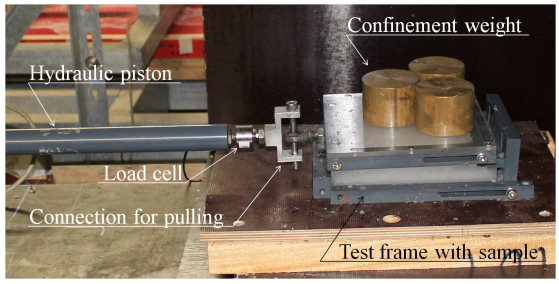

(a) Overview picture of the test rig with the HSVA-frame.

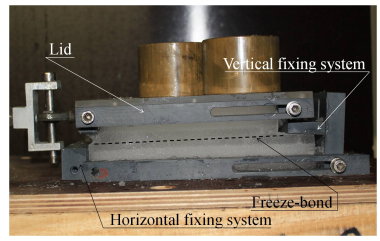

(b) HSVA test frame.

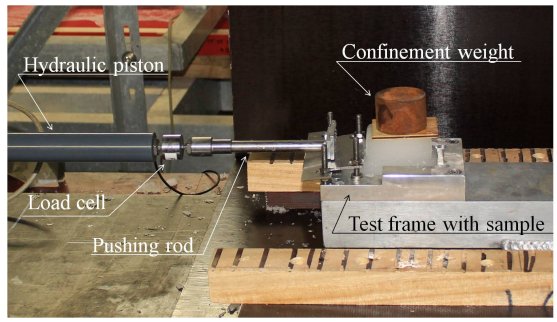

(c) Overview picture of the test rig with the NTNU-frame.

Figure 3.7: Test rig and frames used during the HSVA-experiments.

Shear force was applied to the freeze-bond by pushing or pulling the upper ice-block. A hydraulic piston with a fixed velocity of (mean, standard deviation, max, min) 2.12, 0.14, 2.45, 1.6 mm/s was used. This piston velocity was higher than the piston velocity used by Repetto-Llamazares et al. (2011a), but equal to Repetto-Llamazares and Høyland (2011a). A 1 kN load cell was used to measure the freeze-bond strength. The displacement sensor was built-in to the piston. Force and displacement were recorded with 100 Hz frequency. The test rig and set-up was identical for the two test-frames.

During the freeze-bond strength tests with the HSVA-frame all the confinement weights were placed at the rear end of the lid, see figure 3.7a. This was done in order to prevent the lid from sliding off. For the strongest freeze-bonds it was in addition necessary to keep the lid in place by hand. This was done by vertically pushing the lid down at the rear end. It was difficult to get the connection point between the lid and pulling system aligned, and it was often necessary to apply force to get them connected. This force was often perpendicular to the pulling direction.

3.5.1 Ice properties

Saline model ice, with small crystals, produced in the large ice-basin at HSVA was used in the experiments. The ice was produced after the HSVA-procedure for model ice as described by Evers and Jochmann (1993). This procedure involves spraying 6.9 ppt freezing point temperature saline water with fine water droplets to seed the ice growth. In addition small air bubbles are feed into the ice from below. The air-bubbles are continuously added during the production of the ice-sheet, but are stopped when heating of the ice-sheet starts. This leaves a three to five mm thick layer of less porous ice at the bottom, beeing formed after the heating is initiated. Two horizontal and one vertical cross-sectional thin section of the produced ice is located in appendix C. These show that the produced ice may be classified as S2 ice with a thin granular top layer and a tick columnar layer. The columnar layer contained crystals with a diameter of approximately 2.5 mm. All ice used in the experiments at HSVA were extracted from one ice-sheet, and in the same area of the ice-basin.

After production the ice was heated to a temperature close to the freezing-point, before the ice used to form freeze-bonds were extracted. This is done in order obtain the desired mechanical properties of the ice during model testing. Heating of the ice results in a low ice-strength, and made it difficult to extract

large enough ice-blocks from the basin. The extracted ice-blocks were stored in sealed plastic-bags with the surface intended to form freeze-bonds facing upward. The salinity, density and temperature of the extracted ice is presented in table 3.7. HSVA-model ice extracted after heating was also used by Repetto-Llamazares et al. (2011a).

Table 3.7: Salinity, density and temperature of the HSVA-ice at the time of extraction from the production basin.

ρ_i [kg/m^3]	S [ppt]	T_{core} [°C]
906	3.3	-0.73

As a standard procedure at HSVA the top surface of the ice was wiped off before tests were performed with the ice. This was the only interference of the top surface, since flooding was avoided during extraction. Extraction of bottom surface samples without mechanically affecting this surface was not possible. Due to the weak ice-strength, a smooth plywood plate was used to lift ice-blocks out of the ice-basin. The bottom surface was then glided along the plywood plate in order to get the ice-blocks into the plastic bags. We tried to keep the surface abrasion at a minimum.

For series 100 and 200 the extracted ice-blocks were stored at -7 °C for one and two days before testing. Series 300 ice-blocks were first stored for two days at -20 °C, followed by 15 hours of heating to -7 °C before testing. Ice-crystals were formed on the contact surfaces during storing, from initial moisture in the ice-blocks. By sweeping the top surface with a brush it was possible to almost completely remove these ice-crystals. The ice-crystals could not completely be removed from the bottom surface. This resulted in some increase in the surface roughness compared to the natural bottom surface.

3.5.2 Test configurations

Three test series, named series 100 to 300, were carried out. Each series lasted from one and a half to nine hours. The tests were divided into four test configurations, two using the NTNU-frame and two using the HSVA-frame. A complete test matrix is found in table 3.8, where the number of samples tested per configuration is given. The actual number of samples the different statistical parameters are based on is found in chapter 4. Due to the limited test period

it was not possible to test the configurations with as large spread in the testing sequence as for the NTNU-experiments, see appendix A.

Table 3.8: Test matrix for the HSVA-experiments.

Test-frame	Surface	Additional	Number of test per series: 100	200	300	Total number of tests
NTNU	Top		7	6		13
	Bottom		7	5		12
HSVA	Bottom			13		13
	Bottom	Stored			7	7

The use of two test frames, and thereby two sample dimensions, formed the basis for the test configurations. Two contact surfaces were used with the NTNU-frame, the natural top surface in contact the natural top surface and the natural bottom surface in contact the natural bottom surface. Pictures of these surfaces are seen in figure 3.8. Helgøy (2011) applied these two surface configurations, and used S2 ice with small crystals in their experiments. The two HSVA-frame configurations used the natural bottom surface in contact the natural bottom surface to form freeze-bonds. The temperature in the ice-blocks used with the NTNU-frame was kept at -7 °C at all time. The time - temperature history of the ice-blocks were the dividing factor for the samples tested with the HSVA-frame. For one configuration the ice-blocks were stored at -7 °C at all time. In the other configuration the ice-blocks were first stored at -20 °C for two days, followed by 15 hours of heating to -7 °C. Repetto-Llamazares et al. (2011a) cooled all the ice used in the experiments down to -20 °C, before heating the ice to the desired temperature. Freeze-bond strength testing was performed with an equal air temperature as the initial ice-block temperature, i.e. -7 °C.

Common for all the configurations in the HSVA-experiments was that the ambient air temperature of the submersion basin was -7 °C. Water from the production basin was used in the submersion basin, and the salinity increased from 6.7 to 7.3 ppt from the first to the last test. All samples were assembled "In air". A picture of a HSVA-frame sample before submersion is seen in figure 3.9. The ambient air temperature of the submersion basin in the experiments of Repetto-Llamazares et al. (2011a) is not known, but the initial submersion basin salinity and assembling method was equal to our experiments.

(a) NTNU-frame, Top, $(90 \cdot 40 \cdot 22$ mm)

(b) NTNU-frame, Bottom, $(90 \cdot 40 \cdot 22$ mm)

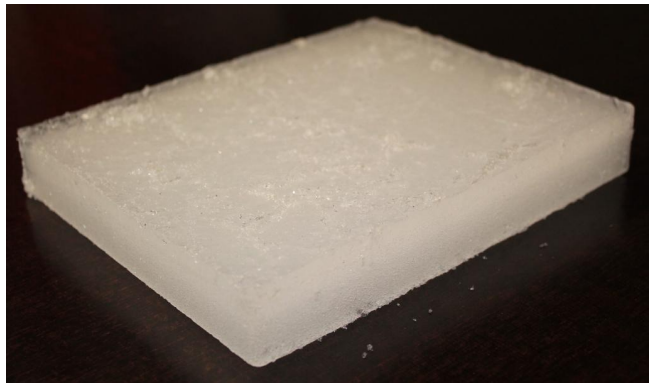

(c) HSVA-frame, $(180 \cdot 140 \cdot 27$ mm)

Figure 3.8: Contact surfaces during the HSVA-experiments.

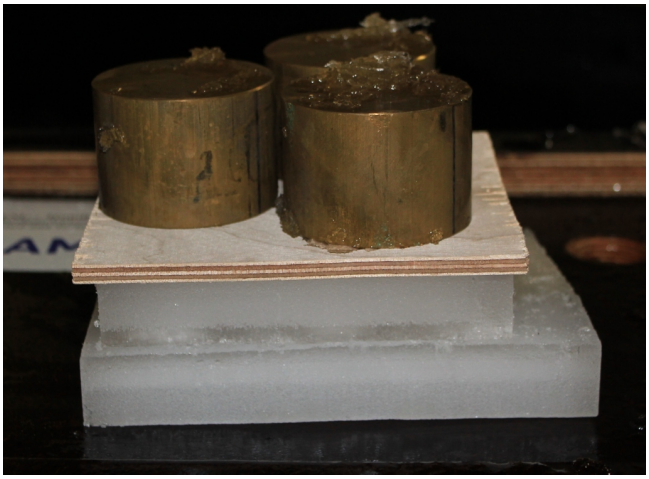

Figure 3.9: HSVA-frame sample before submersion.

3.5.3 Measured variables

The submersion basin salinity was measured in the beginning and end of each test series. Physical properties of equal ice-blocks as the ice-blocks used to form freeze-bonds were measured for series 100 and 200. This included measuring the ice-block dimensions, weight, salinity and core temperature (not series 100). Ice-block dimensions and weight were used to calculate the density. Due to lack of a sufficient amount of ice the salinity was only measured in one sample from series 300. This sample had gone through the same time - temperature history and was cut to the same thickness as the remaining samples, but had a smaller surface area.

Pictures were made of the fractured surfaces after the freeze-bond strength was measured. Both the upper and lower contact surface was photographed, as in the NTNU-experiments. Salinity of the separate ice-blocks were measured, but not for the joint salinity of both ice-blocks. Surface pictures were made of all samples. Five samples miss complete salinity measurements from series 100. This was due to leaking plastic bags during melting of the samples, see details in appendix A. Series 200 and 300 have complete salinity measurements.

3.5.4 Thin sections

One thin section for each of the NTNU-frame configurations, and one thin section with the HSVA-frame sample dimension and contact surface (bottom) was prepared. The HSVA-frame thin section was prepared in two parts due to the width of the sample. Before production the samples were precooled to $-20\ ^{\circ}\mathrm{C}$, and the production temperature was kept at the same level. As for the freeze-bond thin sections prepared in the NTNU-experiments the thin sections were made in the centre of the sample, see figure 3.6.

Chapter 4

Results

4.1 Introduction

Results from the NTNU- and the HSVA-experiments are presented separately throughout this chapter. Full page figures and tables are located in the last pages of this chapter, i.e. figure 4.21 to 4.25 and table 4.6 to 4.9. Additional information and results may be found in the appendixes. Appendix A contains a list presenting chronologically data from each test. Polarized and non-polarized pictures of the freeze-bond and ice-sheet thin sections are located in appendix B and C. Stress - displacement or stress - time curves of each test are presented in appendix D. These diagram's are edited so that the starting point of each curve lies in the area were the freeze-bond started to yield resistance.

The freeze-bond strength (τ_{fb}) has been used in the analyses of the different strength measurements. It is defined as the peak force during a test divided by either the nominal or real contact area between the ice-blocks. The nominal freeze-bond strength ($\tau_{fb,nom}$) has primarily been used in the presentation of the result. Repetto-Llamazares et al. (2011a) and Repetto-Llamazares and Høyland (2011a) also presented the results in form of the nominal freeze-bond strength. The unbounded area (A_{ub}) between the ice-blocks, see section 4.2.4 and 4.3.4, has been used to define the effective freeze-bonded area, and thereby the real freeze-bond strength ($\tau_{fb,real}$).

The freeze-bond strength measurements are presented through box- and point-plots. Point-plots are used to compare the freeze-bond strength for the different test-configurations, test series and applied ice-sheets. For the comparisons where an adequate amount of samples were available, a 95% confidence interval of the mean value have been presented. The t-distribution was used to estimate the interval.

A box-plot presents the quartiles of the assessed data series. For the reader who is not familiar with this sort of data presentation, a short presentation follows. The lower line starts at the lowest obtained value (0% quartile), while the upper line ends at the highest obtained value (100% quartile). Limits of the outer-points of the box are given by the 25 and 75% quartiles, and the mid line is the median (50% quartile). Points outside the upper or lower lines are considered as outliers and has a value larger than $q_{75\%} + 1.5(q_{75\%} - q_{25\%})$ where $q_{25\%}$ and $q_{75\%}$ are the 25% and 75% quartiles, respectively. This means that approximately 99.3% of the data points should be included by the lower and upper line if the data is normally distributed. The upper or lower line stops at the last value included in the defined interval if an outlier is present.

4.2 NTNU-experiments

4.2.1 Physical properties of the ice used in the NTNU-experiments

Spatial variations in colour and transparency were visually seen for Ice 2 and 3. Figure 4.1 shows how some parts of the ice were opaque and white, while other parts were transparent. Brine channels where seen in the opaque parts, while very few brine channels and voids were seen in the transparent parts. The border between the ice crystals seemed to follow the boundary between the opaque and transparent areas. Ice 1 had an evenly opaque coloured structure.

Table 4.1 contains measured data of physical properties of the ice-blocks utilised to form freeze-bonds. The two low salinity samples from series 5000 (Ice 2) and 7000 (Ice 3) were made out of the transparent parts of the ice. These had a salinity of 0.62 and 0.54 ppt, respectively. Pictures of transparent ice-blocks are shown in figure 4.1a and in the lower part of figure 4.1b. Average salinity for the different ice sheets were Ice 1: 1.98 ppt, Ice 2: 1.13 ppt and Ice 3: 1.06 ppt.

(a) Ice 2, series 5000. Ice-sheet thickness = 140 mm. This cross section has been sawn into 40 mm wide pieces in the vertical direction.

(b) Ice 3, series 7000. Ice-sheet thickness = 110 mm.

Figure 4.1: Pictures showing spatial variation in colour and transparency of Ice 2 and 3. The picture shows the full ice-sheet thickness.

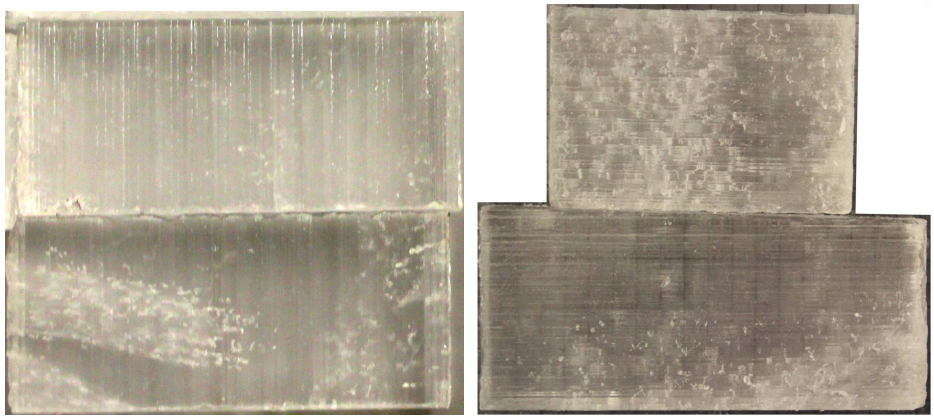

(a) Ice 2 samples, "Cut-Normal". **(b)** Ice 3 samples, "Cut-Parallel".

Figure 4.2: Transparent ice-blocks from Ice 2 and 3.

Table 4.1: Temperature, density and salinity of tested ice-blocks before submersion for the NTNU-experiments.

Series	Block orientation	Ice	ρ_i [kg/m^3]	S [ppt]	T [°C]	m [g]	Dimensions [mm] L	W	H
1000		1	856	1.96	-7.5[a]	70.3	91	41	22
		1	854	2.04[a]	-8.5[a]	70.1	91	41	22
		1	877	1.98	-7.0[a]	71.8	91	40	22.5
2000	Vertical	1	859	1.91	-7.5[a]	72.1	91	41	22.5
3000	Vertical	1	847	2.00	-6.0	71.8	93	40.5	22.5
4000	Vertical	1	845	2.23	-6.9	69.4	91	41	22
	Horizontal	1	864	1.92	-7.2	70.9	91	41	22
	Horizontal-Bottom	1	818	2.34	-6.9	67.9	91	41	22.3
5000	Horizontal	2	910	0.62	-6.6	71.3	89	40	22
	Vertical	2	868	1.64	-6.6	70.3	90	40	22.5
6000	Vertical-Stored	1	856	1.69	-7.1	75.9	92	41	23.5
	Vertical	1	848	2.04	-6.8	69.2	91	39	23
	Horizontal	1	851	1.64	-7.1	68.7	90	39	23
7000	Horizontal-Bottom	3	873	1.44	-6.6	66.7	91	40	21
	Horizontal	3	864	0.54	-6.9	69.2	91	40	22
	Vertical	3	855	1.21	-6.7	69.3	91	40.5	22

[a]Temprature and/or salinity were not messured in the same ice-block as the remaining properties.

The salinity of two larger ice-blocks from Ice 2 were measured, one opaque and one transparent ice-block. These ice-blocks had a cross section of $40 \cdot 60$ [mm] and length equal to the ice-sheet thickness. The transparent sample had a salinity of 0.33 ppt, while the opaque sample had a salinity of 1.91 ppt.

4.2.2 Texture of freeze-bonded samples

Pictures of a selection of the prepared freeze-bond thin sections are presented in figure 4.3. The main findings from analysing the thin sections relate to differences in ice texture between the horizontal and vertical samples, and differences in ice texture between samples from the three ice-sheets.

Ice 1 samples contained columnar crystals, with minor parts entering the wedge out zone for some samples. Ice 2 and 3 samples had larger crystals with a random oriented crystal structure, somewhat tending to a columnar crystal structure for some samples. Vertical configuration samples applying Ice 1 had the columnar crystals aligned parallel to the longitudinal ice-block direction, figure 4.3a. Horizontal configuration Ice 1 samples had the columnar crystals aligned perpendicular to the longitudinal ice-block direction, figure 4.3b. Figure 4.3c shows a vertical configuration sample from Ice 2 with columnar crystals in the upper ice-block, and larger randomly oriented crystals in the lower ice-block. A "Horizontal, Bottom" sample from Ice 3 is seen in figure 4.3d. This sample had nearly a columnar crystal structure, but considerably larger crystals compared to the Ice 1 samples.

No detectable freeze-bond thickness was observed form the thin-sections. Differences at the freeze-bonding surface could be seen between the "Cut-Normal" and "Cut-Parallel" samples. Traces after the groves created during sawing were observed for some of the "Cut-Normal" samples. No groves were visible for the "Cut-Parallel" samples. "Cut-Parallel" samples had the groves parallel with the thin-section plane, while the "Cut-Normal" samples had the groves perpendicular to the thin-section plane. Examination of the thin sections also showed that ice was forming on the upper surface of the lower ice-block in the areas which were not in contact with the upper ice-block.

A relative even distribution of voids over the cross-section of the Ice 1 samples were seen, figure 4.3f. Spatial variations in the distribution of voids were seen for the Ice 2 and 3 samples. Figure 4.3e shows an example, this is the same sample as seen through polarized light in figure 4.3c. By comparing these figures it is

seen that the large crystal on the right side of the lower ice-block corresponds to the area with few voids. Differences in void content related to the crystal structure were seen for all Ice 2 samples, and the majority of the Ice 3 samples.

(a) Series 4000, Vertical, Cut-Parallel, Ice 1

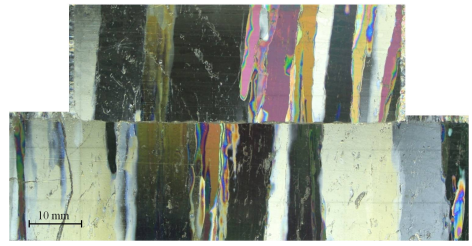

(b) Series 2000, Horizontal, Cut-Normal, Ice 1

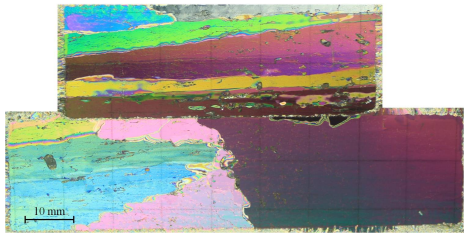

(c) Series 5000, Vertical, Cut-Normal, Ice 2

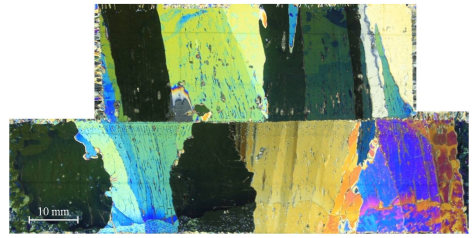

(d) Series 7000, Horizontal, Bottom, Ice 3

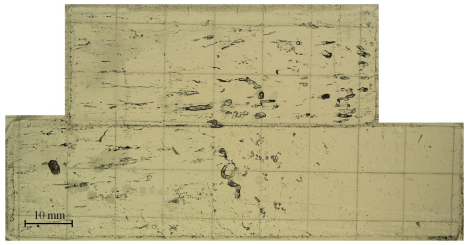

(e) Series 5000, Vertical, Cut-Normal, Ice 2

(f) Series 2000, Horizontal, Cut-Normal, Ice 1

Figure 4.3: Examples of thin sections from the NTNU-experiments.

4.2.3 Ice-block salinity after submersion

Salinity of the two ice-blocks forming the freeze-bonding sample was measured separately and mixed after the freeze-bond strength was measured. Statistical data of these measurements are found in table 4.6. Figure 4.4 shows how the separate ice-block salinity varied between the different configurations for the Ice 1 samples. No particular differences were found between the salinity content of the different configurations. The lower ice-block had highest salinity content for 87 of the 99 samples (88%).

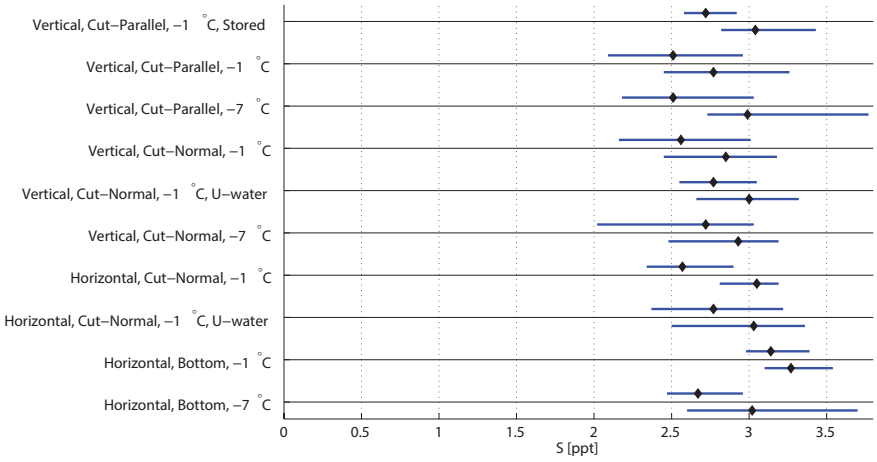

Figure 4.4: Salinity (S) of the upper ice-block (S_u) (above the line) and the lower ice-block (S_l) (below the line) for Ice 1, measured after strength testing. Divided after test configuration. The black mark indicates the average ice-block salinity while the error bars shows the maximum and minimum ice-block salinity.

Figure 4.5 shows a similar plot comparing the ice-block salinity of samples from the three ice-sheets, divided after test configuration. This plot shows that there is a much larger spread in the ice-block salinity for the Ice 2 and 3 samples, compared to the Ice 1 samples. This is also in accordance with the salinity measurements made before submersion, see table 4.1 in section 4.2.1. In particular should the low salinity of the top ice-block for Ice 3 samples in the "Vertical, Cut-Normal, -1 °C" configuration be noticed. This corresponds to the test con-

figuration and applied ice-sheet with the lowest average freeze-bond strength, $\tau_{fb,nom} = 6.1$ kPa.

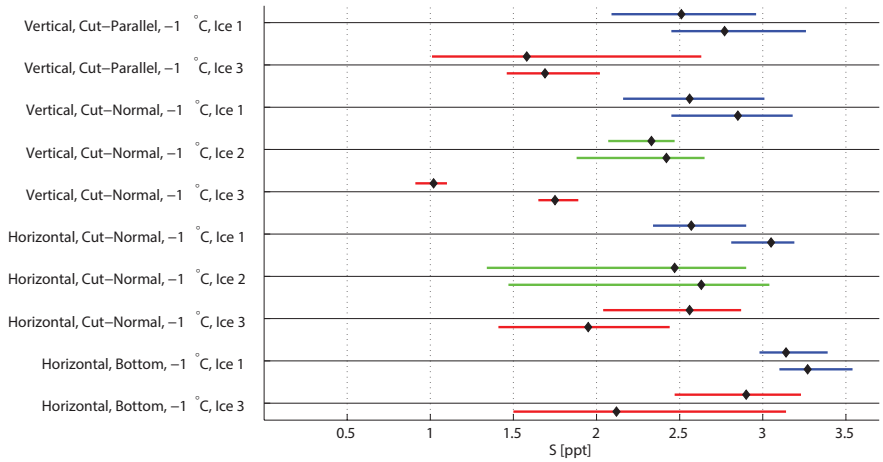

Figure 4.5: Salinity (S) of the upper ice-block (S_u) (above the line) and lower ice-block (S_l)(below the line), measured after strength testing. Divided after test configuration and ice-sheet. The black mark indicates the average ice-block salinity, while the error bars shows the maximum and minimum ice-block salinity. Samples from the three ice-sheets are marked with different colours.

4.2.4 Freeze-bonded area

The freeze-bonded area between the ice-blocks has been estimated from pictures of the fractured surfaces. A selection of these pictures is seen in figure 4.6. The extent of the freeze-bonded area is quantified through the unbounded area (A_{ub}) in percent of the nominal contact area (A_{fb}). Statistical parameters for each configuration is presented in table 4.2. Fully freeze-bonded surfaces were created for the samples assembled "In water", with exception of one sample which had a small unbounded area of 2%. Figure 4.6a shows one of the "In water" samples with a fully freeze-bounded area. All configurations assembled "In air" contained samples with unbounded areas.

Ten of the eighteen samples applying the natural bottom surface of the ice-sheet to form freeze-bonds had fully freeze-bonded surfaces. A surface picture of one samples which not had a fully freeze-bonded surface is seen in figure 4.6b. Common for all these samples were that the extent of the unbounded area was clearly seen, and the shape and the orientation of the area were random.

All samples with a artificial contact surface assembled "In air" had an unbounded area. Common for these samples was that they were bounded along the outer edge, with an unbounded area in the centre of the contact surface. The extension of this unbounded area varied between the different samples. Determination of the unbounded areas was difficult due to a soft transition between the bonded and unbounded areas. As seen in figure 4.6c and 4.6d the boundary between the bonded and unbounded areas to some degree were following the straight grooves made during sawing of the surfaces. The contact surfaces from Ice 2 and 3 samples seemed to contain more moisture than the samples from Ice 1 after fracture.

Table 4.2: Statistics of the unbounded area (A_{ub}) for the NTNU-experiments.

Configuration				Number of samples	A_{ub} [%] Mean	Std	Max	Min
Vertical,	Cut-Parallel,	−1 °C, Stored	Ice 1	13	35	10	52	15
Vertical,	Cut-Parallel,	−1 °C	Ice 1	11	42	10	56	29
			Ice 3	5	52	15	62	26
Vertical,	Cut-Parallel,	−7 °C	Ice 1	10	42	16	66	7
Vertical,	Cut-Normal,	−1 °C	Ice 1	12	37	9	52	16
			Ice 2	6	35	7	48	28
			Ice 3	5	39	14	58	24
Vertical,	Cut-Normal,	−1 °C, In water	Ice 1	12	0	0	0	0
Vertical,	Cut-Normal,	−7 °C	Ice 1	10	39	10	57	26
Horizontal,	Cut-Normal,	−1 °C	Ice 1	11	31	8	45	22
			Ice 2	6	33	10	45	15
			Ice 3	5	28	13	47	16
Horizontal,	Cut-Normal,	−1 °C, In water	Ice 1	12	0.1	0.5	2	0
Horizontal,	Bottom,	−1 °C	Ice 1	6	3	5	13	0
			Ice 3	7	0.1	0.4	1	0
Horizontal,	Bottom,	−7 °C	Ice 1	5	5	10	23	0

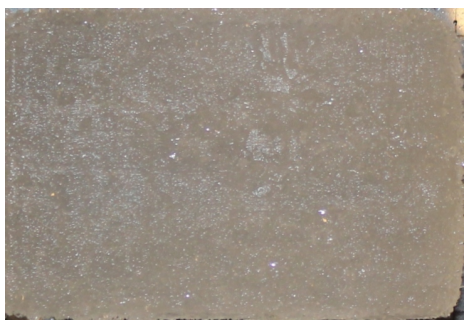

(a) Sample 4006, "In water", Ice 1, $A_{ub} = 0\%$.

(b) Sample 1026, "Bottom", Ice 1, $A_{ub} = 3\%$.

(c) Sample 2000, "Cut-Normal", Ice 1, $A_{ub} = 22\%$.

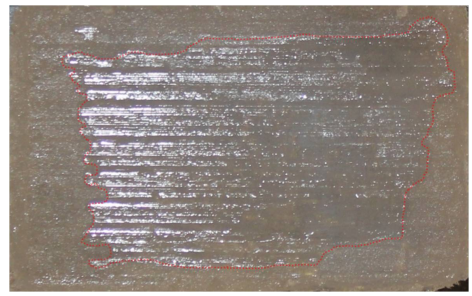

(d) Sample 7010, "Cut-Parallel", Ice 3, $A_{ub} = 59\%$.

Figure 4.6: Pictures of fractured surfaces from the NTNU-experiments, unbounded area (A_{ub}) is marked by a red line.

4.2.5 Freeze-bond strength

Examples of stress - time plots from the freeze-bond strength tests are presented in figure 4.7, equal plots for each test are found in appendix D. The freeze-bond strength is plotted against time due to signal disturbances on the displacement sensor. The plotted time of 1.5 s equals a displacement of 3 mm if a constant piston velocity of 2 mm/s is assumed. Crushing of porous ice accumulated on the face of the upper ice-block during submersion gave a visible contribution to the stress - time curve before the freeze-bond fractured.

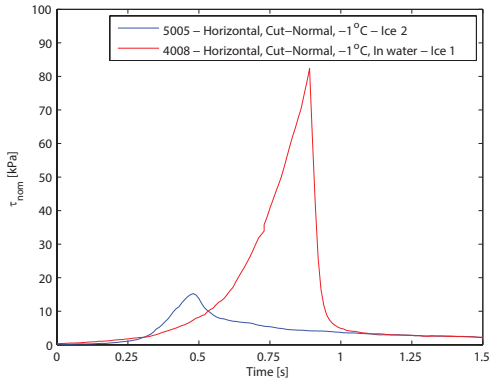

Figure 4.7: Examples of stress - time plots from the NTNU-experiments, sample 4008 and 5005. The plotted time of 1.5 s equals a displacement of ~ 3 mm.

4.2.5.1 Freeze-bond strength vs. test configuration - Ice 1 samples

Ice 1 samples have been used to compare the freeze-bond strength between the test configurations. We have chosen to do so due to the clear difference seen between the physical properties of the three ice-sheets, see section 4.2.1. Statistical parameters for the test configurations is presented in table 4.7. A point-plot of all tests, divided after test configuration, is in addition shown in figure 4.21.

Figure 4.8 shows a box-plot comparing the nominal freeze-bond strength for the vertical samples. A significant difference is seen between the assembled "In

water" configuration and the configurations assembled "In air". By comparing the average nominal freeze-bond strength the samples assembled "In water" were almost two times stronger than the samples assembled "In air". The difference is reduced by comparing the average real freeze-bond strength of the samples, but the assembled "In water" samples was still 1.25 to 1.45 times stronger than the samples assembled "In air", see figure 4.9.

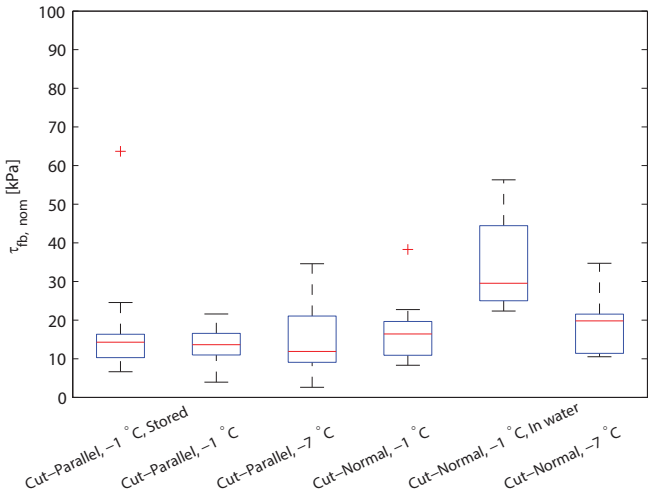

Figure 4.8: Box-plot of the nominal freeze-bond strength ($\tau_{fb,nom}$) for the vertical "Ice 1" samples.

Only minor differences were seen within the vertical configurations assembled "In air". The observed differences relates to variations in the strength distribution, and the "Cut-Parallel, $-1\,^{\circ}$C, Stored" configuration had a very strong outlier, $\tau_{fb,nom} = 63.7$ kPa. Larger differences were seen between the configurations when the real freeze-bond strengths were compared, see figure 4.9. It should be noticed that it was difficult to estimate the unbounded area for the samples with a artificially prepared surface, and some uncertainty must be added to the results from this plot.

A similar box-plot comparing the nominal freeze-bond strength for the horizontal samples is shown in figure 4.10. Two configurations with a Artificially

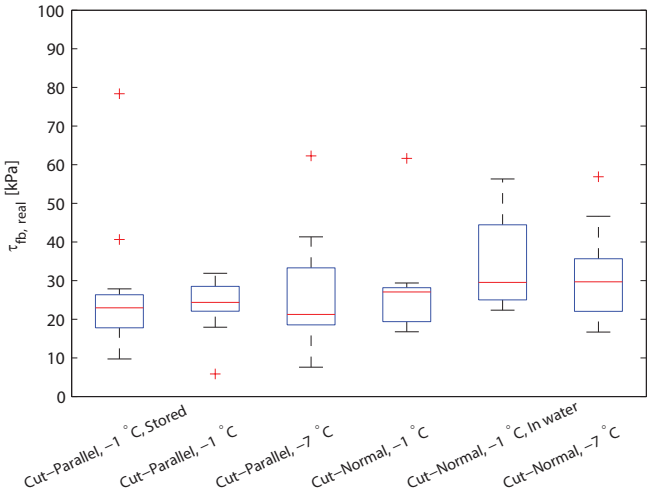

Figure 4.9: Box-plot of the real freeze-bond strength ($\tau_{fb,real}$) for the vertical "Ice 1" samples.

prepared contact surface were used for the horizontal samples. These were equal, except that one configuration was assembled "In air" and the other "In water". A significant difference was seen between these configurations, as for the vertical samples. The "In water" samples had 1.87 times the nominal freeze-bond strength of the "In air" samples. The "Bottom" surface samples assembled "In air" had a freeze-bond strength in the range of the samples with a artificial surface assembled "In water". Fewer samples, five and six, was tested for the "Bottom" configurations. This makes it difficult to obtain good statistics for these configurations. As for the vertical samples, the difference between the "In air" and "In water" samples were reduced when comparing the real freeze-bond strength, but the majority of the "In air" samples were still weaker than the "In water" samples. The "In water" samples were 1.28 times stronger than the "In air" samples when comparing the real freeze-bond strength. Due to small unbounded areas, only minor differences were seen between the nominal and real freeze-bond strength for the "In water" and "Bottom" configurations, see figure 4.11.

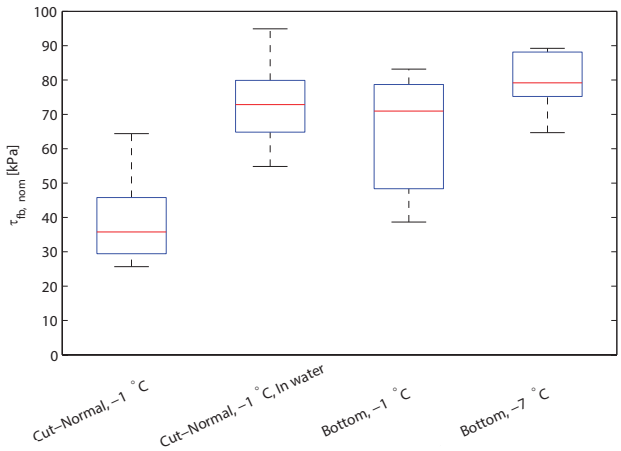

Figure 4.10: Box-plot of the nominal freeze-bond strength ($\tau_{fb,nom}$) for the horizontal "Ice 1" samples.

Both vertical and horizontal samples were made for the configurations "Cut-Normal, −1 °C" and "Cut-Normal, −1 °C, In-water". These samples showed that there was a significant difference in the freeze-bond strength related to

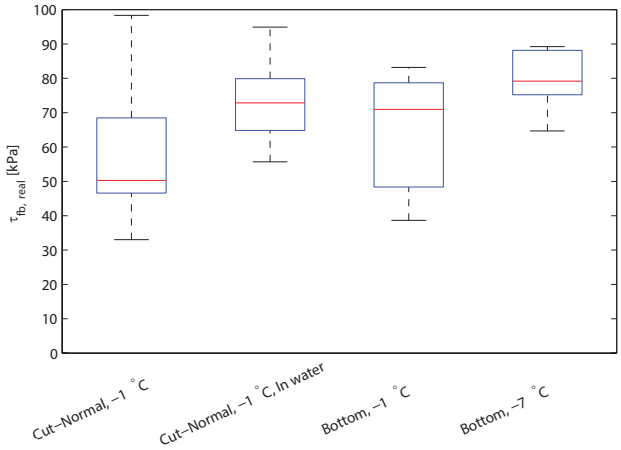

Figure 4.11: Box-plot of the real freeze-bond strength ($\tau_{fb,real}$) for the horizontal "Ice 1" samples.

the ice-block orientation. The horizontal "Cut-Normal, −1 °C" samples was in average 2.2 times stronger than the vertical samples. For the "Cut-Normal, −1 °C, In-water" samples the corresponding ratio between the horizontal and vertical samples were 2.1 times. Both the mentioned ratios were for the nominal freeze-bond strength, corresponding ratios for the real freeze-bond strength were 2.1 for both configurations .

4.2.5.2 Freeze-bond strength vs. ice-sheet - Ice 1, 2 and 3 samples

A box-plot comparing the nominal freeze-bond strength of Ice 1, 2 and 3 for the "Vertical, Cut-Normal, −1 °C" and the "Horizontal, Cut-Normal, −1 °C" samples are seen in figure 4.12. This plot shows that the freeze-bond strength varies between the three ice-sheets, within a configuration. Ice 1 samples yielded the highest freeze-bond strength, both in average and maximum obtained values. This was the case for all four configurations were more than one ice-sheet were applied. A point-plot showing the nominal freeze-bond strength for the four configurations is presented in figure 4.22, and statistical parameters are found in table 4.7.

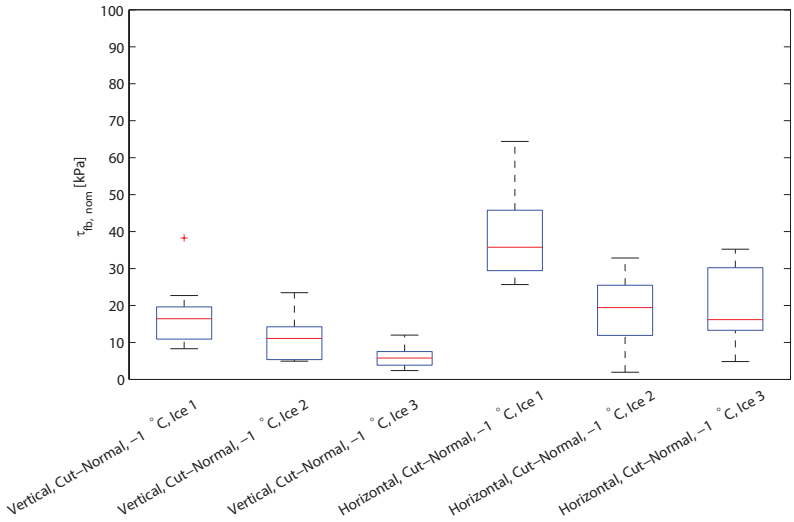

Figure 4.12: Box-plot of the nominal freeze-bond strength ($\tau_{fb,nom}$) for the "Cut-Normal -1 °C" samples for both ice-block directions. Divided after applied ice sheet.

The visual appearance of the ice-blocks have been related to the freeze-bond strength. Ice 1, had as described in section 4.2.2, a organised crystal structure and smaller crystals than Ice 2 and 3. Visible brine channels were seen at the surface of the Ice 1 samples. For horizontal samples the short end of the brine channels were seen at the contact surface. Vertical samples had the brine channels parallel with the longitudinal ice-block direction. Such a classification according to the brine-channel direction was not possible for Ice 2 and 3, and horizontal and vertical ice-blocks could not be distinguished visually.

Large visual differences were seen within the samples from Ice 2 and 3. Transparent ice-blocks, i.e. few brine channels and a low salinity before submersion, yielded the lowest freeze-bond strengths. One of the highly transparent Ice 2 samples had such a low freeze-bond strength that the freeze-bond failed during assembling in the test frame. Higher freeze-bond strengths were obtained if the ice-blocks were opaque, i.e. visible brine channels and a higher salinity before submersion. The intention was to test a wide range of ice-blocks according to the visual appearance. But with only few samples (five to six) per ice-sheet and configuration, it was difficult to obtain good statistics due to the large variations connected to physical differences in the ice-blocks.

Figure 4.13 relates the average nominal freeze-bond strength and the average ice-block salinity after submersion for the three ice-sheets. The "Vertical, Cut-Parallel, -1 °C", "Vertical, Cut-Normal, -1 °C" and "Horizontal, Cut-Normal, -1 °C" configurations were used in this comparison. Different marker types are used to point out the test configurations, while colours are used to distinguish between Ice 1, 2 and 3 samples. This plot shows in general that the lowest freeze-bond strengths were obtained for the samples with lowest salinity after submersion. It may also seem like the "Vertical, Cut-Parallel, -1 °C" and "Vertical, Cut-Normal, -1 °C" configurations has a relatively equal salinity - freeze-bond strength relationship. The salinity - freeze-bond strength relationship is ambiguous for the "Horizontal, Cut-Normal, -1 °C" configuration, but the sample with the highest salinity had the highest freeze-bond strength.

Very different freeze-bond strengths was obtained for the Ice 1 and Ice 3 samples within the "Horizontal, Bottom, -1 °C" configuration. Ice 1 samples had an average nominal freeze-bond strength of 65.1 kPa ($\tau_{fb,real,mean} = 66.7$ kPa), while the Ice 3 samples had an average nominal freeze-bond strength of 14.0 kPa ($\tau_{fb,real,mean} = 14.0$ kPa). A more or less even contact between the ice-blocks from Ice 1 was obtained during assembling. The ice-blocks from Ice 3 were unstable and the top block was rocking against the lower block during assembling.

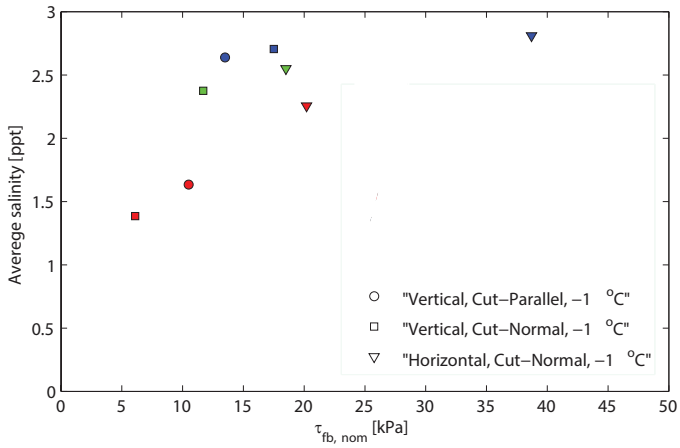

Figure 4.13: Scatter diagram of the average nominal freeze-bond strength and average joint ice-block salinity after submersion for both ice-blocks forming the freeze-bond for the "Vertical, Cut-Parallel, $-1\ ^{\circ}$C" (circular marker), "Vertical, Cut-Normal, $-1\ ^{\circ}$C" (squared marker) and "Horizontal, Cut-Normal, $-1\ ^{\circ}$C" (triangular marker) configurations. The different ice-sheets are indicated by colours: Ice 1: blue, Ice 2: green and Ice 3: red.

4.2.5.3 Freeze-bond strength vs. test series - Ice 1 samples

Figure 4.23 shows a point-plot comparing the freeze-bond strength of the different test series within a test configuration for the Ice 1 samples. Statistics of each test series are presented table 4.8. The average nominal freeze-bond strength is somewhat different for the different series within a configuration. For some configurations the range in obtained freeze-bond strength varied less within a series than within the whole configuration, no clear trends were found.

4.3 HSVA-experiments

4.3.1 Physical properties of the ice used in the HSVA-experiments

The ice-blocks used in the HSVA-experiments were homogeneous and had uniform physical properties, with a salinity of 1.8 to 2.2 ppt before submersion. Lowest salinity was measured for the "NTNU-frame, Bottom" samples, although the measured differences were small. The top-surface ice-blocks had clearly the most even surface. The temperature, density and salinity of the ice-blocks utilised to form freeze-bonds are presented in table 4.3.

Table 4.3: Temperature, density and salinity of tested ice-blocks before submersion for the HSVA-experiments.

Series	Configuration		ρ_i [kg/m^3]	S [ppt]	T [°C]	m [g]	Dimensions [mm] L	W	H
100	NTNU-frame,	Top	889	2.1		72.0	90.0	40.0	22.5
	NTNU-frame,	Bottom	854	1.9		41.0	60.0	40.0	20.0
200	NTNU-frame,	Top	880	2.1	-6.2	70.0	88.0	41.5	21.8
	NTNU-frame,	Bottom	860	1.8	-5.6	65.0	90.0	39.8	21.1
	HSVA-frame		825	2.1	-6.7	560.0	179.5	140.0	27.0
	HSVA-frame		845	2.2	-6.5	446.0	141.0	140.0	26.8
300	HSVA-frame,	Stored		2.0					

4.3.2 Texture of freeze-bonded samples

A columnar crystal structure with the crystals aligned perpendicular to the freeze-bonded surface was seen for the bottom surface samples. The top surface samples had a granular crystal structure at the freeze-bonding surface. Equal crystal structures may be expected to have been present for all the prepared samples. This is due to the uniform ice properties seen within the prepared ice-blocks and thin sections. A picture of the "NTNU-frame, Top" thin section and a one part of the "HSVA-frame" thin section is seen in figure 4.14. It was not possible to detect any differences in the void content between the samples from the thin sections.

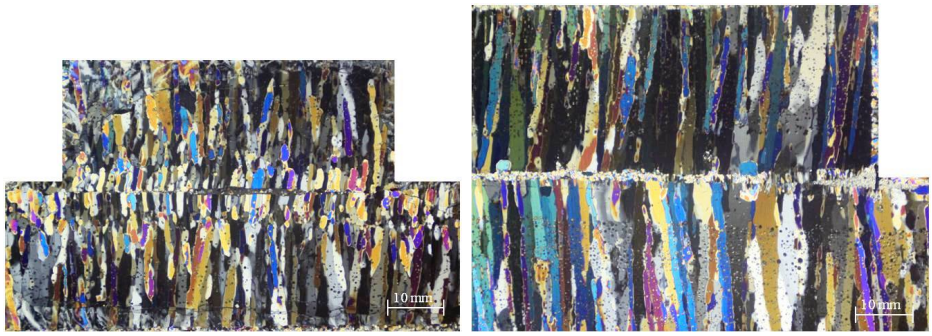

(a) NTNU-frame, Top sample **(b)** HSVA-frame, Part II

Figure 4.14: Examples of thin sections from the HSVA-experiments.

Gaps were present between the two freeze-bonding surfaces for the prepared thin sections. A gap extending over a small part of the freeze-bond was seen for the two NTNU-frame thin sections, see figure 4.15a and 4.15c. Perfect contact between the surfaces was seen for the remaining parts of the freeze-bond. A gap filled with re-frozen ice was seen over the entire width of the freeze-bond for the HSVA-frame thin section. This implies that it seems like the freeze-bond had a thickness of around 2 mm for this sample, see 4.15b and 4.15d.

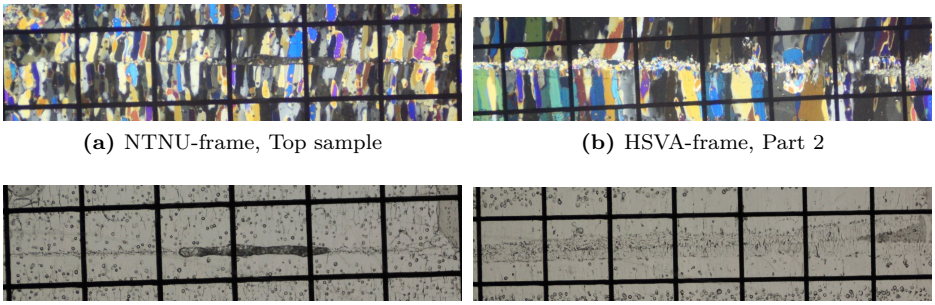

(a) NTNU-frame, Top sample **(b)** HSVA-frame, Part 2

(c) NTNU-frame, Top sample **(d)** HSVA-frame, Part 2

Figure 4.15: Segments of the freeze-bond thin sections from the HSVA-experiments showing gapes found in the freeze-bond. The grid size is 10 by 10 mm.

4.3.3 Ice-block salinity after submersion

There were no noteworthy differences in the salinity content of the ice-blocks from the different configurations after strength testing. A plot showing the spread of the upper and lower ice-block salinity for each configuration is seen in figure 4.16. The salinity content was highest in the lower ice-block for 38 of the 40 samples (95%). Statistical parameters for each configuration are found in table 4.4. The range of the measured salinities varied between 2.1 and 3.3 ppt.

Table 4.4: Statistics of the ice-block salinity (S) after strength testing for the upper ice-block (S_u) and lower ice-block (S_l) for the HSVA-experiments.

Configuration		Number of samples	S_u [ppt] Mean	Std	Max	Min	S_l [ppt] Mean	Std	Max	Min
NTNU-frame,	Top	12[a]	2.7	0.1	2.8	2.6	3.0	0.2	3.3	2.7
NTNU-frame,	Bottom	11	2.4	0.1	2.6	2.1	2.8	0.1	3.0	2.6
HSVA-frame,		11	2.5	0.1	2.7	2.4	2.7	0.1	2.8	2.6
HSVA-frame,	Stored	6	2.4	0.1	2.5	2.3	2.6	0.1	2.7	2.5

[a] S_l consists of 11 samples.

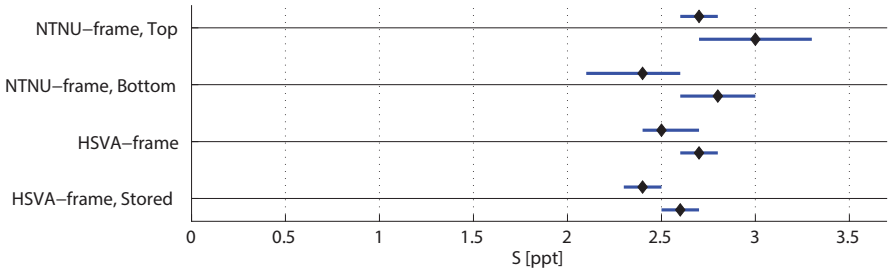

Figure 4.16: Salinity (S) of the upper ice-block (S_u) (above the line) and the lower ice-block (S_l) (below the line) for the HSVA-experiments. Divided after test configuration. The black mark indicates the average ice-block salinity while the error bars shows the maximum and minimum ice-block salinity.

4.3.4 Freeze-bonded area

Pictures of the fractured surfaces have been used to estimate the freeze-bonded area. Examples of these pictures are seen in figure 4.17. In general the unbounded areas were small, but the "NTNU-frame, Top" configuration had the clearly largest unbounded areas for this set of experiments. A random orientation and shape was seen for all the unbounded areas. Statistical parameters for each configuration are presented in table 4.5.

Table 4.5: Statistics of the unbounded area (A_{ub}) for the HSVA-experiments.

Configuration		Number of samples	A_{ub} [%] Mean	Std	Max	Min
NTNU-frame,	Top	12	10	11	41	0
NTNU-frame,	Bottom	12	2	5	17	0
HSVA-frame,		11	4	5	15	0
HSVA-frame,	Stored	6	3	4	11	0

4.3.5 Freeze-bond strength

Examples of stress - displacement plots are shown in figure 4.18, and equal plots for each test is found in appendix D. Plotted displacement for the two

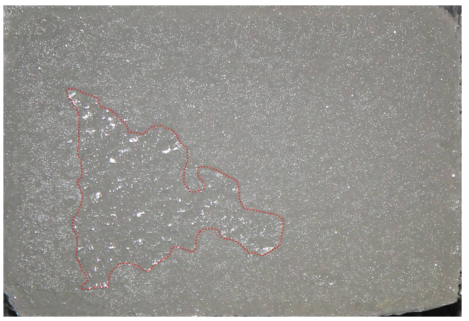

(a) Sample 102, "NTNU-frame, Top", $A_{ub} = 17\%$

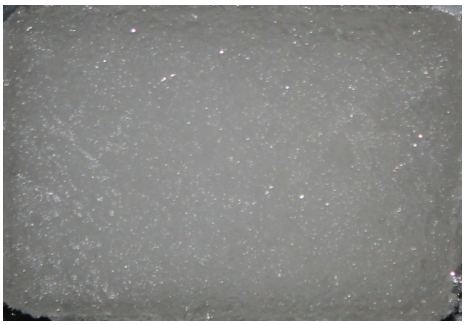

(b) Sample 107, "NTNU-frame, Bottom", $A_{ub} = 0\%$

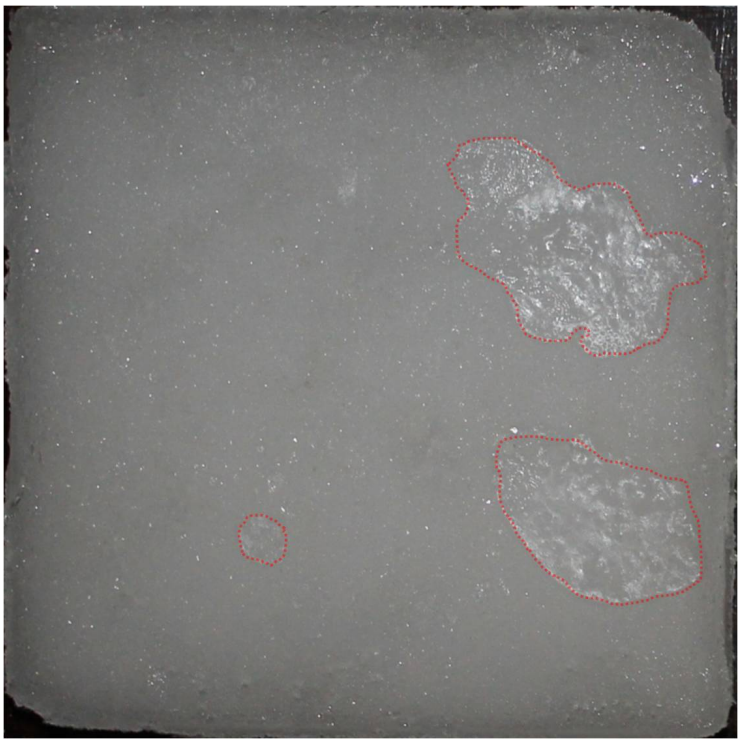

(c) Sample 301, "HSVA-frame, Stored", $A_{ub} = 11\%$

Figure 4.17: Pictures of fractured surfaces from the HSVA-experiments, the unbounded area (A_{ub}) is marked by a red line.

configurations using the NTNU-frame are 3 mm. Samples from the HSVA-frame configurations are plotted over a displacement of 10 mm. This was necessary in order to include the whole stress - displacement curves. Movements in the frame and possible larger deformations of the ice-blocks were found as reasons for this large increase in deformation before freeze-bond fracture. Visible movements of the freeze-bonded sample, sliding of the lid in both the vertical and horizontal direction and deformations of the lid at the connection point for the pulling system were seen. The top-block was often seen to make a jump when the freeze-bond fractured. This jump was largest for the strongest samples.

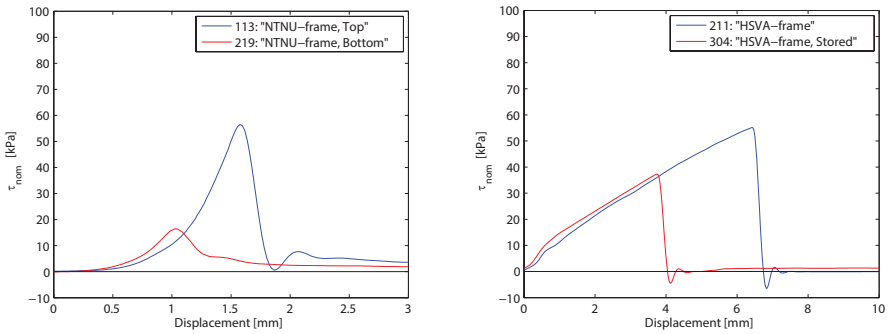

(a) NTNU-frame size samples, Sample 133 and 219.

(b) HSVA-frame size samples, Sample 211 and 304.

Figure 4.18: Examples of stress - displacement plots for the HSVA-experiments.

4.3.5.1 Freeze-bond strength vs. test configuration

A box-plot comparing the nominal freeze-bond strength for the four test configurations is presented in figure 4.19. Highest freeze-bond strengths were found for the "NTNU-frame, Top" configuration. This configuration had in average 1.5 times stronger freeze-bonds than the "NTNU-frame, Bottom" configuration. The difference between these configurations was, as seen in figure 4.24, significant. In real freeze-bond strength was the corresponding ratio 1.6 times. A point-plot of the nominal freeze-bond strengths for the four test configurations is seen in figure 4.24. The mean values with 95% confidence limits are indicated above each configuration. Statistical parameters are presented in table 4.9.

Only minor differences were seen between the two configurations using the HSVA-frame. It should be noticed that only six samples were tested for the "HSVA-frame, Stored" configuration. Close to equal freeze-bond strengths were obtained for the two HSVA-frame configurations and the "NTNU-frame, Bottom" configuration. The bottom surface was utilised as a common contact surface for these three configurations. Average nominal freeze-bond strength for these configurations were 30.67, 29.75 and 32.89 kPa.

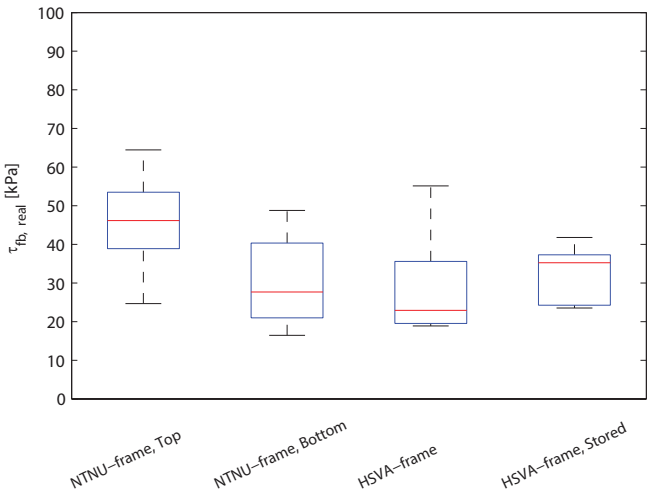

Figure 4.19: Box-plot of the nominal freeze-bond strength ($\tau_{fb,nom}$) for the HSVA-experiments ("HSVA-frame" samples all bottom surfaces).

4.3.5.2 Freeze-bond strength vs. test series

No particular differences were seen between the freeze-bond strength for the different test series. This assessment was done for the two NTNU-frame configurations, which were the only tested in several series. Freeze-bond strength measurements for the two series are seen in figure 4.25, and statistical parameters are found in table 4.9.

4.3.5.3 Failure mode for the HSVA-frame samples

A vertical fracture of the lower ice-block occurred for two of the 200 series samples and for one of the 300 series samples. The lower ice-block fractured around 30 to 50 mm from the rear end of the upper ice-block. Examples are seen in figure 4.20. The lid was pushed down at the rear end of the lid by hand during strength testing for the 300 series sample. No extra pressure was added for the two 200 series samples. Converted to nominal freeze-bond strength, the fracture force of the 300 series sample equalled a freeze-bond strength of 40.5 kPa.

A considerable pressure was added by hand to the rear end of the lid for the strongest samples, which failed in shear at the freeze-bonded surface. This was done for sample 209 and 211 ($\tau_{fb,nom} = 51.12$ and 55.15 kPa) and sample 301 ($\tau_{fb,nom} = 41.80$ kPa). Adding this pressure might have prevented these samples from failing with a vertical fracture of the lower ice-block.

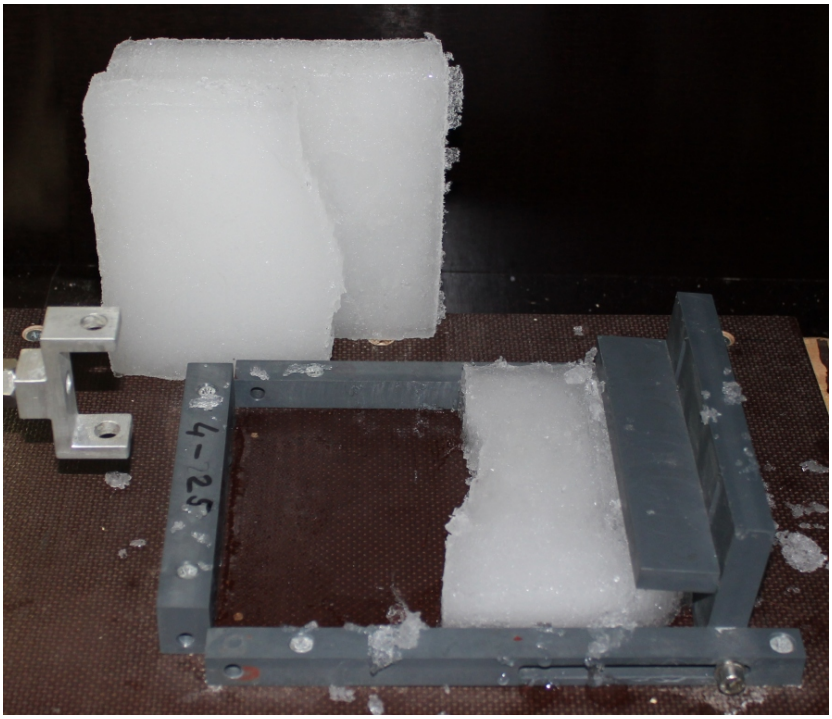

(a) Sample 200

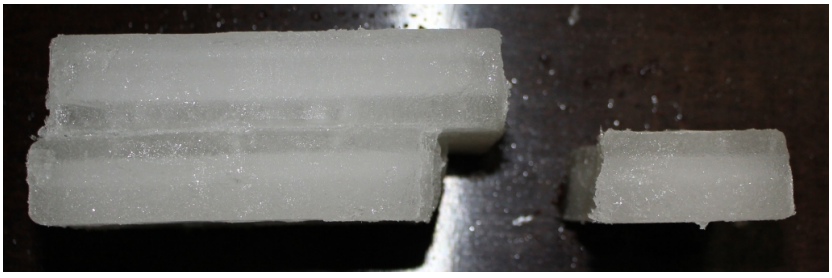

(b) Sample 300

Figure 4.20: Vertical failure of the lower ice-block for the HSVA-frame samples.

Table 4.6: Statistics of the ice-block salinity (S) after strength testing for the upper ice-block (S_u), lower ice-block (S_l) and the combined salinity of both ice-blocks (S_{tot}) for the NTNU-experiments.

Configuration				Number of samples	S_u [ppt] Mean	Std	Max	Min	S_l [ppt] Mean	Std	Max	Min	S_{tot} [ppt] Mean
Vertical,	Cut-Parallel,	−1 °C, Stored	Ice 1	11	2.72	0.10	2.92	2.58	3.04	0.16	3.43	2.82	2.88
Vertical,	Cut-Parallel,	−1 °C	Ice 1	11	2.51	0.25	2.96	2.09	2.77	0.27	3.26	2.45	2.93
			Ice 3	5	1.58	0.72	2.63	1.01	1.69	0.22	2.02	1.46	1.63
Vertical,	Cut-Parallel,	−7 °C	Ice 1	10[a]	2.51	0.29	3.03	2.18	2.99	0.31	3.77	2.73	2.81
Vertical,	Cut-Normal,	−1 °C	Ice 1	12	2.56	0.25	3.01	2.16	2.85	0.25	3.18	2.45	2.74
			Ice 2	6	2.33	0.15	2.47	2.07	2.42	0.29	2.65	1.88	2.34
			Ice 3	5[b]	1.02	0.08	1.10	0.91	1.75	0.11	1.89	1.65	1.48
Vertical,	Cut-Normal,	−1 °C, In water	Ice 1	12	2.77	0.17	3.05	2.55	3.00	0.18	3.32	2.66	2.89
Vertical,	Cut-Normal,	−7 °C	Ice 1	10	2.68	0.34	3.03	2.02	2.88	0.27	3.19	2.44	2.80
Horizontal,	Cut-Normal,	−1 °C	Ice 1	11	2.57	0.21	2.90	2.34	3.05	0.10	3.19	2.81	2.85
			Ice 2	6[c]	2.36	0.63	2.90	1.34	2.48	0.71	3.04	1.47	2.56
			Ice 3	5	2.56	0.34	2.87	2.04	1.95	0.42	2.44	1.41	2.17
Horizontal,	Cut-Normal,	−1 °C, In water	Ice 1	12	2.77	0.25	3.22	2.37	3.03	0.25	3.36	2.50	2.86
Horizontal,	Bottom,	−1 °C	Ice 1	6	3.14	0.16	3.39	2.98	3.27	0.17	3.54	3.10	3.19
			Ice 3	7	2.90	0.32	3.23	2.47	2.12	0.66	3.14	1.50	2.42
Horizontal,	Bottom,	−7 °C	Ice 1	5	2.67	0.21	2.96	2.47	3.02	0.41	3.70	2.60	2.83

[a] S_u consists of 9 samples.
[b] S_{tot} consists of 4 samples.
[c] S_{tot} consists of 5 samples.

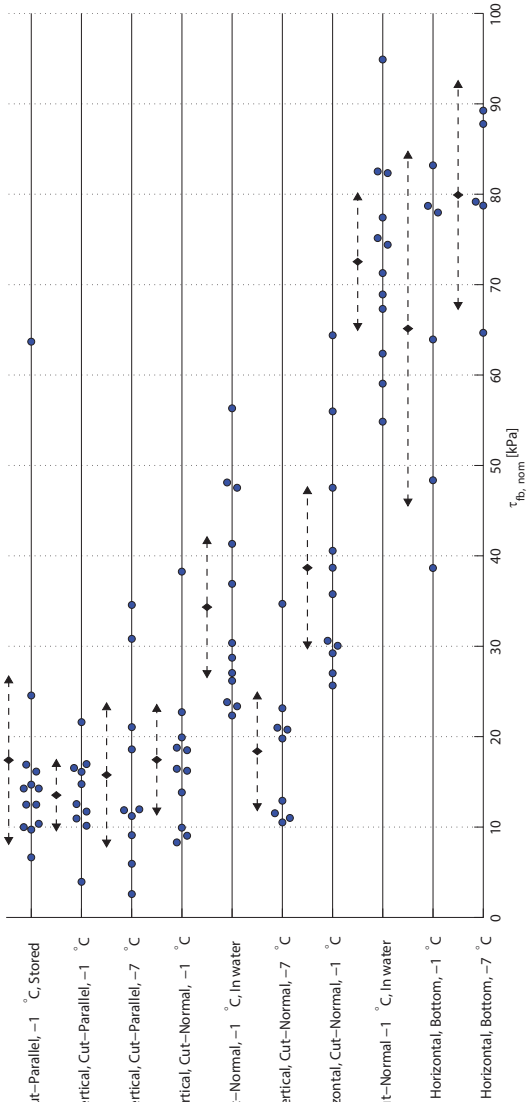

Figure 4.21: Point-plot of the nominal freeze-bond strength ($\tau_{fb,nom}$) for "Ice 1", grouped after test configuration for the NTNU-experiments. Average nominal freeze-bond strength, with 95% confidence limits are indicated in black above each configuration. To avoid overlapping are data points located above and below the line.

Table 4.7: Statistics of the nominal and real freeze-bond strength (τ_{fb}) grouped after test configuration for the NTNU-experiments. Both separate and joint statistics are presented for the test configurations were more than one ice-sheet was applied.

Configuration				Number of samples	$\tau_{fb,nom}$ [kPa] Mean	Std	Max	Min	$\tau_{fb,real}$ [kPa] Mean	Std	Max	Min	A_{ub} [%] Mean
Vertical,	Cut-Parallel,	−1 °C, Stored	Ice 1	13	17.4	14.6	63.7	6.7	26.1	17.5	78.4	9.7	35
Vertical,	Cut-Parallel,	−1 °C	Joint	15	12.5	5.7	21.6	3.2	23.3	11.0	47.7	5.8	45
			Ice 1	10	13.5	4.8	21.6	3.9	23.5	7.6	31.9	5.8	42
			Ice 3	5	10.5	7.3	19.9	3.2	23.0	17.1	47.7	7.9	52
Vertical,	Cut-Parallel,	−7 °C	Ice 1	10	15.8	10.5	34.6	2.6	26.2	16.1	62.3	7.6	42
Vertical,	Cut-Normal,	−1 °C	Joint	22	13.3	8.3	38.3	2.4	21.0	12.5	61.6	3.3	37
			Ice 1	11	17.5	8.4	38.3	8.3	27.4	12.3	61.6	16.8	37
			Ice 2	6	11.7	7.0	23.5	4.9	17.9	10.5	35.7	7.5	35
			Ice 3	5	6.1	3.6	12.0	2.4	10.5	6.5	21.0	3.3	39
Vertical,	Cut-Normal,	−1 °C, In water	Ice 1	12	34.3	11.5	56.3	22.3	34.3	11.5	56.3	22.3	0
Vertical,	Cut-Normal,	−7 °C	Ice 1	9	18.4	7.9	34.7	10.5	31.0	13.2	56.9	16.7	40
Horizontal,	Cut-Normal,	−1 °C	Joint	21	29.5	15.2	64.4	1.9	42.5	22.7	98.3	3.5	31
			Ice 1	11	38.7	12.6	64.4	25.7	56.6	19.6	98.3	33.0	31
			Ice 2	5	18.5	11.3	32.8	1.9	26.5	15.3	46.1	3.5	33
			Ice 3	5	20.2	11.9	35.3	4.8	27.3	15.1	43.9	9.1	28
Horizontal,	Cut-Normal,	−1 °C, In water	Ice 1	12	72.5	11.1	94.9	54.8	72.6	11.0	94.9	55.7	0.1
Horizontal,	Bottom,	−1 °C	Joint	13	37.6	29.7	83.2	6.7	38.3	30.1	83.2	6.7	1
			Ice 1	6	65.1	18.2	83.2	38.7	66.7	17.9	83.2	44.6	3
			Ice 3	7	14.0	8.6	27.5	6.7	14.0	8.6	27.8	6.7	0.1
Horizontal,	Bottom,	−7 °C	Ice 1	5	79.9	9.8	89.2	64.7	84.3	4.5	89.9	79.2	5

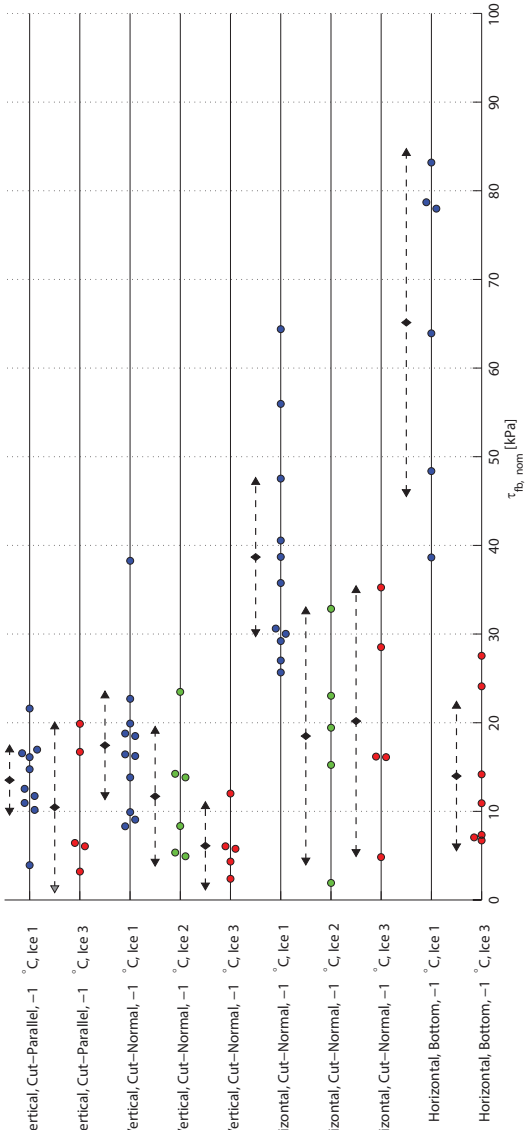

Figure 4.22: Point-plot of the nominal freeze-bond strength ($\tau_{fb,nom}$) for the NTNU-experiments. Grouped after applied ice-sheet and test configuration. Average nominal freeze-bond strength, with 95% confidence limits are indicated in black above each configuration. To avoid overlapping are data points located above and below the line, Ice 1: blue, Ice 2: green and Ice 3: red.

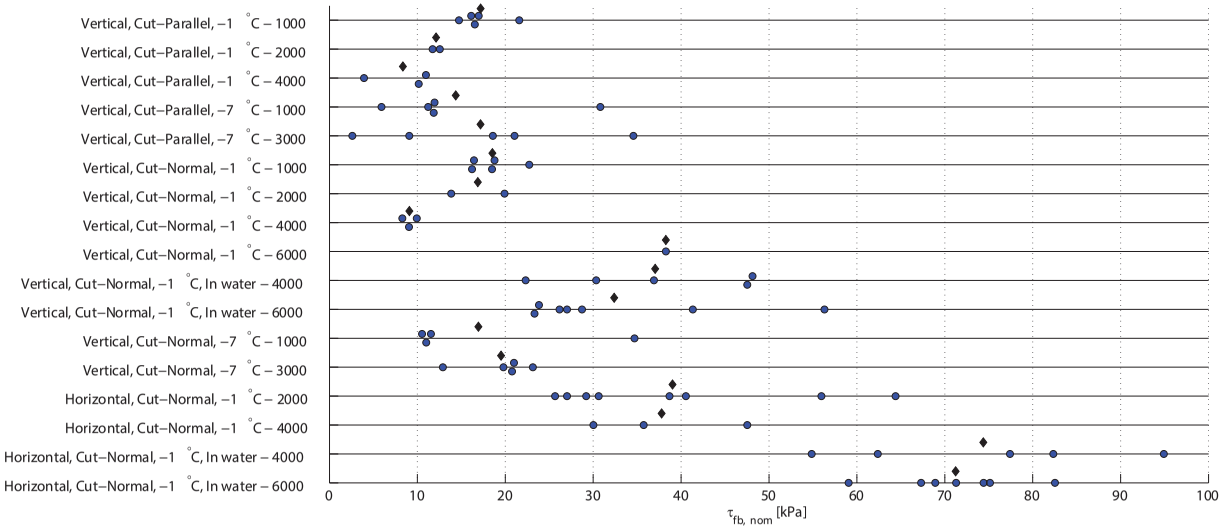

Figure 4.23: Point-plot of the nominal freeze-bond strength ($\tau_{fb,nom}$) for the NTNU-experiments. Grouped after test configuration and series. Average nominal freeze-bond strength is marked in black above each data series. To avoid overlapping are data points located above and below the line.

Table 4.8: Statistics of the nominal and real freeze-bond strength (τ_{fb}) grouped after test configuration and series for the NTNU-experiments.

Configuration			Series	Number of samples	$\tau_{fb,nom}$ [kPa] Mean	Std	Max	Min	$\tau_{fb,real}$ [kPa] Mean	Std	Max	Min	A_{ub} [%] Mean
Vertical,	Cut-Parallel,	−1 °C	1000	5	17.2	2.6	21.6	14.8	26.9	4.65	31.9	22.1	36
			2000	2	12.1	0.6	12.5	11.7	25.8	3.9	28.5	23.0	53
			4000	3	8.4	3.9	11.0	3.9	16.3	9.8	25.1	5.8	44
Vertical,	Cut-Parallel,	−7 °C	1000	5	14.4	9.5	30.8	5.9	20.1	8.1	33.3	11.0	33
			3000	5	17.2	12.2	34.6	2,6	32.3	20.6	62.3	7.6	50
Vertical,	Cut-Normal,	−1 °C	1000	5	18.5	2.6	22.7	16.2	27.2	0.9	28.5	26.0	32
			2000	2	16.9	4.3	19.9	13.8	25.4	5.6	29.4	21.5	34
			4000	3	9.1	0.8	9.9	8.3	17.7	1.0	18.7	16.8	48
			6000	1	38.3		38.3	38.3	61.6		61.6	61.6	38
Vertical,	Cut-Normal,	−1 °C, In water	4000	5	37.1	11.1	48.1	22.3	37.1	11.1	48.1	22.3	0
			6000	7	32.4	12.2	56.3	23.3	32.4	12.2	56.3	23.3	0
Vertical,	Cut-Normal,	−7 °C	1000	4	16.9	11.9	34.7	10,5	29.2	18.9	56.9	16.7	42
			3000	5	19.5	3.9	23.1	12.9	32.5	8.5	46.6	23.6	39
Horizontal,	Cut-Normal,	−1 °C	2000	8	39.0	14.3	64.4	25.7	55.4	21.2	98.3	33.0	29
			4000	3	37.8	8.9	47.5	30.0	60.0	18.1	80.9	48.8	36
Horizontal,	Cut-Normal,	−1 °C, In water	4000	5	74.4	16.0	94.9	54.8	74.6	15.7	94.9	55,7	0,3
			6000	7	71.2	7.3	82.5	59.0	71.2	7.3	82.5	59.0	0

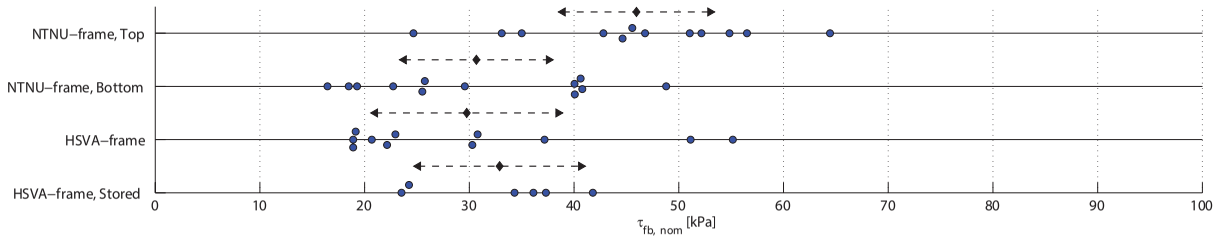

Figure 4.24: Point-plot of nominal freeze-bond strength ($\tau_{fb,nom}$) for the HSVA-experiments, grouped after test configuration. Average nominal freeze-bond strength with 95% confidence limits are indicated in black above each configuration.

Table 4.9: Statistics of the nominal ($\tau_{fb,nom}$) and the real ($\tau_{fb,real}$) freeze-bond strength for the HSVA-experiments, grouped after test configuration and series.

Configuration		Series	Number of samples	$\tau_{fb,nom}$ [kPa] Mean	Std	Max	$\tau_{fb,real}$ [kPa] Min	Mean	Std	Max	Min	A_{ub} [%] Mean
NTNU-frame,	Top	Joint	12	46.0	11.1	64.5	24.7	50.7	10.8	69.7	25.4	10
		100	7	43.2	10.7	56.5	24.7	46.4	11.1	56.5	25.4	7
		200	5	49.8	11.6	64.5	33.1	56.7	7.7	69.7	49.0	12
NTNU-frame,	Bottom	Joint	12	30.7	10.9	48.8	16.5	31.6	11.8	50.0	16.5	2
		100	7	33.8	11.4	48.8	18.5	34.0	11.7	50.0	18.5	0.6
		200	5	26.3	9.5	40.6	16.5	28.3	12.5	48.8	16.5	5
HSVA-frame		200	11	29.8	13.0	55.2	18.9	30.8	12.7	55.7	19.0	4
HSVA-frame,	Stored	300	6	32.9	7.4	41.8	23.5	34.2	8.8	47.1	23.6	3

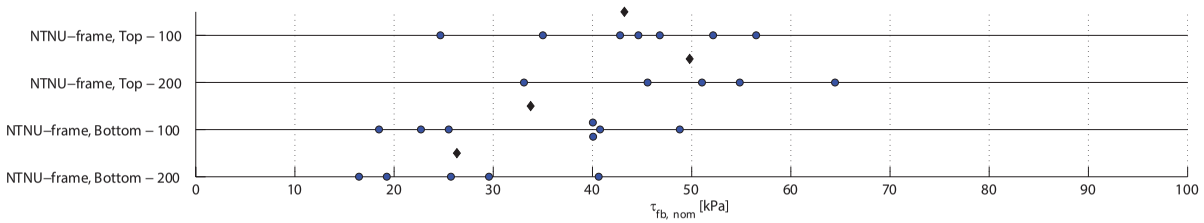

Figure 4.25: Point-plot of nominal freeze-bond strength ($\tau_{fb,nom}$) for the HSVA-experiments, grouped after test series. Average nominal freeze-bond strength is marked in black above each data series. To avoid overlapping are data points located above and below the line.

Chapter 5

Discussion

5.1 Introduction

A discussion of the results is presented in this chapter. Section 5.2 evaluates how the 14 test configurations have affected the freeze-bond strength. In general Ice 1 samples from the NTNU-experiments and all samples from the HSVA-experiments are used in this evaluation. Comments are in addition made to the results of Helgøy (2011). The following section, section 5.3, discuss the reproducibility of the results from Repetto-Llamazares et al. (2011a) and Repetto-Llamazares and Høyland (2011a). In section 5.4 an assessment of the coherence between the surface roughness and unbounded area is presented. This is followed by section 5.5 where a discussion of how the physical properties of the ice-blocks affect the freeze-bond strength is presented. The last section of this chapter, 5.6, evaluates the test set-up and gives general remarks on uncertainties related to our experiments.

5.2 Freeze-bond strength vs. test configuration

Equivalent freeze-bond strengths were obtained for a number of the applied test configurations, see section 4.2.5 and 4.3.5. The following list summarises the factors which are found to have, and not to have an effect on the freeze-bond

strength. This list are made on the basis of Ice 1 samples from the NTNU-experiments and all HSVA samples.

Factors which ***did*** have an effect on the freeze-bond strength:

- Ice-block direction; "Vertical" and "Horizontal" ice-blocks.
- Assembling conditions; "In air" and "In water".
- Contact surface; artificially produced and natural top or bottom of the ice-sheet.

Factors which ***did not*** have an effect on the freeze-bond strength:

- Sawing direction of the contact surface; "Cut-Normal" and "Cut-Parallel".
- Time - temperature history of the ice-blocks.
- Ambient air temperature of the submersion basin; -1 °C and -7 °C.
- Sample dimensions; Small "NTNU-frame" ($A_{fb} = 24\,\mathrm{cm}^2$) and Large "HSVA-frame" samples ($A_{fb} = 196\,\mathrm{cm}^2$).

A further discussion of the above mentioned points follows in the remaining parts of this section. As an implication of the listed similarities it has been found convenient to merge test configurations into new groups. From the NTNU-experiments the following five Ice 1 configurations are merged into the group "Vertical, In air - *New*":

"Vertical, Cut-Parallel, -1 °C, Stored,", "Vertical, Cut-Parallel, -1 °C", "Vertical, Cut-Parallel, -7 °C", "Vertical, Cut-Normal, -1 °C" and "Vertical, Cut-Normal, -7 °C".

In addition the Ice 1 bottom surface configurations are merged into the group "Horizontal, Bottom - *New*". This applies to the configurations:

"Horizontal, Bottom, -1 °C" and "Horizontal, Bottom, -7 °C".

From the HSVA-experiments the following three configurations are merged into the group "HSVA, Bottom - *New*":

"HSVA-frame", "HSVA-frame, Stored" and "NTNU-frame, Bottom".

A box-plot comparing the three new and the four original configurations are presented in figure 5.1. Statistical parameters of all of these groups are in addition presented in table 5.1.

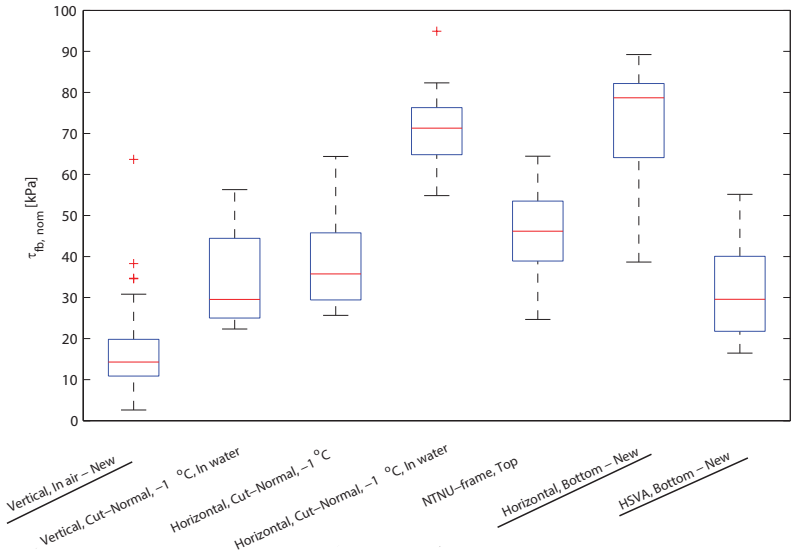

Figure 5.1: Box-plot of the nominal freeze-bond strength ($\tau_{fb,nom}$) for the three new and four original configurations. Includes Ice 1 samples from the NTNU-experiments and all HSVA samples.

Table 5.1: Summary of the nominal freeze-bond strength ($\tau_{fb,nom}$) for the three new and four original configurations. Includes Ice 1 samples from the NTNU-experiments and all HSVA samples.

Configuration		Number of samples	$\tau_{fb,nom}$ [kPa] Mean	Std	Max	Min
Vertical,	In air - *New*	53	16.5	9.9	63.7	2.6
Vertical,	Cut-Normall, −1 °C, In water	12	34.3	11.5	56.3	22.3
Horizontal,	Cut-Normall, −1 °C	11	38.7	12.6	64.4	25.7
Horizontal,	Cut-Normall, −1 °C, In water	12	72.5	11.1	94.9	54.8
NTNU-frame,	Top	12	46.0	11.1	64.5	24.7
Horizontal,	Bottom - *New*	11	71.9	16.2	89.2	38.7
HSVA,	Bottom - *New*	29	30.8	10.9	55.2	16.5

5.2.1 Vertical and Horizontal ice-blocks

"Vertical" and "Horizontal" ice-blocks were used in the NTNU-experiments, see figure 3.3. The results clearly showed that the horizontal ice-blocks yielded the highest freeze-bond strengths, with an average of two times stronger freeze-bonds than for the vertical ice-blocks, see table 5.2. Vertical Ice 1 ice-blocks had the columnar crystals aligned parallel with the freeze-bond, and horizontal Ice 1 ice-blocks had the columnar crystals aligned normal to the freeze-bond. No previous description of this phenomenon is known, and we suggest that the alignment of the brine channels is an important factor in explaining this phenomenon. The brine channels are considered important in relation to two factors. Firstly in relation to the permeability of the ice-blocks, and secondly in relation to the adhesive strength between the ice formed in the freeze-bond and the ice in the surrounding surfaces.

Table 5.2: Summary of the nominal freeze-bond strength ($\tau_{fb,nom}$) for the horizontal and vertical Ice 1 samples with an artificially prepared contact surface from the NTNU-experiments.

Configuration			Number of samples	$\tau_{fb,nom}$ [kPa] Mean	Std	Max	Min
Vertical,	In air		53	16.5	9.9	63.7	2.6
Horizontal,	Cut-Normal,	−1 °C	11	38.7	12.6	64.4	25.7
Vertical,	Cut-Normal,	−1 °C, In water	12	34.3	11.5	56.3	22.3
Horizontal,	Cut-Normal,	−1 °C, In water	12	72.5	11.1	94.9	54.8

Brine is expelled when ice is formed in the freeze-bond. This brine has two possibilities to drain, horizontally along the freeze-bonded surface or vertically through the surrounding ice-blocks. Higher brine drainage is assumed to result in stronger freeze-bonds. The brine channels of the horizontal Ice 1 ice-blocks were seen to be perpendicularly aligned to the freeze-bonded surface. Vertical Ice 1 ice-blocks had the brine channels parallel with the freeze-bonded surface. Horizontal ice-blocks are from this assumed to have the highest permeability. This would further lead to increased brine drainage, and hence stronger freeze-bonds.

A higher adhesive strength between the ice formed in the freeze-bond and the surrounding surfaces may be an additional explanation. This is also due to the perpendicular alignment of the brine channels. The crystal structure of the horizontal ice blocks would in addition have the c-axis aligned parallel with the

freeze-bond. Both these points are suggested as possible contributions leading to a higher degree of interlocking between the newly formed ice and the microstructure of the freeze-bonding ice-blocks.

5.2.2 Ambient air temperature of the submersion basin

The influence on the freeze-bond strength of having the water temperature in the submersion basin at, or slightly above the freezing-point was investigated through keeping the ambient air temperature of the basin at two levels, -1 °C and -7 °C. This was done as a part of the NTNU-experiments. Ice was continuously formed in the basin with an ambient air temperature of -7 °C, while no ice was formed in the basin during sample submersion with an ambient air temperature of -1 °C. No detectable differences were found within the obtained freeze-bond strengths. A summary of the measured freeze-bond strengths for the configurations tested at the two temperature levels are presented is table 5.3. The difference in freeze-bond strength between the two bottom surface configurations, as discussed in section 5.2.5, is considered to be an effect of the contact surface, and not of the ambient air temperature.

Table 5.3: Summary of the nominal freeze-bond strength ($\tau_{fb,nom}$) for the configurations tested while keeping the ambient air temperature of the submersion basin at two levels, -1 °C and -7 °C.

Configuration			Number of samples	$\tau_{fb,nom}$ [kPa] Mean	Std	Max	Min
Vertical,	Cut-Parallel,	-1 °C	10	13.5	4.8	21.6	3.9
Vertical,	Cut-Parallel,	-7 °C	10	15.8	10.5	34.6	2.6
Vertical,	Cut-Normal,	-1 °C	11	17.5	8.4	38.3	8.3
Vertical,	Cut-Normal,	-7 °C	9	18.4	7.9	34.7	10.5
Horizontal,	Bottom,	-1 °C	6	65.1	18.2	83.2	38.7
Horizontal,	Bottom,	-7 °C	5	79.9	9.8	89.2	64.7

5.2.3 Assembling method, "In air" and "In water"

Two assembling methods were used during the NTNU-experiments, assembling "In air" and "In water", this had a significant effect on the freeze-bond strength. Ratios between the freeze-bond strength for the "In air" and "In water" samples

are found in table 5.4. These ratios show that the "In water" samples are stronger than the "In air" samples, also if the real freeze-bond strengths are compared. We do not have an explanation to this phenomenon, but consider it as an interesting observation that freeze-bonds assembled "In water" is stronger than freeze-bonds assembled "In air". In nature freeze-bonds develops as a part of ice-ridges created in water.

Table 5.4: Ratio between the average "In air" and "In water" freeze-bond strength (τ_{fb}) for the configurations assembled under both conditions.

Vertical, Cut-Normall, -1 °C		Horizontal, Cut-Normall, -1 °C	
$\frac{\tau_{fb,nom,Inair}}{\tau_{fb,nom,Inwater}}$	$\frac{\tau_{fb,real,Inair}}{\tau_{fb,real,Inwater}}$	$\frac{\tau_{fb,nom,Inair}}{\tau_{fb,nom,Inwater}}$	$\frac{\tau_{fb,real,Inair}}{\tau_{fb,real,Inwater}}$
0.51	0.80	0.53	0.78

We have only tested the effects of assembling the samples "In air" and "In water" for artificially prepared contact surfaces. This implies that we do not known how this effect would influence the freeze-bond strength for naturally created surfaces.

5.2.4 Time - Temperature history of the ice-blocks

Time - temperature history of the ice-blocks used to form freeze-bonds were found as one of the main differences between the previous investigations. Repetto-Llamazares et al. (2011a) and Repetto-Llamazares and Høyland (2011a) either exposed the ice-blocks to, or stored the ice-blocks at -20 °C. Helgøy (2011) kept a constant temperature of -7.5 °C in the ice-blocks. The effect of cooling the ice was studied both during the NTNU- and HSVA-experiments. These measurements are summed up in table 5.5. In the NTNU-experiments the ice was stored in pre-cut dimensions, since this was the procedure of Repetto-Llamazares and Høyland (2011a). No noteworthy differences in the freeze-bond strength were found in relation to the time - temperature history in either the NTNU- or HSVA-experiments. This implies that the processes occurring during cooling of the ice from -7 to -20 °C do not affect the freeze-bond strength.

Table 5.5: Summary of the nominal freeze-bond strength ($\tau_{fb,nom}$) for the configurations tested with stored (−20 °C) and non-stored (−7 °C) samples.

Configuration				Number of samples	$\tau_{fb,nom}$ [kPa] Mean	Std	Max	Min
Vertical,	Cut-Parallel,	−1 °C	Ice 1	10	13.5	4.8	21.6	3.9
Vertical,	Cut-Parallel,	−1 °C, Stored	Ice 1	13	17.4	14.6	63.7	6.7
HSVA-frame				11	29.8	13.0	55.2	18.9
HSVA-frame,	Stored			6	32.9	7.4	41.8	23.5

5.2.5 Contact surface

Two main types of contact surfaces were used during the experiments: natural surfaces; "Top" and "Bottom" and artificially prepared surfaces; "Cut-Normal" and "Cut-Parallel". The main results for the different surfaces are recapitulated in table 5.6. In general the strongest freeze-bonds were obtained for the natural contact surfaces of the ice-sheet. Weaker freeze-bonds were obtained for the artificially prepared surfaces. An assessment of the influence on the freeze-bonds strength from the different contact surfaces follows.

Table 5.6: Summary of the nominal freeze-bond strength ($\tau_{fb,nom}$) for the defined groups of contact surfaces. Results from Helgøy (2011) are in addition presented. "Vertical" "−1 °C" and "−7 °C" samples are presented together since no difference was found in relation to the ambient air temperature.

Configuration			Number of samples	$\tau_{fb,nom}$ [kPa] Mean	Std	Max	Min
NTNU-frame,	Top		12	46.0	11.1	64.5	24.7
Horizontal,	Bottom - *New*	Ice 1	11	71.9	16.2	89.2	38.7
HSVA,	Bottom - *New*		29	30.8	10.9	55.2	16.5
Horizontal,	Bottom, −1 °C	Ice 3	7	14.0	8.6	27.5	6.7
Vertical,	Cut-Parallel, −1 °C & −7 °C	Ice 1	20	14.6	8.0	34.6	2.6
Vertical,	Cut-Normal, −1 °C & −7 °C	Ice 1	20	17.9	7.9	38.3	8.3
Helgøy (2011),	Top - Top		11	28.5	12.3	54.0	9.5
Helgøy (2011),	Bottom - Bottom		12	62.5	22.3	114.8	37.4

5.2.5.1 Artificially prepared surfaces

Two artificially prepared surfaces with an equal surface roughness were used during the NTNU-experiments. These were made by either having the groves made during sawing of the surface normal to or parallel with the longitudinal ice-block direction, see figure 3.4. Equal freeze-bond strengths were obtained for the two surfaces. At dry conditions it may be assumed that a higher shear force would be present for the samples with normal groves. This is due to a higher friction between these surfaces. An implication is that there does not seem to be any connection between the initial friction between the ice-blocks, and the freeze-bond strengths observed after submersion. A requirement may be that the global surface roughness of the ice-blocks is equal so that an equal freeze-bond strength is able to develop between the ice-blocks, see section 5.4.

5.2.5.2 Natural bottom surfaces

Three different levels of freeze-bond strengths were in general observed for the freeze-bonds created between two natural bottom surfaces. The Ice 1 samples from the NTNU-experiments yielded the highest freeze-bond strengths, with an average nominal freeze-bond strength of 71.9 kPa. Secondly followed the "Bottom" samples from the HSVA-experiments, with an average nominal freeze-bond strength of 30.8 kPa. Weakest freeze-bonds were found for the Ice 3 samples from the NTNU-experiments, with an average nominal freeze-bond strength of 14.0 kPa. Freeze-bonds developed between two natural bottom surfaces were also investigated by Helgøy (2011). An average nominal freeze-bond strength of 62.5 kPa were reported from their measurements. A box-plot comparing the obtained freeze-bond strengths from these four groups are shown in figure 5.2.

The spread in obtained freeze-bond strengths is large, with a difference of 88.2 kPa between the weakest and strongest sample. This implies that physical differences in the freeze-bonding process have occurred. An even surface with a clearly visible skeleton layer was seen for the Ice 1 samples. Except for a larger crystal diameter the Ice 1 surfaces were by eye equal to the bottom surfaces used by Helgøy (2011). These samples do also have comparable freeze-bond strengths. The bottom surface of the Ice 3 and HSVA samples seemed to be more eroded. In addition increased surface roughness of these samples was seen as an effect of ice formed on the surfaces after extraction of ice from the production basin. Ice 3 samples are believed to have the highest surface roughness,

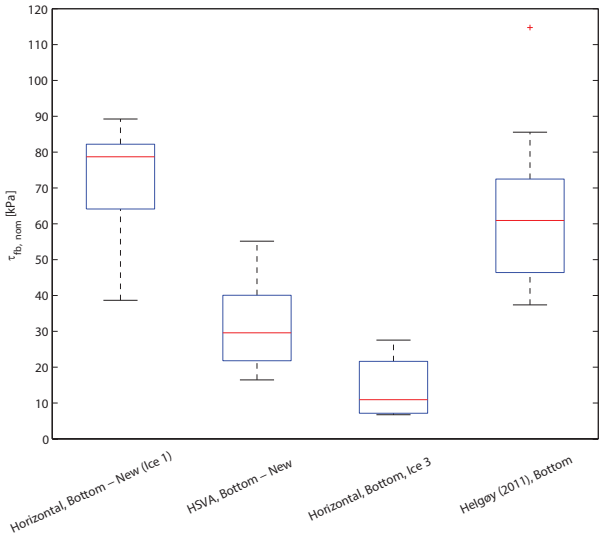

Figure 5.2: Box-plot of the nominal freeze-bond strength ($\tau_{fb,nom}$) for the three defined groups of "Bottom" samples. Results from the "Bottom - Bottom" configuration of Helgøy (2011) are in addition presented.

and had in addition different physical properties, see section 4.2.1.

Eroded surfaces in connection with a higher surface roughness for the Ice 3 and HSVA samples are probably the main explanation to the difference in measured freeze-bond strengths. Different physical properties of the Ice 3 samples may in addition have contributed to a further reduction of the freeze-bond strengths for these samples.

This shows that it is difficult to obtain a reproducible bottom surface. It is also considered problematic that the surface roughness is increased after extraction from the production basin due to of moisture re-crystallised on the surface. An assumption drawn from this observation may be that stronger freeze-bonds are created in-situ since the surface erosion would be less.

5.2.5.3 Natural top surfaces

Top surface samples were tested during the HSVA-experiments. Previous investigations using an equal surface combination were performed by Helgøy (2011). Both these investigations applied scaled S2 ice with small crystals. A comparison of these two groups are seen in figure 5.3. We can not explain why we obtained stronger freeze-bonds than Helgøy (2011). However, one important difference in the production process of the ice used in the two experiments has been found. Air bubbles were feed into the HSVA ice, this was not done for the ice used by Helgøy (2011). Changing the physical properties of the ice close to the surface may lead to higher freeze-bond strength. As discussed in section 5.2.1 an increased permeability and adhesive strength of the surface may lead to increased freeze-bond strengths. Shafrova and Høyland (2008) measured highest freeze-bond strengths for ice-foot ice with a high gas content (20%). They explain the strong freeze-bonds to be an effect of the reduced thermal conductivity of the porous ice, which leaves more cold for the development of freeze-bonds, see section 2.3.3. This may be an additional explanation to the difference in freeze-bond strength between our, and the experiments of Helgøy (2011).

5.2.6 Ice-block size

Two sample dimensions were applied during the HSVA-experiments. Both sample sizes used the natural bottom surface of the ice-sheet to form freeze-bonds. The large samples had an 8.17 times larger nominal contact area than the small

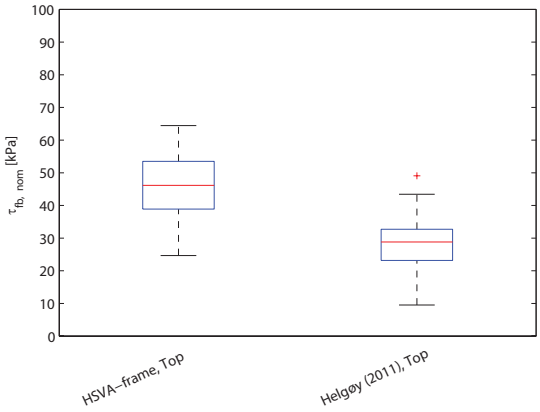

Figure 5.3: Box-plot of the nominal freeze-bond strength ($\tau_{fb,nom}$) for the "HSVA-frame, Top" samples and the "Top - Top" configuration samples from Helgøy (2011).

samples. A summary of these measurements are found in table 5.7. Equivalent freeze-bond strengths were measured for the two sample dimensions. The average freeze-bond strength for the small ("NTNU-frame") samples was 30.7 kPa, while the large ("HSVA-frame") samples had an average freeze-bond strength of 30.8 kPa.

Table 5.7: Summary of the nominal freeze-bond strength ($\tau_{fb,nom}$) for the small ("NTNU-frame" size) and the large ("HSVA-frame" size) samples from the HSVA-experiments. Since no significant differences were found in relation to the time - temperature history for the two "HSVA-frame" size configurations are these presented together.

Configuration	Number of samples	$\tau_{fb,nom}$ [kPa] Mean	Std	Max	Min
NTNU-frame, Bottom	12	30.7	10.9	48.8	16.5
HSVA-frame samples	17	30.8	11.2	55.2	18.9

It may be concluded from these measurements that the freeze-bond strength is not dependent on the nominal contact area between the ice-blocks for the sample dimensions and contact surfaces used in our experiments. We presume

that this conclusion only would be valid for the surface conditions applied in our experiments. If a smoother surface had been applied to form the freeze-bond, the freeze-bonding mechanism would probably be different. As discussed in section 5.4 a freeze-bond would most likely only be developed along the outer edges of the freeze-bonding surface. This would further lead to a larger unbounded area between the ice-blocks, and hence a reduced freeze-bond strength.

5.3 Previous investigations and reproducibility

Previous experimental investigations of the freeze-bond strength with a similar test set-up as the one used in our investigation where performed by Ettema and Schaefer (1986), Repetto-Llamazares et al. (2011a), Repetto-Llamazares and Høyland (2011a), Helgøy (2011) and Astrup (2011). A main goal of our work was to investigate the reproducibility of the experiments by Repetto-Llamazares et al. (2011a) and Repetto-Llamazares and Høyland (2011a). A thoroughly comparison between their and our work is therefore presented in section 5.3.1 and 5.3.2.

Experimental investigations of freeze-bonds were also performed by Shafrova and Høyland (2008) and Marchenko and Chenot (2009). A review of these investigations and the work of Repetto-Llamazares et al. (2011a) have been presented by Repetto-Llamazares and Høyland (2011b). The experimental procedures used in these experiments were different from the one used in our experiments. Accordingly it is difficult to compare these experiments with the experiments done in this thesis. Further discussions of the work of Shafrova and Høyland (2008) and Marchenko and Chenot (2009) are therefore not included here.

5.3.1 Repetto-Llamazares et al. (2011a)

Comparing our results from the HSVA-experiments with the results from Repetto-Llamazares et al. (2011a) was beneficial because the same ice type and the same test-frame were used during both experiments. Both sets of experiments were performed at HSVA. Investigating the freeze-bond strength in relation to the submersion time (Δt), initial temperature (T_i) and confinement pressure (σ) was the main goal of the work by Repetto-Llamazares et al. (2011a). Although Repetto-Llamazares et al. (2011a) applied a wide range of these parameters, it is

not a full consistency between the test parameters used by Repetto-Llamazares et al. (2011a) and ours. We chose to use equal test parameters (Δt, T_i, σ, V, T_i) both during the NTNU- and HSVA-experiments. This was done in order to ensure a full comparability between the two sets of experiments. We identified the test series 3000 ($\Delta t = 5$ min samples) from Repetto-Llamazares et al. (2011a) to be the test configuration lying closest to our experiments. This is also the configuration which resulted in highest freeze-bond strengths in their experiments. A comparison of test parameters and results from series 3000 ($\Delta t = 5$ min samples) from Repetto-Llamazares et al. (2011a) and our experiments are presented in table 5.8.

Table 5.8: Comparison of the test parameters for test series 3000 ($\Delta t = 5$ min) from Repetto-Llamazares et al. (2011a) (-RLetal (2011a)-) and the HSVA-frame samples form our experiments.

	RLetal (2011a)	Our
Test frame	Equal to the our experiments.	Equal to the experiments by RLetal (2011a).
Ice	HSVA model-ice extracted after heating.	HSVA model-ice extracted after heating.
Freeze-bonded area, A_{fb}	$140 \cdot 140$ [mm]	$140 \cdot 140$ [mm]
Ice-block thickness, h_b	25 to 35 mm	27 mm
Contact surface	Random combinations of the natural top and bottom of the ice-sheet.	Only the natural bottom in contact with the natural bottom.
Initial temprature, T_i	-7.5 °C	-7.0 °C
Time - temprature history	Cooled down and stored at -20 °C, subsequently heated to T_i.	Both cooled down and stored at -20 °C, and stored at -7 °C throughout the whole storage period.
Piston velocity, V	0.7 and 0.78 mm/s	2 mm/s
Submersion time, Δt	5 min	10 min
Submersion basin salinity, S_{sb}	8.4 ppt	6.9 to 7.3 ppt
Confinement pressure, σ_{sub}	0.66 kPa	1.9 kPa
Confinement pressure, σ_{test}	0.66 kPa	2.2 kPa
Average freeze-bond strength:	$\tau_{fb,nom} \approx 20$ kPa	$\tau_{fb,nom} = 30.9$ kPa
Maximum freeze-bond strength:	$\tau_{fb,nom} = 29.5$ kPa	$\tau_{fb,nom} = 55.2$ kPa
Minimum freeze-bond strength:	N/A	$\tau_{fb,nom} = 18.9$ kPa

Five test parameters are seen to be different, h_b, V, Δt, σ and the contact surface. Two of these are related to the test parameters defined by Repetto-Llamazares et al. (2011a), namely Δt and σ. The closest submersion times to our

experiments used by Repetto-Llamazares et al. (2011a) were 1, 5 and 20 min, from which 5 min submersion time yielded the highest freeze-bond strengths. Confinement pressures above 0.66 kPa by Repetto-Llamazares et al. (2011a) were only used for submersion times of 20 h. The following list assesses how the five test parameters are considered to have affected the freeze-bond strength.

- Exact ice-block thickness in the experiments of Repetto-Llamazares et al. (2011a) is not known, but the ice-blocks might have been somewhat thicker than the 27 mm thick ice-blocks used in our experiments. Thicker ice-blocks would lead to a higher tension in the freeze-bond during strength testing. It has not been investigated how a combination of tension and shear affects the freeze-bond strength, and it is therefore difficult to quantify if this leads to a reduced freeze-bond strength. From the experience of observing the fracture process of the freeze-bonds the difference in ice-block thickness is not considered to be able to cause the observed strength differences, even though it might have contributed.

- The surface roughness was not measured in either our or the experiments of Repetto-Llamazares et al. (2011a). We used a fixed surface combination of the natural bottom in contact with the natural bottom while Repetto-Llamazares et al. (2011a) randomly used the natural top and bottom of the ice-sheet to form the freeze-bonds. The quality and surface combination may, as discussed in section 5.2.5, affect the freeze-bond strength. For our NTNU-frame size samples were the strongest freeze-bonds measured for the configuration with the top surface in contact with the top surface, while Helgøy(2011) measured the strongest freeze-bonds for the freeze-bonds created between two bottom surfaces. We are uncertain of how the surface properties have contributed to the observed strength differences, but it is likely that they have.

- The difference in piston velocity is not considered to contribute to the obtained differences in freeze-bond strength. Astrup (2011) performed freeze-bond measurements with piston velocities of 1 and 10 mm/s without finding any noteworthy differences in the freeze-bond strength.

- The effect of increasing the submersion time from 5 to 10 min is considered to give a possible contribution to the observed strength difference. Repetto-Llamazares et al. (2011a) proved that the freeze-bond strength follows a bell-shaped time - strength relationship, with highest freeze-bond strengths observed after 5 min submersion. Submersion times of 1, 5, 20 min and higher were used in the establishment of this relation-

ship. Increasing freeze-bond strengths from 5 to 10 min submersion time is considered possible.

- Increasing freeze-bond strengths with increasing confinement pressure has been proved by Repetto-Llamazares et al. (2011a). Increasing the confinement pressure from 0.66 to 1.9 kPa during submersion would most likely have contributed to higher freeze-bond strengths in our measurements. A Mohr-Coulomb failure criterion was established by Repetto-Llamazares et al. (2011a) to describe the evolution of the freeze-bond strength with increasing confinement pressure, see equation 2.1. They only reports cohesion (c_τ = 1.1 to 4.5 kPa) and friction angels (ϕ_τ = 11 to 34°) for submersion times of 20 h, so their values are not found adequate to use in describing our test conditions. Corresponding parameters based on the results of Repetto-Llamazares et al. (2011a) and us, see table 5.8, would be a friction angle of 83° and a cohesion of 14.6 kPa. This friction angle is considered to be unrealistic high, and shows that a higher confinement pressure in our experiments not alone was responsible for the increase in freeze-bond strength.

From the assessed differences it could be concluded that it is likely that our results could be compared with the results from Repetto-Llamazares et al. (2011a). The measured difference is mainly explained by different confinement pressures (0.66 vs. 1.9 kPa) and submersion times (5 vs. 10 min). Thicker ice-blocks and different contact surfaces are considered to be possible additional reasons to the obtained difference in freeze-bond strength.

5.3.2 Repetto-Llamazares and Høyland (2011a)

One objective of the NTNU-experiments was to see if we by changing the ice-block direction, the surface properties, the ambient air temperature of the submersion basin and the time - temperature history of the ice-blocks managed to reproduce the results by Repetto-Llamazares and Høyland (2011a). All these parameters were stated by Helgøy (2011) as possible reasons for the difference in freeze-bond strength between their results, and the results of Repetto-Llamazares and Høyland (2011a). Repetto-Llamazares and Høyland (2011a) obtained the lowest known freeze-bond strengths for the confinement pressure, submersion time and initial ice-block temperature used in our experiments (σ_{sub} = 1.9 kPa, σ_{test} = 2.04 kPa, Δt = 10 min and T_i = −7 °C). It should be noticed that Repetto-Llamazares and Høyland (2011a) only tested

between 2 and 4 samples per configuration, 27 in total. None of these configurations had an average freeze-bond strength above 4 kPa. Repetto-Llamazares and Høyland (2011a) commented that they did not know the reason for the low freeze-bond strengths, but states that it probably was related to the surface quality of the ice-blocks. A summary of the test parameters and results used by Repetto-Llamazares and Høyland (2011a), Helgøy (2011) and in our experiments is presented in table 5.9.

We established six configurations with in total 90 samples to see if we managed to reproduce the freeze-bond strengths of Repetto-Llamazares and Høyland (2011a). The test configurations are summarised in table 5.10. A discussion of the relation between the test configurations and measured freeze-bond strengths have already been presented in section 5.2. For the Ice 1 samples assembled "In air" no significant differences were found between the five vertical ice-block configurations. The horizontal samples gave considerably higher freeze-bond strengths. By the use of an artificially prepared contact surface lower freeze-bond strengths than those measured by Helgøy (2011) were obtained. But the freeze-bond strengths were still significantly higher than those reported by Repetto-Llamazares and Høyland (2011a). Changing the ambient air temperature of the submersion basin and the time - temperature history of the ice-blocks did not have any influence on the freeze-bond strength.

We believe that the main explanation to the difference in obtained freeze-bond strengths by Repetto-Llamazares and Høyland (2011a) and Helgøy (2011) is associated with different physical properties of the applied ice-blocks. The lowest freeze-bond strengths in our experiments were obtained for the "Vertical, Cut-Normal, $-1\,^{\circ}$C" configuration applying Ice 3 samples and "Horizontal, Cut-Normal, $-1\,^{\circ}$C" configuration applying Ice 2 samples, $\tau_{fb,nom,min} = 2.4$ and 1.9 kPa, respectively. As seen in section 4.2.5 weak samples were connected with the transparent parts of the ice, i.e. a low salinity and few brine channels. The relation between the physical properties of the ice-blocks and obtained freeze-bond strengths is further discussed in section 5.5. Repetto-Llamazares and Høyland (2011a) have not reported the physical properties of the ice-blocks used in their experiments, except that the ice was made from 8 ppt saline water. Pictures from their experimental work shows many transparent ice-blocks.

Both changing the ice-block direction from horizontal to vertical ice-blocks and the contact surface from natural top and bottom to an artificially prepared contact surface were found to reduce the freeze-bond strengths compared to Helgøy (2011). Even with this reduction the freeze-bond strength was considerably

Table 5.9: Comparison of test parameters applied by Repetto-Llamazares and Høyland (2011a) (−RL&H(2011a)−), Helgøy (2011) and in our experiments.

	RL&H (2011a)	Helgøy (2011)	Our
Test frame:	Equal to Helgøy (2011).	Equal to RL&H (2011a).	New aluminium frame.
Ice:	Un-scaled laboratory made saline ice.	Laboratory made saline ice with small crystals.	Un-scaled laboratory made saline ice.
Ice production basin:	"Frysis II"	"Frysis II"	"Frysis II"
Produced ice-sheet thickness:	200 mm	22 to 30 mm	110 to 188 mm
Production basin water salinity:	8 ppt	8 ppt	8 ppt
Ice production temperature:	−20 °C	−20 °C	−20 °C with periods at −7 °C
Freeze-bonded area, A_{fb}:	$60 \cdot 40$ [mm]	$60 \cdot 40$ [mm]	$60 \cdot 40$ [mm]
Ice-block thickness, h_b:	22 mm	22 mm	22 mm
Contact surface:	Artificially produced.	Natural top and bottom.	Artificially produced.
Initial temprature, T_i:	−7.0 °C	−7.5 °C	−7.0 °C
Time - temprature history:	Exposed to −20 °C, stored at −7 °C. Final sample dimensions prepared before storing.	Stored at −7.5 °C	Exposed to −20 °C and stored in final sample dimensions at −7 °C, in addition to samples stored in large ice-blocks at −7 °C.
Piston velocity, V:	2 mm/s	1 mm/s	2 mm/s
Submersion time, Δt:	10 min	10 min	10 min
Submersion basin salinity, S_{sb}:	8 ppt	8 ppt	8 to 9.1 ppt
Confinement pressure, σ_{sub}:	1.9 kPa	1.9 kPa	1.9 kPa
Confinement pressure, σ_{test}:	2.04 kPa	2.04 kPa	2.04 kPa
Nominal freeze-bond strengths:	$\tau_{fb,mean} = 3.6$ kPa	$\tau_{fb,mean} = 28.5$ to 62.5 kPa	$\tau_{fb,mean} = 6.1$ to 38.7 kPa

Table 5.10: Summary of the nominal freeze-bond strength ($\tau_{fb,nom}$) for the six configurations prepared in order to reproduce the results of Repetto-Llamazares and Høyland (2011a).

Configuration				Number of samples	$\tau_{fb,nom}$ [kPa] Mean	Std	Max	Min
Vertical,	Cut-Parallel,	−1 °C, Stored	Ice 1	13	17.4	14.6	63.7	6.7
Vertical,	Cut-Parallel,	−1 °C	Ice 1	10	13.5	4.8	21.6	3.9
			Ice 3	5	10.5	7.3	19.9	3.2
Vertical,	Cut-Parallel,	−7 °C	Ice 1	10	15.8	10.5	34.6	2.6
Vertical,	Cut-Normal,	−1 °C	Ice 1	11	17.5	8.4	38.3	8.3
			Ice 2	6	11.7	7.0	23.5	4.9
			Ice 3	5	6.1	3.6	12.0	2.4
Vertical,	Cut-Normal,	−7 °C	Ice 1	9	18.4	7.9	34.7	10.5
Horizontal,	Cut-Normal,	−1 °C	Ice 1	11	38.7	12.6	64.4	25.7
			Ice 2	5	18.5	11.3	32.8	1.9
			Ice 3	5	20.2	11.9	35.3	4.8

higher than those reported by Repetto-Llamazares and Høyland (2011a). We suggest that the low freeze-bond strengths reported by Repetto-Llamazares and Høyland (2011a) are related to the physical properties of the ice used to form freeze-bonds in their experiments.

5.4 Surface roughness vs. unbounded area

It was in general observed five different states of the unbounded area between the freeze-bounding ice-blocks. These were, ordered after the extent of the unbounded area:

- Fully freeze-bonded surfaces. This was observed for the samples assembled "In water", with exception of 1 of the 24 samples which had a small (2%) unbounded area.
- Ice 3 "Bottom" samples from the NTNU-experiments with an almost fully freeze-bonded surfaces, $A_{ub,mean} = 0.1\%$. These samples were from a visual assessment considered to have the highest surface roughness. One of the seven samples had an unbounded area.

- The Ice 1 "Bottom" samples from the NTNU-experiments and the "Bottom" samples from the HSVA-experiments form the following group. These samples had a joint average unbounded area of 3.2%. Twenty-one of the forty samples were found to have an unbounded area.
- "NTNU-frame, Top" samples from the HSVA-experiments had an average unbounded area of 10%. This surface is considered to have the lowest surface roughness of the two natural surfaces. From these 13 samples was there only 2 without an unbounded area.
- Largest unbounded areas were found for the samples with an artificially prepared surface, assembled "In air". These had a joint average unbounded area of 37%. These samples are considered to have the most even surfaces applied in our experiments, and all samples contained an unbounded area.

Statistical parameters for each of these groups are presented in table 5.11. Results from Helgøy (2011), who is the only author who previously has described the unbounded area, are presented together with our results in this table.

Table 5.11: Statistical parameters of the unbounded area (A_{ub}) for the five groups defined after the state of the unbounded area. Results from Helgøy (2011) are in addition presented.

Configuration	Number of samples	A_{ub} [%] Mean	Std	CV[a]	Max	Min
"In water" samples	24	0.1	0.4	4.9	2	0
Ice 3 "Bottom"samples	7	0.1	0.4	2.6	1	0
"Horizontal, Bottom" and "HSVA, Bottom" samples	40	3.5	5.5	1.6	23	0
"NTNU-frame, Top" samples	13	10	11	1.1	41	0
Artificially preapared surfaces	94	37	12	0.3	66	7
Helgøy (2011), "Bottom - Bottom" samples	21	4	5	1.2	15	0
Helgøy (2011), "Top - Top" samples	22	15	10	0.6	33	0

[a]Coefficient of variation.

The artificially prepared surfaces were found to have the most even and reproducible surface conditions in our experiments. Repetto-Llamazares and Høyland (2011a) do also comment that their surfaces (sawn by a band-saw) from a visual assessment where smoother than the surfaces used by Repetto-Llamazares et al. (2011a) (natural top and bottom of HSVA-model ice). A special feature of the artificially prepared surfaces assembled "In air", was that they were bounded along the outer edge of the contact surface. A varying size unbounded area was located in centre of the freeze-bonding surface, see figure 5.4. This is considered

to be an effect of the initial surface contact between the ice-blocks. During submersion water would penetrate into the freeze-bonding surface. For the even artificially prepared surfaces, it is assumed that water penetrates slowly, and start to freeze before water has covered the entire surface.

(a) Sample 1015, "Cut-Normal", Ice 1, A_{ub} = 31%.

(b) Sample 5007, "Cut-Normal", Ice 2, A_{ub} = 45%.

Figure 5.4: Pictures of fractured surfaces for samples with an artificially prepared surface, the unbounded area (A_{ub}) is marked by a red line.

The described mechanism is considered to be the main explanation to the different levels of unbounded areas. Highest surface roughness is considered to have been present for the Ice 3 "Bottom" samples from the NTNU-experiments. A high surface roughness would allow a high inflow of water, and thereby creating a small unbounded area. The remaining "Bottom" samples and the "NTNU-frame, Top" samples are considered to be in the intermediate stage between the two stated outer limits. A fully freeze-bonded surface was induced to the samples assembled "In water". The unbounded areas reported by Helgøy (2011) for their "Bottom - Bottom" and "Top - Top" configurations is, as seen in table 5.11, comparable to our unbounded areas for the corresponding surface configurations.

On the basis of these results we suggest that the initial surface roughness of the two freeze-bonding surfaces yields a significant contribution to the unbounded area observed after fracture. Creation of unnatural even surfaces by sawing the contact surface showed a significant effect on the freeze-bonding process. It seems like both a low surface roughness (artificially prepared surfaces) and a high surface roughness (Ice 3 "Bottom" samples) gives weaker freeze-bonds. For a low surface roughness water would not be able to cover the whole freeze-bonding

surface, while a high surface roughness leaves a gap between the surfaces of such a thickness that the freeze-bond strength is reduced. We do believe that this phenomenon should be considered when performing laboratory investigations of ice-rubble with artificially produced surfaces. Both the unbounded area and freeze-bond strengths observed for the artificially produced surfaces assembled "In air" are seen to be different from the freeze-bond strengths and unbounded areas of the samples with natural surfaces. The result may be that the freeze-bond strength is underestimated in ice-rubble with artificially prepared surfaces.

5.5 Freeze-bond strength vs. ice-properties

Three different types of ice were in general used in our experiments, namely Ice 1, Ice 2 and 3 and the HSVA-model ice. Both Ice 1 from the NTNU-experiments and the HSVA-model ice have been classified as S2 sea ice. The columnar crystals of Ice 1 had roughly four times the diameter of the columnar crystals in the HSVA-model ice. The ice-crystals found for Ice 2 and 3 in the NTNU-experiments were considerably larger than for Ice 1. These crystals were in addition randomly organized, though somewhat tending to a columnar structure. The salinity and the visual appearance of Ice 2 and 3 were also different from Ice 1 and the HSVA-model ice, see section 4.2.1.

Different freeze-bond strengths were obtained for the three groups of ice. The varying physical properties of Ice 2 and 3 are considered as the main explanation for the observed differences in freeze-bond strengths between Ice 1 on one hand, and Ice 2 and 3 on the other. The differences in freeze-bond strength between the HSVA samples and the NTNU samples using the natural ice-sheet surfaces is considered to be an effect of the surface conditions, see section 5.2.5 and 5.4.

Salinity measurements, thin section analysis and visual observations of the ice-blocks have been the main sources used for characterising the physical properties of the ice. The freeze-bond measurements at NTNU applying an artificial contact surface proved that a lower freeze-bond strength was obtained for Ice 2 and 3 than for Ice 1, see table 5.12. A clear difference between the samples from Ice 1 and Ice 2/3 was observed in the visual appearance of the ice-blocks. Ice 1 had an even opaque colour, while some opaque and some highly transparent ice-blocks were seen for Ice 2 and 3. The visually transparent ice-blocks yielded the lowest freeze-bond strengths. A low salinity and few brine channels and voids are physical properties which have been connected to the transparent ice-blocks.

Higher freeze-bond strengths were obtained if the ice-blocks had an opaque look. Physical properties connected to the opaque ice-blocks are a higher salinity and a higher number of brine channels and voids. The visual assessment have been supported by salinity measurements before and after submersion, section 4.2.1 and 4.2.3, and analysis of thin sections, section 4.2.2.

Table 5.12: Summary of the nominal freeze-bond strength ($\tau_{fb,nom}$) for the configurations in the NTNU-experiments which applied more than one ice-sheet.

Configuration				Number of samples	$\tau_{fb,nom}$ [kPa] Mean	Std	Max	Min
Vertical,	Cut-Parallel,	−1 °C	Ice 1	10	13.5	4.8	21.6	3.9
			Ice 3	5	10.5	7.3	19.9	3.2
Vertical,	Cut-Normal,	−1 °C	Ice 1	11	17.5	8.4	38.3	8.3
			Ice 2	6	11.7	7.0	23.5	4.9
			Ice 3	5	6.1	3.6	12.0	2.4
Horizontal,	Cut-Normal,	−1 °C	Ice 1	11	38.7	12.6	64.4	25.7
			Ice 2	5	18.5	11.3	32.8	1.9
			Ice 3	5	20.2	11.9	35.3	4.8
Horizontal,	Bottom,	−1 °C	Ice 1	6	65.1	18.2	83.2	38.7
			Ice 3	7	14.0	8.6	27.5	6.7

We are suggesting the same explanation for the difference in freeze-bond strength between Ice 1 and Ice 2/3 as the reason for the differences in freeze-bond strengths for the vertical and horizontal ice-blocks, see section 5.2.1. As suggested in this section a high permeability of the freeze-bonding surfaces would result in higher freeze-bond strengths. A large difference in permeability is considered to have been present between the opaque and transparent ice-blocks, with lowest permeability for the transparent ice-blocks. It was visually seen that the surface of the transparent ice-blocks seemed to contain more moisture after fracture. A smooth and dense structure of the transparent ice-blocks would in addition probably lead to a lower adhesive strength for these samples. The changing crystal direction and crystal size would further lead to a changing orientation of the crystal structure in relation to the freeze-bond. This may in addition affect the freeze-bond strength.

In addition to a large spatial variability of the physical properties of Ice 2 and 3, the crystal size of these ice-sheets are considered to be too large compared to the sample size. With the possibility of having just a few crystals per sample, spatial variations of the contacting ice-blocks be able to give a large scatter in

the freeze-bond strength within a configuration.

5.6 Assessment of the experimental procedure

The experimental set-up used in this thesis is in general considered advantageous. The main reason is that the effects from different factors on the freeze-bond strength easily are isolated. In addition small samples are used, which are easy to handle and small amounts of ice are required for the experiments. Small samples with an natural top or bottom surface are in addition easier to extract from the ice production basin. We tried to extract top surface samples during the NTNU-experiments, but did not manage to extract ice without flooding the top surface. Top surface samples were extracted both during the HSVA-experiments and in the experiments by Helgøy (2011), without flooding.

The largest weakness of the experimental set-up used in our experiments is that the procedure of strength testing applies a small tension to the freeze-bond. Shafrova and Høyland (2008) utilized a test set-up with the freeze-bond aligned at 45° as a part of a sample tested in uniaxial compression. The advantage of such a set up is that there is no tension applied to the freeze-bond. Disadvantages of such a test set-up would be that larger samples are required, and that it is much more difficult to apply a constant confinement pressure. Another possibility is a experimental set-up that has been applied in rock mechanics. This set-up applies three ice-blocks lying on top of each other, and thereby creating two freeze-bonds. In such a set-up the upper and lower ice-blocks are fixed, while force is applied to the middle ice-block. We have not in detail studied this set-up, but we are in general having doubts since we have seen a large scatter of the obtained freeze-bond strengths within a configuration. This would in particular create a challenge when testing the natural top or bottom surface.

We consider producing and extracting ice with equal properties to be one of the largest challenges in our experiments. We attempted to produce three equal ice-sheets during the NTNU-experiments. The differences in freeze-bond strength related to the salinity, density and crystal structure of the produced ice-sheets were found by a coincidence. We do in general believe that the in-homogeneity we found for Ice 2 and 3 was so large that these ice-sheets were not suitable for small-scale experiments. For further experiments should it also be developed a method to prevent moisture from re-crystallize on the natural surfaces, after extraction of ice from the production basin. Extracting ice without heating

the ice from the production temperature is considered simplest. This does not mean that ice needs to be extracted at an air temperature of $-20\,^{\circ}\mathrm{C}$, but the ice-strength should not be particularly reduced. The mechanical abrasion of the bottom surface of the HSVA-model ice is considered to be too large, it was in addition difficult to extract large enough ice-blocks. In the case of further freeze-bond experiments at HSVA is it recommended to extract ice before the ice is heated. For further freeze-bond experiments at NTNU a method for producing ice with uniform physical properties should be developed.

5.6.1 Test frames

Two test frames were applied during our experiments. The NTNU-frame is considered to be easiest to handle, and it is seen as an advantage that the pushing piston was independent from the test frame. It was troublesome to connect the lid of the HSVA-frame to the pulling system. An additional effect of this was that an initial stress was applied to the freeze-bond, before the piston was activated. Large deformations and problems with fixing the lid to the upper ice-block during strength testing were in addition experienced for the HSVA-frame. The stiffer NTNU-frame seams to better reflect the fracture process of the freeze-bond.

The largest challenge with the pulling system of the HSVA-frame was that the lid slipped in rear end of the upper ice-block. This resulted in the problem of a vertical fracture of the lower ice-block, since a higher bending moment was induced to the sample. The pushing piston used with the NTNU-frame is considered to have been stable in the vertical direction, no visible vertical movements were seen during interaction between the piston and the sample.

The overall experience with the test frame designed for the NTNU-experiments were good, and it is recommended to use this frame in further experiments. We do believe that too many disadvantages are seen for the HSVA-frame to recommend further experiments to be performed with this frame. If a new test frame should be designed for HSVA-frame size samples, is it recommended to ensure that force is applied as low as possible on the face of the upper ice-block. This would keep the bending moment in the samples at a minimum.

5.6.2 Uncertainties

The largest identified uncertainty related to the freeze-bond strength measurements is connected to the surface properties of the ice-blocks. The surface roughness has only been quantified through qualitative measures. This is considered to be unfavourable. We did in addition lack a good way to quantify the condition of the natural top and bottom surface of the ice-sheet.

An additional vertical force was applied by hand to the rear end of the lid for the strongest HSVA-frame samples. How this pressure has affected the freeze-bond strength measurements is not known.

The unbounded areas of the ice-blocks were estimated from pictures made of the fractured surfaces. These pictures were uploaded to the software "AutoCAD", that was used to calculate the stated area. The border of the unbounded area was determined by eye, and it was for some samples challenging to determine the transition between the bounded and unbounded area. This applies specially to the artificially prepared surfaces.

Density measurements of the ice were dependent on volumetric measurements of the samples. The volume of the samples was calculated from dimensional measurements of the length, width and height of the samples. As previously explained the surfaces of the samples were uneven, which means that some uncertainty must be added to the dimensional measurements. This uncertainty would further affect the calculation of the sample volume and density.

Chapter 6

Conclusions

6.1 Summary

One hundred and eighty one freeze-bond strength tests have been performed and analysed in this thesis. In the ice laboratory of the Department of Civil and Transport Engineering at NTNU 136 samples divided into 10 test configurations were tested. At HSVA 45 samples divided into 4 test configurations were tested. The reproducibility of the experiments performed by Repetto-Llamazares et al. (2011a) and Repetto-Llamazares and Høyland (2011a), and how the freeze-bond strength varies with the salinity, density and crystal size and orientation of the ice-blocks used to form freeze-bonds were investigated. We do in particular consider our work to be an important contribution in the process of carrying out more accurate small-scale laboratory investigations of single freeze-bonds and freeze-bonds formed as a part of ice-rubble in the future.

6.2 Conclusions

The main conclusion from our experiments is:

- The freeze-bond strength developed between two saline ice-blocks is strongly dependent on the physical properties of the freeze-bonding ice-blocks.

The following tested factors were found ***to*** affect the freeze-bond strength:

1. Ice-block salinity; Weak freeze-bonds were obtained for freeze-bonds created between ice-blocks with a low initial salinity ($S < \sim 1$ ppt), while stronger freeze-bonds were obtained if the ice-blocks had a high initial salinity ($S > \sim 2$ ppt).
2. Ice-block direction; Ice-blocks with the columnar crystal structure parallel with the longitudinal ice-block direction gave weaker freeze-bonds than ice-blocks with the columnar crystal structure normal to the longitudinal ice-block direction.
3. Assembling conditions; Putting the ice-blocks in contact with each other in air gave weaker freeze-bonds than if the ice-blocks were put in contact with each other in water.
4. Contact surface; Artificially prepared surfaces gave the weakest freeze-bonds while the natural ice-sheet bottom surface gave the strongest freeze-bonds, an intermediate freeze-bond strength was found for the natural top surface of the ice-sheet.

The following tested factors were found ***not to*** affect the freeze-bond strength:

5. Time - temperature history of the ice-blocks; Ice-blocks constantly stored at -7 °C or exposed to/stored at -20 °C.
6. Grove direction of the contact surface for the artificially prepared surfaces; Groves normal to or parallel with the loading direction.
7. Sample dimensions; Small samples ($A_{fb} = 24$ cm^2) or Large samples ($A_{fb} = 196$ cm^2)
8. Submersion basin temperature; Freezing-point temperature water or slightly above.

Other important results are considered to be:

- We did not manage to reproduce the results of Repetto-Llamazares et al. (2011a) and Repetto-Llamazares and Høyland (2011a). The difference between the results of Repetto-Llamazares et al. (2011a) and us have mainly been explained by the use of a different submersion time (5 vs. 10 min) and confinement pressure (0.66 vs. 1.9 kPa). We do however considerer the results of Repetto-Llamazares et al. (2011a) to be reproducible. We did not manage to obtain as low average freeze-bond strengths as reported

by Repetto-Llamazares and Høyland (2011a). The obtained difference is suggested to be explained by different physical properties of the ice used in the two experiments, we believe they used transparent ice-blocks with a low salinity.

- The surface roughness affects the nominal contact area between the freeze-bonding ice-blocks. A low surface roughness (artificially prepared surfaces) gives a large unbounded area between the ice-blocks, while a high surface roughness (Ice 3 "Bottom" samples) gives a close to fully freeze-bonded surface between the ice-blocks.

6.3 Recommendations for further work

The importance of the relation between freeze-bond strengths and the physical properties of the freeze-bonding ice-blocks are highlighted in this thesis. We do consider further investigations of this relation to be important. These investigations should in particular consider the stated hypothesis of how the permeability and adhesive strength of the freeze-bonding surface correlates to the freeze-bond strength.

Surface properties of the freeze-bonding ice-blocks have been related to the freeze-bond strength. The following list suggests additional studies which should be performed regarding this relation:

- Different levels of freeze-bond strengths are found for freeze-bonds developed between two natural bottom surfaces. It is suggested to develop a method for quantifying the state of the surface, and relate this to the freeze-bond strength.
- Equal freeze-bond strengths were measured for the two sample dimensions applied in our experiments. We have suggested that this is a combined effect of the surface roughness and nominal contact area between the freeze-bonding ice-blocks. It is in general believed that a large nominal contact area and an even surface would lead to low freeze-bond strengths. This relation needs further investigations.
- A new method of assembling the freeze-bonding sample "In water" was applied. This effect was only studied for artificially prepared surfaces. How it affects the freeze-bond strength for natural contact surfaces is not

known.

All experiments performed in this thesis used the same initial ice-block temperature (T_i), submersion time (Δt) and confinement pressure (σ_{sub}, σ_{test}). How our results vary with these parameters needs further investigation.

Bibliography

Astrup, O. S. (2011). *Rubble properties and ad freeze-bonds in first-year ridges*, TBA4550 Marine Civil Engineering; Specialization Project, Norwegian University of Science and Technology.

Astrup, O. S. (2012). *Experimental investigations and analytical analysis of ice rubble: Shear box and pile testing*, TBA4920 Marine Civil Engineering; Master Thesis, Norwegian University of Science and Technology.

Bailey, E. (2011). *The Consolidation and Strength of Rafted Sea Ice*, PhD thesis, University College London.

Ettema, R. and Schaefer, J. A. (1986). Experiments on freeze-bonding between ice blocks in floating ice rubble, *Journal of Glaciology* **32**(112): 397–403.

Evers, K. U. and Jochmann, P. (1993). An advanced technique to improve the mechanical properties of model ice developed at the HSVA ice tank, *Proceedings of the 12th international Conference on Port and Ocean Engineering under Arctic Conditions (POAC)*, Hamburg, Germany, pp. 877–888.

Harrison, J. D. and Tiller, W. A. (1963). *Controlled Freezing of Water. In Ice and Snow - Properties, Processes and Applications (W. D. Kingery, Ed.)*, MIT Press, MA. pp. 215-225.

Helgøy, H. (2011). *Study of freeze-bond strength in relation to the contact surfaces for small-scale experiments*, TBA4550 Marine Civil Engineering; Specialization Project, Norwegian University of Science and Technology.

Høyland, K. V. (2007). Morphology and small-scale strength of ridges in the North-western Barents Sea, *Cold Regions Science and Technology* **48**: 169–187.

Høyland, K. V. (2010). Thermal aspects of model basin ridges, *20th IAHR International Symposium on Ice*, Lahti, Finland.

ISO-19906 (2010). *Petroleum and natural gas industries - arctic offshore structures*, International Standardization organization, Geneva, Switzerland.

Liferov, P. and Bonnemaire, B. (2005). Ice rubble behaviour and strength: Part I. Review of testing and interpretation of results, *Cold Regions Science and Technology* **41**: 135–151.

Løset, S., Shkhinek, K. N., Gudmested, O. T. and Høyland, K. V. (2006). *Actions from ice on arctic offshore and coastal structures*, LAN. pp. 53-56 & pp. 100-103.

Marchenko, A. and Chenot, C. (2009). Regelation of ice blocks in the water and on the air, *Proceedings of the 20th international Conference on Port and Ocean Engineering under Arctic Conditions (POAC)*, Luleå, Sweden.

Repetto-Llamazares, A. H. V. and Høyland, K. V. (2011a). Experiments on the relation between freeze-bond and ice rubble strength, Part II: Freeze-bond experiments and comparison with numerical simulations, *Proceedings of the 21th international Conference on Port and Ocean Engineering under Arctic Conditions (POAC)*, Montréal, Canada.

Repetto-Llamazares, A. H. V. and Høyland, K. V. (2011b). Review in experimental studies on freeze-bonds, *Proceedings of the 21th international Conference on Port and Ocean Engineering under Arctic Conditions (POAC)*, Montréal, Canada.

Repetto-Llamazares, A. H. V., Høyland, K. V. and Evers, K. U. (2011a). Experimental studies on shear failure of freeze-bonds in saline ice: Part I. Set-up, failure mode and freeze-bond strength, *Cold Regions Science and Technology* **65**: 286–297.

Repetto-Llamazares, A. H. V., Høyland, K. V. and Kim, E. (2011b). Experimental studies on shear failure of freeze-bonds in saline ice: Part I. Ice-ice friction after failure and failure energy, *Cold Regions Science and Technology* **65**: 298–307.

Serré, N. (2011). *Study of the rubble ice action in scale-model ice ridge impact on seabed structures*, PhD thesis, Norwegian University of Science and Technology.

Serré, N., Repetto-Llamazares, A. H. V. and Høyland, K. V. (2011). Experiments on the relation between freeze-bond and ice rubble strength, Part I: Shear box experiments, *Proceedings of the 21th international Conference on Port and Ocean Engineering under Arctic Conditions (POAC)*, Montréal, Canada.

Shafrova, S. and Høyland, K. V. (2008). The freeze-bond strength in first-year ice ridges. small-scale field and laboratory experiments, *Cold Regions Science and Technology* **54**: 54–71.

Weeks, W. F. (2010). *On Sea Ice*, University of Alaska Press. pp. 78-143.

Appendix A

Freeze-bond test data

Test #	Configuration			$\tau_{fb,nom}$ [kPa]	$\tau_{fb,real}$ [kPa]	$\bar{V}$ [mm/s]	S_U [ppt]	S_L [ppt]	S_{tot} [ppt]	A_{ub} [%]
1000	Vertical,	Cut-Normal,	-1°C				2.16	2.62	2.41	35
	Remark: Piston collided with vertical fixing system.									
1001	Vertical,	Cut-Parallel,	-1°C				2.44	2.74	2.62	48
	Remark: Piston collided with vertical fixing system.									
1002	Vertical,	Cut-Normal,	-1°C	16.23	27.07	2.07	2.40	2.92	2.71	40
1003	Vertical,	Cut-Parallel,	-1°C	16.12	24.79	2.03	2.46	2.79	2.62	35
1004	Vertical,	Cut-Normal,	-1°C	18.49	27.13	2.08	2.42	2.83	2.65	32
1005	Vertical,	Cut-Parallel,	-1°C	16.55	31.91	2.09	2.77	2.47		48
1006	Vertical,	Cut-Normal,	-1°C	18.77	28.49	2.01	2.57	2.65	2.61	34
1007	Vertical,	Cut-Parallel,	-1°C	21.60	31.89	1.94	2.62	2.66		32
1008	Vertical,	Cut-Normal,	-1°C	16.43	26.03	1.93	2.58	2.63	2.59	37
1009	Vertical,	Cut-Parallel,	-1°C	16.96	23.94	2.06	2.57	2.80	2.68	29
1010	Vertical,	Cut-Normal,	-1°C	22.71	27.17	2.02	2.62	3.14	2.92	16
1011	Vertical,	Cut-Parallel,	-1°C	14.75	22.09	1.95	2.96	2.64	2.81	33
1012	Vertical,	Cut-Normal,	-7°C				2.30	2.44	2.36	26
	Remark: The freeze-bond seemed to be broken before strength testing.									
1013	Vertical,	Cut-Parallel,	-7°C		11.22	18.63	2.05	2.47	2.73	2.64	40
1014	Horizontal,	Bottom,	-7°C		89.24	89.87	2.07	2.47	2.60	2.55	1
1015	Vertical,	Cut-Normal,	-7°C		11.54	16.68	2.05	2.36	2.60	2.52	31
1016	Vertical,	Cut-Parallel,	-7°C		11.86	19.31	2.10	2.28	2.74	2.58	39
1017	Horizontal,	Bottom,	-7°C		64.67	83.58	1.94	2.96	2.94	2.94	23
1018	Vertical,	Cut-Normal,	-7°C		10.52	17.41	2.03	2.02	2.48	2.31	40
1019	Vertical,	Cut-Parallel,	-7°C		30.83	33.30	2.00	2.30	2.75	2.60	7
1020	Horizontal,	Bottom,	-7°C		87.78	87.78	2.07	2.47	2.95	2.73	0
1021	Vertical,	Cut-Normal,	-7°C		34.70	56.89	2.04	2.78	2.95	2.90	39

Test #	Configuration			$\tau_{fb,nom}$ [kPa]	$\tau_{fb,real}$	$\bar{V}$ [mm/s]	S_U	S_L [ppt]	S_{tot}	A_{ub} [%]
1022	Vertical,	Cut-Parallel,	-7°C	11.95	18.53	2.04	2.28	2.81	2.63	36
1023	Vertical,	Cut-Normal,	-7°C	11.01	25.78	1.98	2.62	2.89	2.85	57
1024	Horizontal,	Bottom,	-7°C	79.18	79.18	2.03	2.75	3.70	3.16	0
1025	Vertical,	Cut-Parallel,	-7°C	5.93	10.95	1.93	2.18	2.95	2.48	46
1026	Horizontal,	Bottom,	-7°C	78.74	81.03	1.98	2.71	2.90	2.79	3
2000	Horizontal,	Cut-Normal,	-1°C	29.22	37.62	1.93	2.38	3.01	2.75	22
2001	Vertical,	Cut-Normal,	-1°C	19.92	29.37	2.11	2.32	2.45	2.39	32
2002	Horizontal,	Cut-Normal,	-1°C	64.40	98.32	2.17	2.61	3.07	2.86	35
2003	Horizontal,	Cut-Normal,	-1°C	40.56	52.62	1.99	2.36	3.00	2.74	22
2004	Vertical,	Cut-Parallel,	-1°C	11.73	23.03	2.03	2.27	2.61	2.47	49
2005	Horizontal,	Cut-Normal,	-1°C	30.61	45.92	2.08	2.56	3.06	2.84	33
2006	Horizontal,	Cut-Normal,	-1°C	55.97	73.48	2.05	2.34	2.95	2.71	24
2007	Vertical,	Cut-Normal,	-1°C	13.84	21.50	2.18	2.35	2.66		36
2008	Horizontal,	Cut-Normal,	-1°C	27.01	48.63	1.96	2.60	3.19	2.95	44
2009	Horizontal,	Cut-Normal,	-1°C	25.67	33.02	2.02	2.34	2.81	2.63	22
2010	Vertical,	Cut-Parallel,	-1°C	12.54	28.52	2.14	2.46	2.45		56
2011	Horizontal,	Cut-Normal,	-1°C	38.69	53.46	1.99	2.57	3.13	2.90	28
3000	Vertical,	Cut-Normal,	-7°C	20.78	32.01	2.02	3.03	3.06	3.04	35
3001	Vertical,	Cut-Parallel,	-7°C	2.59	7.57	2.03	2.53	3.77	3.31	66
3002	Vertical,	Cut-Normal,	-7°C	12.92	23.57	2.06	2.84	3.11	2.98	45
3003	Vertical,	Cut-Parallel,	-7°C	21.04	41.33	2.11	2.83	2.97	2.90	49
3004	Vertical,	Cut-Normal,	-7°C	21.00	30.83	2.10	2.92	3.08	3.00	32
3005	Vertical,	Cut-Parallel,	-7°C	34.58	62.27	2.08	2.72	2.94	2.85	44
3006	Vertical,	Cut-Normal,	-7°C	23.13	46.64	2.07	2.88	3.01	2.94	50
3007	Vertical,	Cut-Parallel,	-7°C	18.60	27.31	2.05		3.05	3.02	32

Test #	Configuration			$\tau_{fb,nom}$ [kPa]	$\tau_{fb,real}$ [kPa]	$\bar{V}$ [mm/s]	S_U	S_L [ppt]	S_{tot}	A_{ub} [%]
3008	Vertical,	Cut-Normal,	-7°C	19.78	29.68	2.05	3.03	3.19	3.11	33
3009	Vertical,	Cut-Parallel,	-7°C	9.09	23.21	2.07	3.03	3.20	3.11	61
4000	Horizontal,	Bottom,	-1°C	38.65	44.62	2.07	3.21	3.10	3.12	13
4001	Horizontal,	Cut-Normal,	-1°C	47.53	80.91	1.85	2.89	3.10	3.00	41
4002	Vertical,	Cut-Normal,	-1°C	9.05	18.68	2.00	2.96	3.08	3.02	52
4003	Horizontal,	Bottom,	-1°C	83.19	83.19	2.06	3.23	3.43	3.34	0
4004	Vertical,	Cut-Parallel,	-1°C	10.16	17.95	1.98	2.71	3.26	3.01	43
4005	Horizontal,	Cut-Normal,	-1°C, In water	62.37	62.37	1.94	3.00	3.17	3.07	0
4006	Vertical,	Cut-Normal,	-1°C, In water	22.33	22.33	2.04	2.73	3.32	3.06	0
4007	Horizontal,	Cut-Normal,	-1°C	30.04	48.75	2.05	2.74	3.06	2.93	38
4008	Horizontal,	Cut-Normal,	-1°C, In water	82.34	82.34	2.08	2.91	3.15	3.04	0
4009	Vertical,	Cut-Normal,	-1°C	8.30	16.77	2.01	2.67	3.16	2.96	51
4010	Vertical,	Cut-Parallel,	-1°C	3.93	5.83	2.03	2.31	3.23	2.87	33
4011	Horizontal,	Bottom,	-1°C	48.37	48.37	2.06	3.39	3.54	3.45	0
4012	Vertical,	Cut-Normal,	-1°C, In water	47.53	47.53	2.02	2.75	3.29	3.09	0
4013	Horizontal,	Cut-Normal,	-1°C	35.76	50.28	2.11	2.90	3.12	3.04	29
4014	Horizontal,	Cut-Normal,	-1°C, In water	54.84	55.70	1.98	3.22	3.18	3.17	2
4015	Vertical,	Cut-Normal,	-1°C	9.93	17.52	2.03	2.65	2.92	2.81	43
4016	Vertical,	Cut-Parallel,	-1°C	10.96	25.13	2.01	2.09	2.84	2.57	56
4017	Vertical,	Cut-Normal,	-1°C, In water	48.13	48.13	1.98	2.70	2.88	2.79	0
4018	Horizontal,	Bottom,	-1°C	78.70	80.00	2.03	2.98	3.20	3.09	2
4019	Horizontal,	Cut-Normal,	-1°C, In water	77.43	77.43	2.04	2.81	3.18	2.79	0
4020	Vertical,	Cut-Normal,	-1°C, In water	30.35	30.35	2.10	2.55	2.96	2.63	0
4021	Horizontal,	Bottom,	-1°C	63.93	64.82	2.05	2.99	3.17	3.09	1
4022	Horizontal,	Cut-Normal,	-1°C, In water	94.91	94.91	1.93	2.59	3.25	2.76	0

Test #	Configuration				$\tau_{fb,nom}$ [kPa]	$\tau_{fb,real}$	$\bar{V}$ [mm/s]	S_U	S_L [ppt]	S_{tot}	A_{ub} [%]
4023	Vertical,	Cut-Normal,	-1°C,	In water	36.91	36.91	2.03	2.77	3.10	2.92	0
4024	Horizontal,	Bottom,	-1°C		77.98	79.47	1.96	3.06	3.19	3.07	2
5000	Vertical,	Cut-Normal,	-1°C		5.36	7.47	2.07	2.39	2.27	2.30	28
5001	Horizontal,	Cut-Normal,	-1°C					1.81	1.68		35
	Remark: The freeze-bond failed during assembling of sample in test-frame.										
5002	Vertical,	Cut-Normal,	-1°C		14.24	22.58	2.09	2.07	2.57	2.35	37
5003	Horizontal,	Cut-Normal,	-1°C		23.04	27.15	1.98	2.79	3.00	2.90	15
5004	Vertical,	Cut-Normal,	-1°C		23.47	35.72	1.96	2.45	2.65	2.55	34
5005	Horizontal,	Cut-Normal,	-1°C		15.25	24.74	1.96	2.66	3.04	2.88	38
5006	Vertical,	Cut-Normal,	-1°C		4.93	9.93	2.08	2.47	1.88	2.09	48
	Remark: Freeze-bond formed from transparent ice-blocks.										
5007	Horizontal,	Cut-Normal,	-1°C		1.94	3.52	1.95	1.34	1.47	1.41	45
	Remark: Freeze-bond formed from transparent ice-blocks.										
5008	Vertical,	Cut-Normal,	-1°C		13.83	19.70	2.06	2.34	2.57		30
5009	Horizontal,	Cut-Normal,	-1°C		19.44	30.96	2.10	2.90	2.93	2.91	37
5010	Vertical,	Cut-Normal,	-1°C		8.36	12.46	2.01	2.25	2.55	2.41	33
5011	Horizontal,	Cut-Normal,	-1°C		32.84	46.09	2.09	2.67	2.73	2.69	29
6000	Vertical,	Cut-Parallel,	-1°C,	Stored	63.68	78.37	2.02	2.73	3.17	2.99	19
6001	Vertical,	Cut-Parallel,	-1°C,	Stored	24.55	40.63	1.98	2.81	3.04	2.92	40
6002	Vertical,	Cut-Parallel,	-1°C,	Stored	16.90	27.87	2.05	2.65	3.01	2.86	39
6003	Vertical,	Cut-Parallel,	-1°C,	Stored	14.28	24.62	2.08	2.92	3.06	2.97	42
6004	Vertical,	Cut-Parallel,	-1°C,	Stored	14.70	24.49	2.04	2.58	3.02	2.83	40
6005	Vertical,	Cut-Parallel,	-1°C,	Stored	6.65	9.70	2.01	2.84	2.82	2.82	31
6006	Vertical,	Cut-Parallel,	-1°C,	Stored	10.37	18.99	2.03	2.66	2.95	2.83	45
6007	Vertical,	Cut-Parallel,	-1°C,	Stored	9.72	13.48	1.99	2.64	2.97	2.84	28

Test #	Configuration				$\tau_{fb,nom}$ [kPa]	$\tau_{fb,real}$ [kPa]	$\bar{V}$ [mm/s]	S_U [ppt]	S_L [ppt]	S_{tot}	A_{ub} [%]
6008	Vertical,	Cut-Parallel,	-1°C,	Stored	14.27	22.97	2.03	2.75	2.98	2.90	38
6009	Vertical,	Cut-Parallel,	-1°C,	Stored	16.13	19.01	2.05	2.66	2.94	2.80	15
6010	Vertical,	Cut-Normal,	-1°C		38.27	61.64	2.14	3.01	3.18	3.08	38
6011	Horizontal,	Cut-Normal,	-1°C,	In water	71.29	71.29	2.05	2.37	3.36	2.97	0
6012	Vertical,	Cut-Normal,	-1°C,	In water	28.73	28.73	1.93	3.05	3.05	3.05	0
6013	Horizontal,	Cut-Normal,	-1°C,	In water	67.31	67.31	2.11	2.86	3.08	2.97	0
6014	Vertical,	Cut-Normal,	-1°C,	In water	23.82	23.82	2.04	3.04	2.87	2.95	0
6015	Horizontal,	Cut-Normal,	-1°C,	In water	74.40	74.40	2.03	2.89	2.50	2.65	0
6016	Vertical,	Cut-Normal,	-1°C,	In water	41.33	41.33	1.99	3.01	2.94	2.94	0
6017	Horizontal,	Cut-Normal,	-1°C,	In water	68.92	68.92	2.01	2.61	2.77		0
6018	Vertical,	Cut-Normal,	-1°C,	In water	26.18	26.18	2.03	2.69	2.66	2.67	0
6019	Horizontal,	Cut-Normal,	-1°C,	In water	71.29	71.29	2.03	2.37	3.36	2.97	0
6020	Vertical,	Cut-Normal,	-1°C,	In water	27.03	27.03	1.97	2.61	2.91	2.75	0
6021	Horizontal,	Cut-Normal,	-1°C,	In water	75.14	75.14	2.05	2.37	2.74	2.55	0
6022	Vertical,	Cut-Normal,	-1°C,	In water	56.32	56.32	2.07	2.64	2.96	2.84	0
6023	Horizontal,	Cut-Normal,	-1°C,	In water	59.06	59.06	2.00	2.65	2.97	2.84	0
6024	Vertical,	Cut-Normal,	-1°C,	In water	23.34	23.34	2.03	2.75	3.07	2.96	0
6025	Vertical,	Cut-Parallel,	-1°C,	Stored	12.48	18.57	2.06	2.70	3.43	2.91	33
6026	Vertical,	Cut-Parallel,	-1°C,	Stored	12.48	25.82	2.03				52
6027	Vertical,	Cut-Parallel,	-1°C,	Stored	10.00	15.35	2.02				35
7000	Horizontal,	Bottom,	-1°C		27.54	27.80	2.07	3.23	3.14	3.15	1
7001	Horizontal,	Cut-Normal,	-1°C		4.83	9.13	2.11	2.04	1.41	1.65	47
7002	Vertical,	Cut-Parallel,	-1°C,		16.70	32.85	2.03	2.63	2.02	2.24	49
7003	Vertical,	Cut-Normal,	-1°C		2.41	3.30	2.10	1.09	1.68	1.42	27
7004	Horizontal,	Bottom,	-1°C		10.91	10.91	2.05	3.23	1.68	2.30	0

Test #	Configuration			$\tau_{fb,nom}$ [kPa]	$\tau_{fb,real}$	$\bar{V}$ [mm/s]	S_U	S_L [ppt]	S_{tot}	A_{ub} [%]
7005	Horizontal,	Cut-Normal,	-1°C	28.54	43.93	1.98	2.87	2.44	2.57	35
7006	Vertical,	Cut-Parallel,	-1°C,	6.07	8.20	2.02	1.11	1.51	1.34	26
7007	Vertical,	Cut-Normal,	-1°C	6.05	7.92	2.07	1.10	1.89	1.55	24
7008	Horizontal,	Bottom,	-1°C	7.05	7.05	2.10	2.47	1.89	2.07	0
7009	Horizontal,	Cut-Normal,	-1°C	16.10	19.92	1.96	2.73	2.25	2.40	19
7010	Vertical,	Cut-Parallel,	-1°C,	3.23	7.90	2.01	2.03	1.46	1.67	59
7011	Vertical,	Cut-Normal,	-1°C	5.79	9.99	2.05	1.06	1.84	1.52	42
7012	Horizontal,	Bottom,	-1°C	14.18	14.18	2.04	2.62	2.07	2.23	0
7013	Horizontal,	Cut-Normal,	-1°C	16.17	21.44	1.99	2.39	1.65	1.91	25
7014	Vertical,	Cut-Parallel,	-1°C,	6.42	18.49	1.91	1.11	1.71	1.41	65
7015	Vertical,	Cut-Normal,	-1°C	12.00	20.97	2.07	0.96	1.65	1.42	43
7016	Horizontal,	Bottom,	-1°C	24.10	24.10	2.00	2.62	2.94	2.89	0
7017	Horizontal,	Cut-Normal,	-1°C	35.25	42.16	1.97	2.76	2.00	2.34	16
7018	Vertical,	Cut-Parallel,	-1°C,	19.87	47.69	2.03	1.01	1.74	1.47	58
7019	Vertical,	Cut-Normal,	-1°C	4.33	10.37	2.04	0.91	1.70		58
7020	Horizontal,	Bottom,	-1°C	7.36	7.36	2.08	3.11	1.50	2.15	0
7016	Horizontal,	Bottom,	-1°C	6.73	6.73	2.05	3.00	1.60	2.16	0
100	NTNU-frame,	Top		35.00	38.16	2.23	2.7	3.3		8
101	NTNU-frame,	Bottom		40.08	40.08	2.19	2.1			0
102	NTNU-frame,	Top		44.64	53.54	2.14	2.6	2.9		17
103	NTNU-frame,	Bottom		25.50	25.70	2.04	2.4	2.8		1
104	NTNU-frame,	Top		24.66	25.43	2.03	2.6	2.7		3
105	NTNU-frame,	Bottom		22.71	22.71	2.04	2.5	3.0		0
106	NTNU-frame,	Top		46.78	48.79	2.04				4
107	NTNU-frame,	Bottom		18.47	18.47	2.04	2.3	2.8		0

Test #	Configuration		$\tau_{fb,nom}$ [kPa]	$\tau_{fb,real}$ [kPa]	$\bar{V}$ [mm/s]	S_U	S_L [ppt]	S_{tot}	A_{ub} [%]
108	NTNU-frame,	Top	52.16	54.64	2.03		3.0		5
109	NTNU-frame,	Bottom	48.80	50.05	2.03		2.7		3
110	NTNU-frame,	Bottom	40.04	40.22	2.03	2.4	2.7		0
111	NTNU-frame,	Top	42.79	47.88	2.02	2.8	3.0		11
112	NTNU-frame,	Bottom	40.77	40.94	2.03	2.5	2.9		0
113	NTNU-frame,	Top	56.51	56.51	2.03	2.6	3.2		0
200	HSVA-frame,	Bottom							
	Remark: Lower ice-block got vertical fracture before the freeze-bond failed.								
201	HSVA-frame,	Bottom	20.69	21.97	2.21	2.6	2.7		6
202	HSVA-frame,	Bottom						2.7	
	Remark: Lower ice-block got vertical fracture before the freeze-bond failed.								
203	HSVA-frame,	Bottom	22.93	23.74	2.24	2.7	2.7		3
204	HSVA-frame,	Bottom	37.17	37.57	1.60	2.6	2.7		1
205	HSVA-frame,	Bottom	30.29	33.21	2.12	2.6	2.8		9
206	HSVA-frame,	Bottom	18.89	22.13	2.26	2.4	2.7		15
207	HSVA-frame,	Bottom	30.78	31.23	2.11	2.5	2.8		1
208	HSVA-frame,	Bottom	19.15	19.15	2.26	2.5	2.7		0
209	HSVA-frame,	Bottom	51.12	51.24	2.13	2.4	2.6		0
	Remark: Vertical pressure added by hand to rear end of lid.								
210	HSVA-frame,	Bottom	22.15	24.26	2.27	2.6	2.7		9
211	HSVA-frame,	Bottom	55.15	55.65	2.13	2.5	2.6		1
	Remark: Vertical pressure added by hand to rear end of lid.								
212	HSVA-frame,	Bottom	18.91	18.98	2.20	2.6	2.7		0
213	NTNU-frame,	Top	45.55	49.02	2.45	2.6	3.1		7
214	NTNU-frame,	Bottom	40.63	48.76	2.18	2.5	2.6		17

Test #	Configuration			$\tau_{fb,nom}$ [kPa]	$\tau_{fb,real}$	$\bar{V}$ [mm/s]	S_U	S_L [ppt]	S_{tot}	A_{ub} [%]
215	NTNU-frame,	Top					2.7	3.1		14
	Remark: Collision between piston and vertical fixing system.									
216	NTNU-frame,	Top		33.10	56.38	2.28	2.6	2.8		41
217	NTNU-frame,	Bottom		19.27	20.89	2.17	2.4	2.8		8
218	NTNU-frame,	Top		64.45	69.68	2.11	2.7	3.0		8
219	NTNU-frame,	Bottom		16.45	16.45	2.09	2.6	2.8		0
220	NTNU-frame,	Top		51.05	53.74	2.08	2.6	3.0		5
221	NTNU-frame,	Bottom		25.74	25.74	2.05	2.6	2.7		0
222	NTNU-frame,	Top		54.84	54.84	2.04	2.8	2.7		0
223	NTNU-frame,	Bottom		29.57	29.57	2.05	2.4	2.7		0
300	HSVA-frame,	Bottom,	Stored						2.4	
	Remark: Lower ice-block got vertical fracture before the freeze-bond failed.									
301	HSVA-frame,	Bottom,	Stored	41.80	47.12	2.24	2.4	2.5		11
	Remark: Vertical pressure added by hand to rear end of lid.									
302	HSVA-frame,	Bottom,	Stored	24.24	24.87	2.27	2.5	2.7		3
303	HSVA-frame,	Bottom,	Stored	36.12	37.16	2.20	2.4	2.6		3
304	HSVA-frame,	Bottom,	Stored	37.30	37.63	2.18	2.3	2.5		1
305	HSVA-frame,	Bottom,	Stored	34.33	34.67	1.79	2.4	2.6		1
306	HSVA-frame,	Bottom,	Stored	23.52	23.62	1.95	2.5	2.7		0

Appendix B

Freeze-bond thin sections

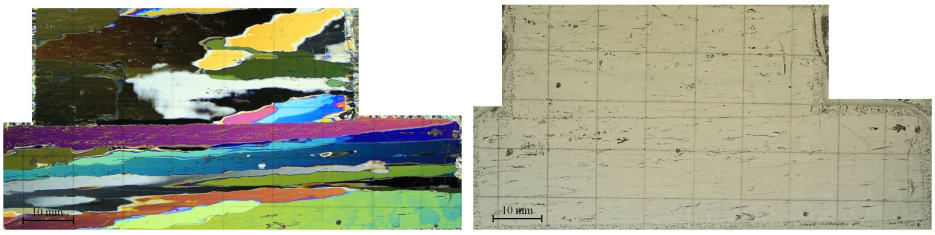

(a) Polarized **(b)** Transparent

Figure B.1: NTNU: Series 1000, Vertical, Cut-Normal, Ice 1

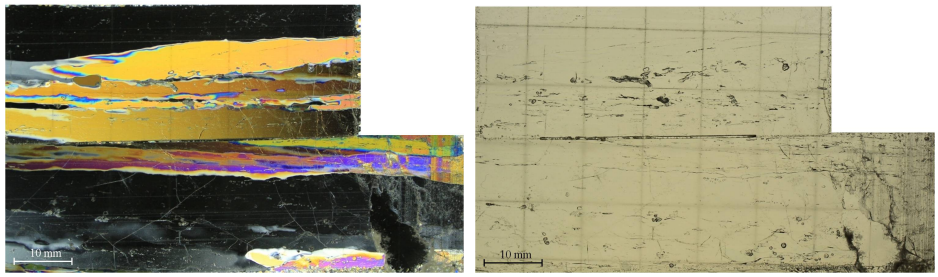

(a) Polarized **(b)** Transparent

Figure B.2: NTNU: Series 1000, Vertical, Cut-Parallel, Ice 1

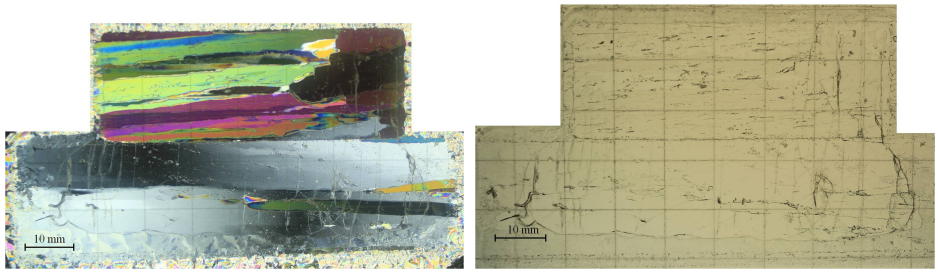

(a) Polarized **(b)** Transparent

Figure B.3: NTNU: Series 4000, Vertical, Cut-Normal, In water, Ice 1

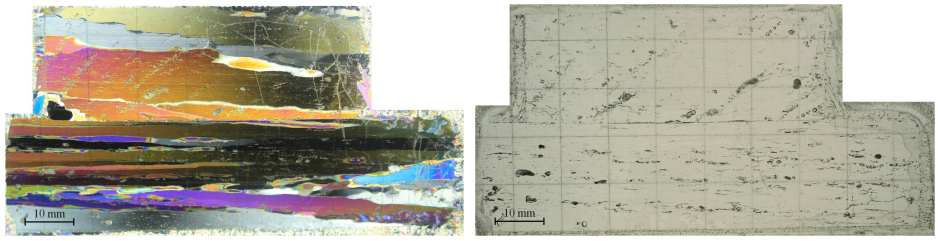

(a) Polarized **(b)** Transparent

Figure B.4: NTNU: Series 4000, Vertical, Cut-Parallel, Ice 1

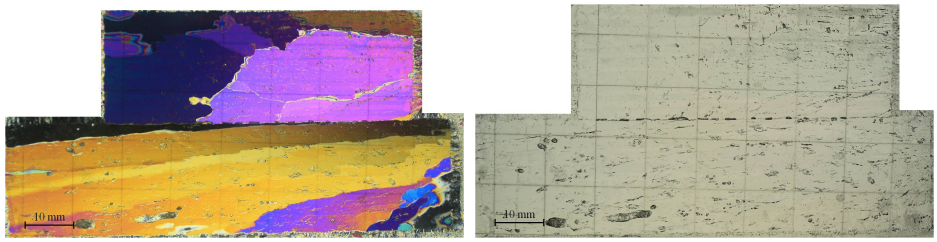

(a) Polarized **(b)** Transparent

Figure B.5: NTNU: Series 5000, Vertical, Cut-Normal, Ice 2

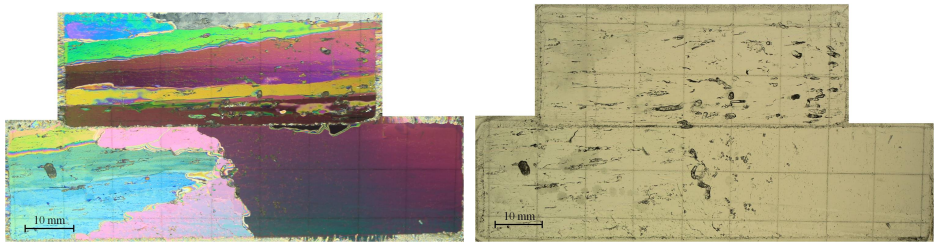

(a) Polarized **(b)** Transparent

Figure B.6: NTNU: Series 5000, Vertical, Cut-Normal, Ice 2

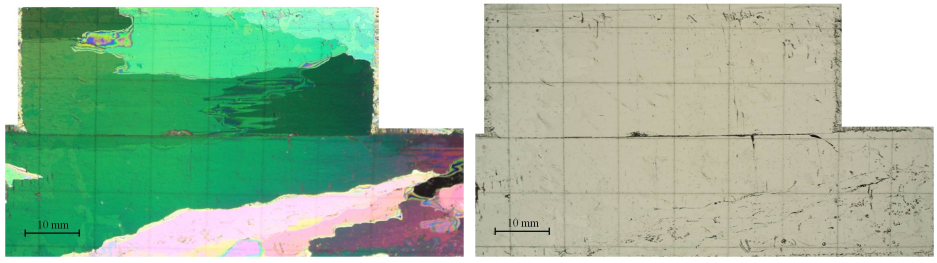

(a) Polarized **(b)** Transparent

Figure B.7: NTNU: Series 5000, Vertical, Cut-Normal, Ice 3

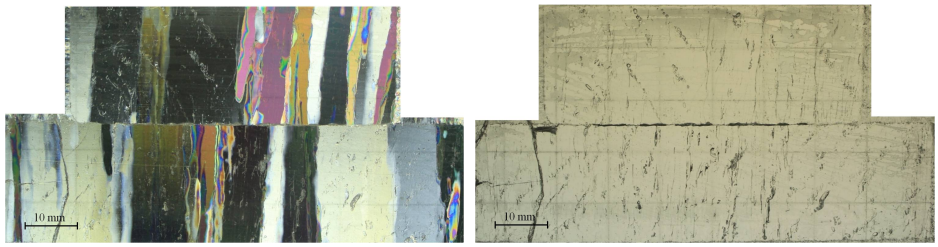

(a) Polarized **(b)** Transparent

Figure B.8: NTNU: Series 2000, Horizontal, Cut-Normal, Ice 1

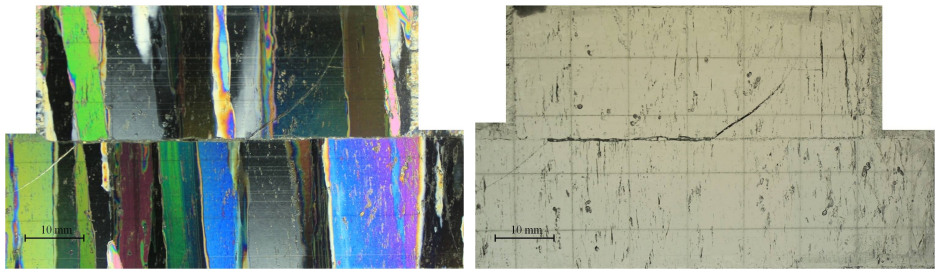

(a) Polarized **(b)** Transparent

Figure B.9: NTNU: Series 2000, Horizontal, Cut-Normal, Ice 1

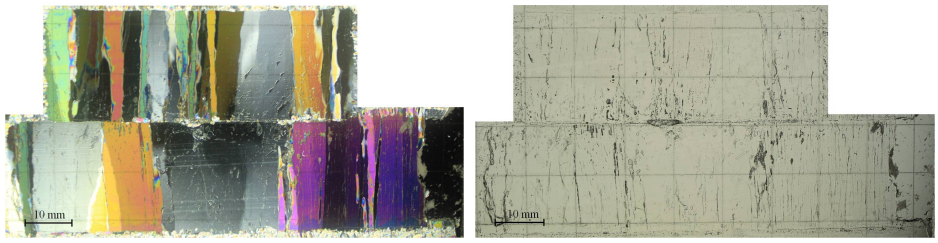

(a) Polarized **(b)** Transparent

Figure B.10: NTNU: Series 4000, Horizontal, Cut-Normal, In water, Ice 1

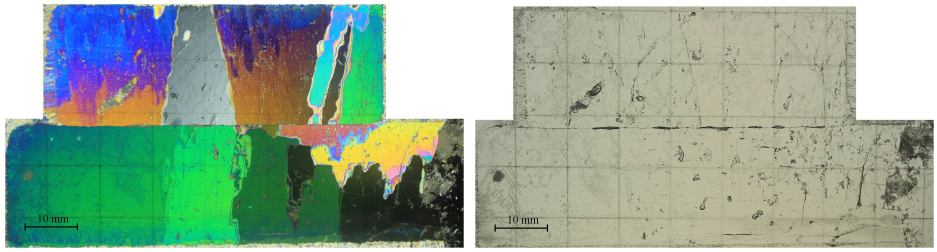

(a) Polarized **(b)** Transparent

Figure B.11: NTNU: Series 5000, Horizontal, Cut-Normal, Ice 2

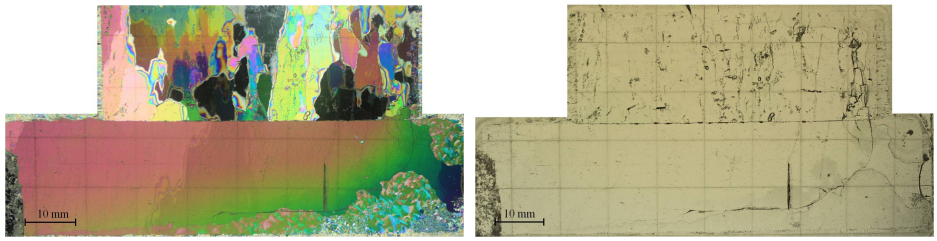

(a) Polarized **(b)** Transparent

Figure B.12: NTNU: Series 5000, Horizontal, Cut-Normal, Ice 2

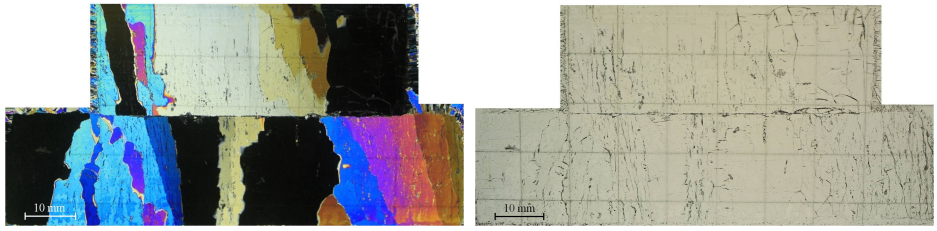

(a) Polarized **(b)** Transparent

Figure B.13: NTNU: Series 7000, Horizontal, Cut-Normal, Ice 3

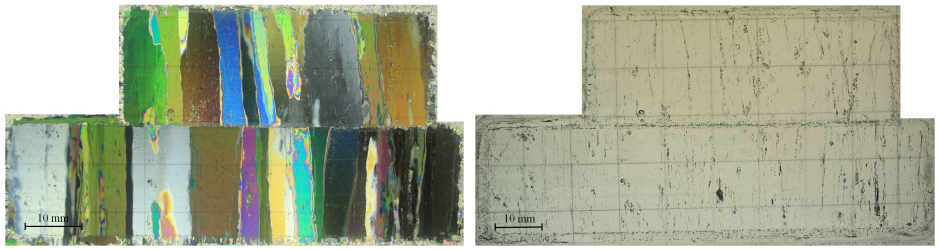

(a) Polarized **(b)** Transparent

Figure B.14: NTNU: Series 4000, Horizontal, Bottom, Ice 1

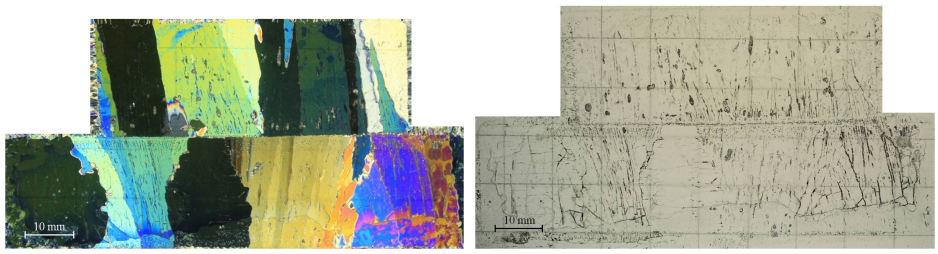

(a) Polarized **(b)** Transparent

Figure B.15: NTNU: Series 7000, Horizontal, Bottom, Ice 3

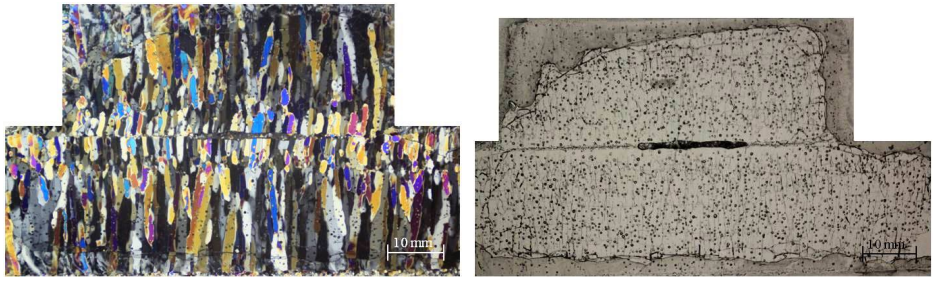

(a) Polarized **(b)** Transparent

Figure B.16: HSVA: NTNU-frame, Top

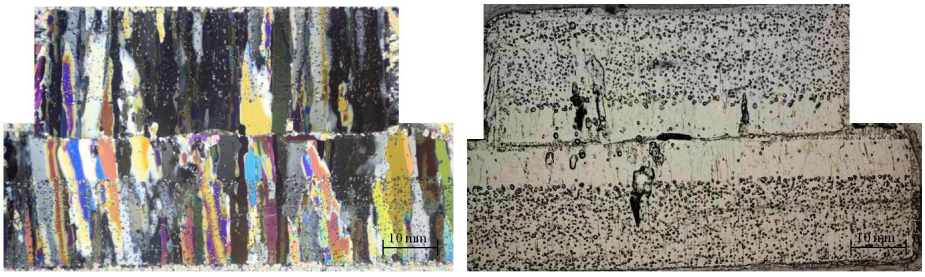

(a) Polarized **(b)** Transparent

Figure B.17: HSVA: NTNU-frame, Bottom

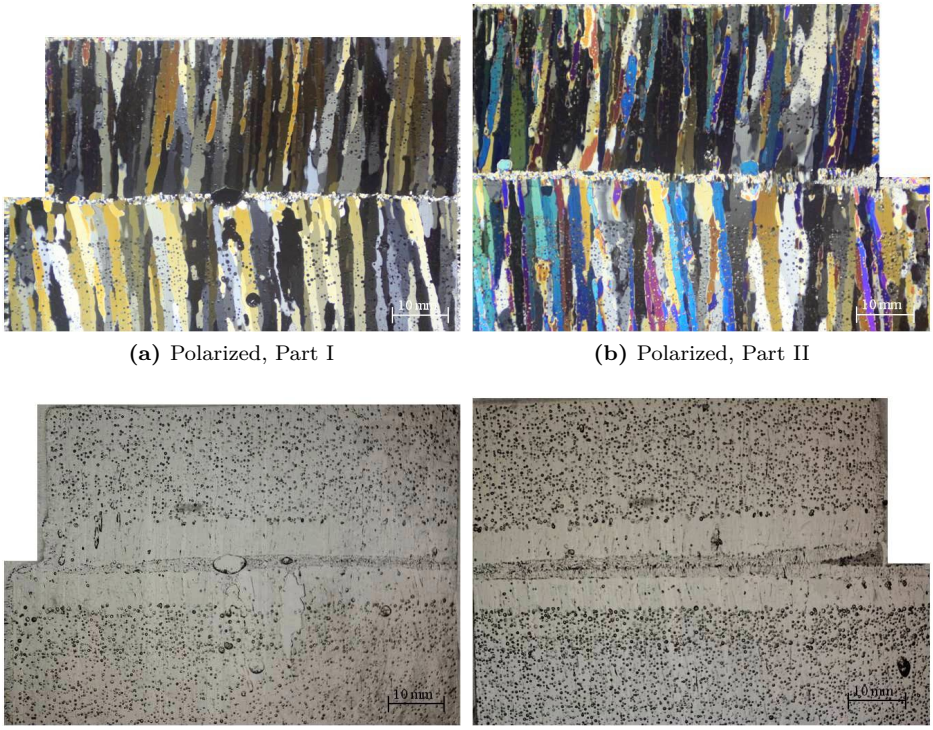

(a) Polarized, Part I

(b) Polarized, Part II

(c) Transparent, Part I

(d) Transparent, Part II

Figure B.18: HSVA: HSVA-frame

Appendix C

Ice-sheet texture

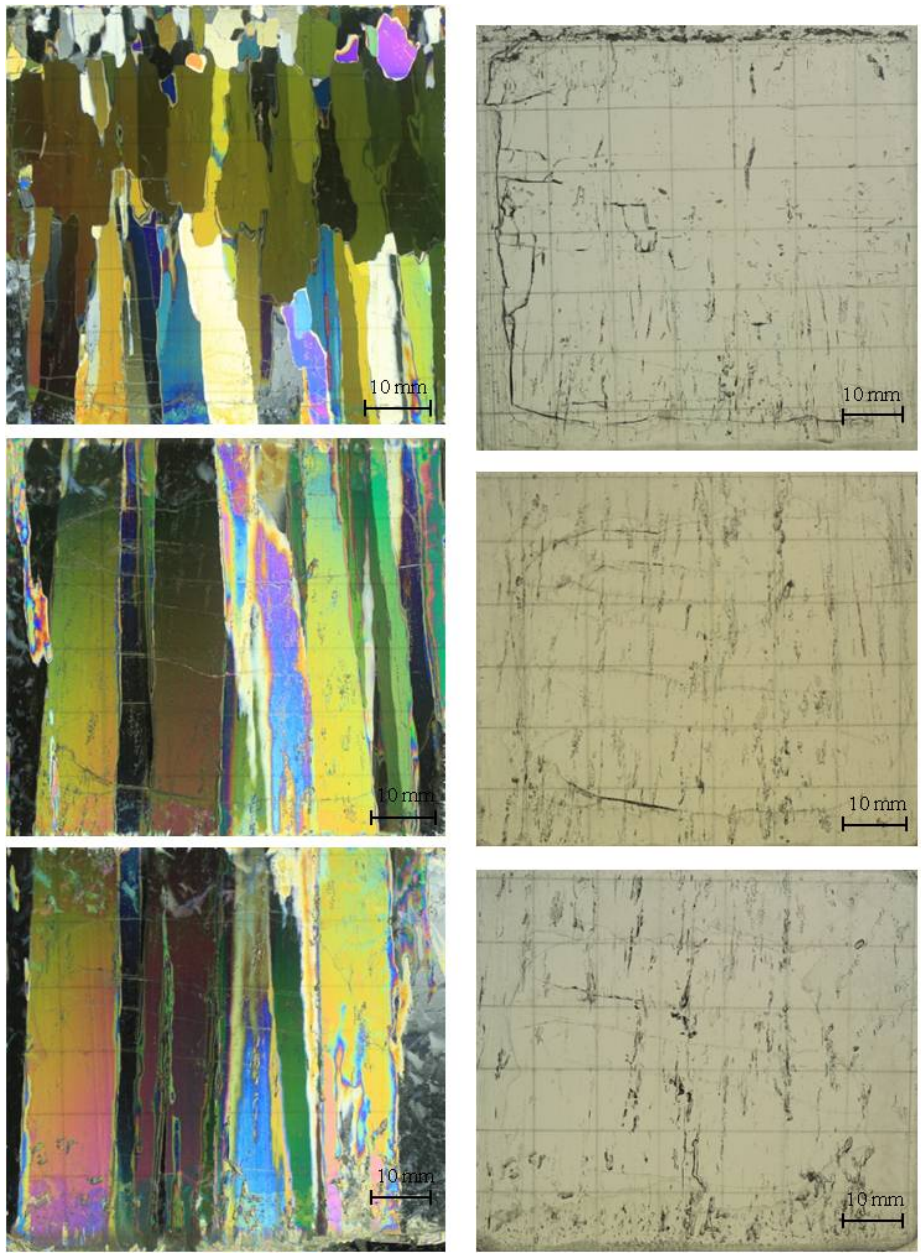

(a) Polarized **(b)** Transparent

Figure C.1: NTNU: Ice 1, Vertical cross-section.

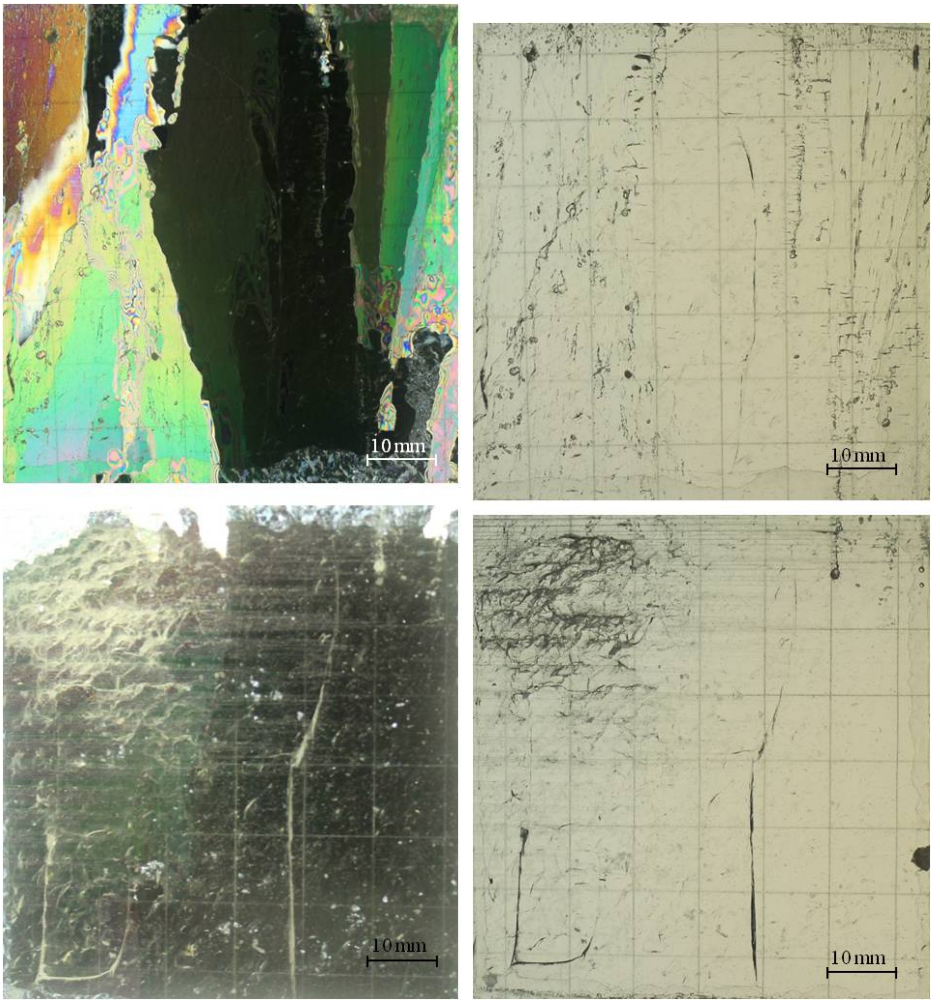

(a) Polarized **(b)** Transparent

Figure C.2: NTNU: Ice 2, Vertical cross-section.

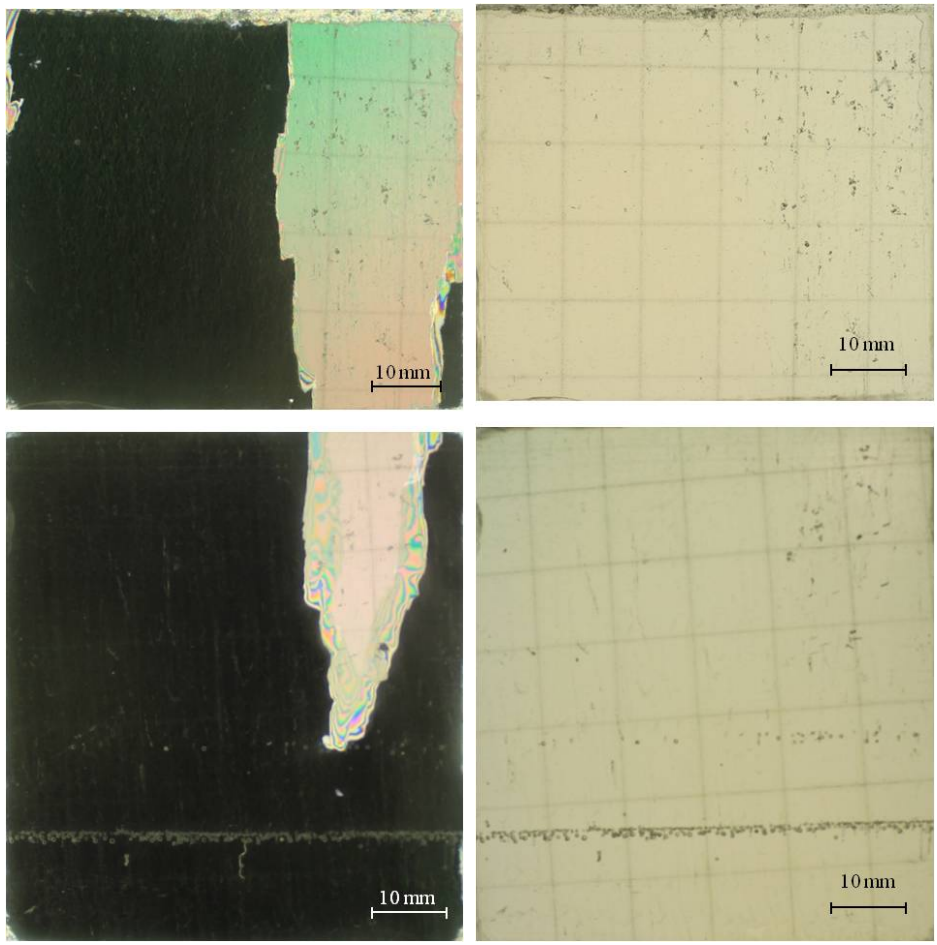

(a) Polarized **(b)** Transparent

Figure C.3: NTNU: Ice 3, Vertical cross-section.

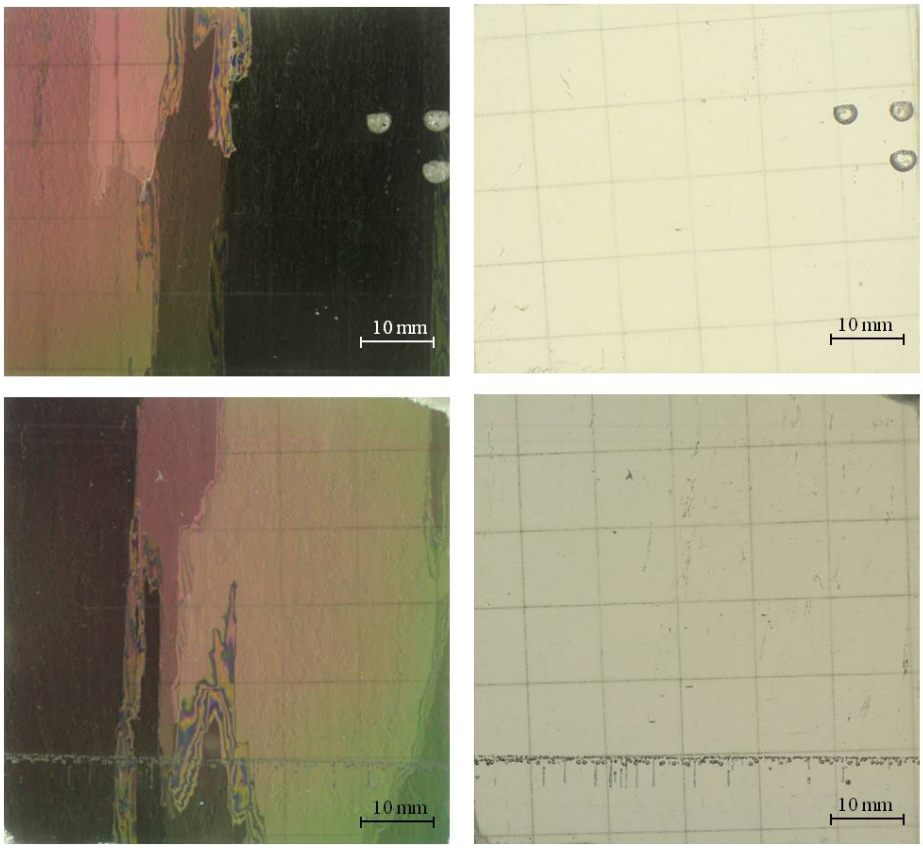

(a) Polarized **(b)** Transparent

Figure C.4: NTNU: Ice 3, Vertical cross-section.

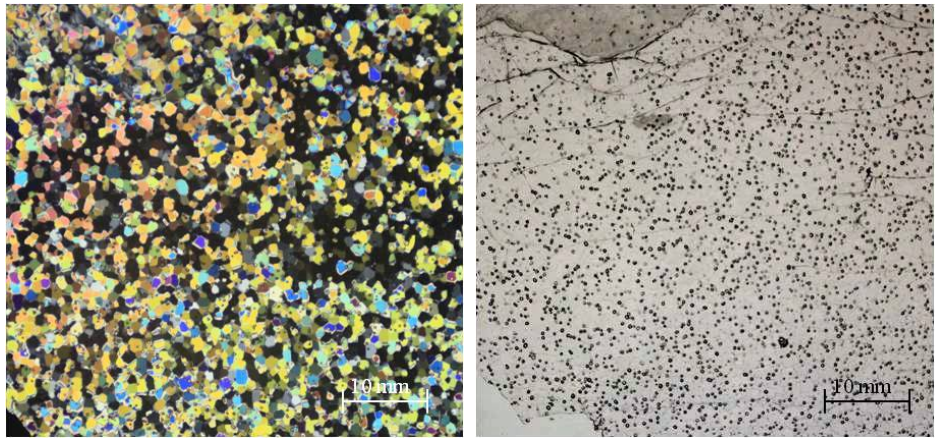

(a) Polarized **(b)** Transparent

Figure C.5: HSVA: Horizontal cross-section, made at the top of the ice-sheet.

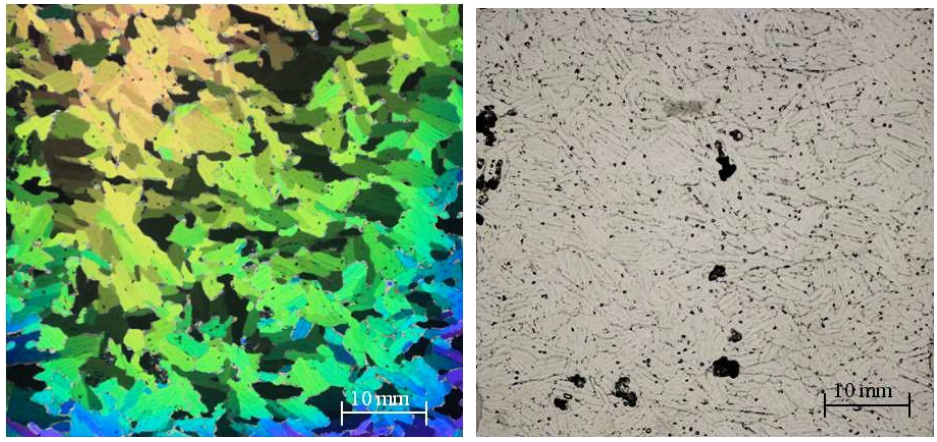

(a) Polarized **(b)** Transparent

Figure C.6: HSVA: Horizontal cross-section, made at the bottom of the ice-sheet.

(a) Polarized

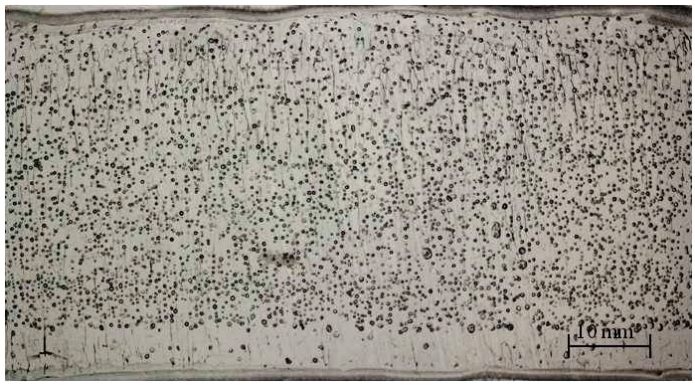

(b) Transparent

Figure C.7: HSVA: Vertical cross-section.

Appendix D

Stress - time/displacement diagrams

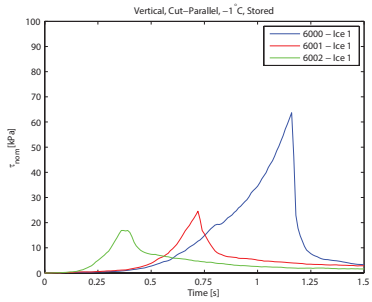
Vertical, Cut–Parallel, –1 °C, Stored
6000 – Ice 1
6001 – Ice 1
6002 – Ice 1
τnom [kPa]
Time [s]

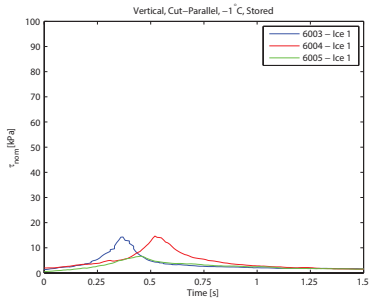
Vertical, Cut–Parallel, –1 °C, Stored
6003 – Ice 1
6004 – Ice 1
6005 – Ice 1
τnom [kPa]
Time [s]

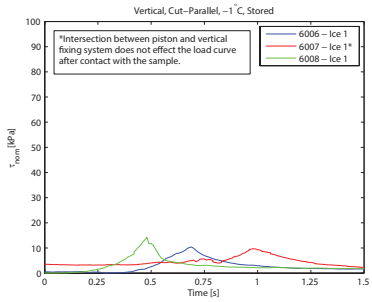
Vertical, Cut–Parallel, –1 °C, Stored
*Intersection between piston and vertical fixing system does not effect the load curve after contact with the sample.
6006 – Ice 1
6007 – Ice 1*
6008 – Ice 1
τnom [kPa]
Time [s]

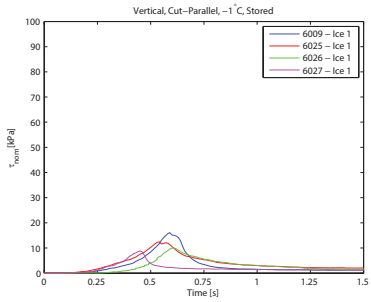
Vertical, Cut–Parallel, –1 °C, Stored
6009 – Ice 1
6025 – Ice 1
6026 – Ice 1
6027 – Ice 1
τnom [kPa]
Time [s]

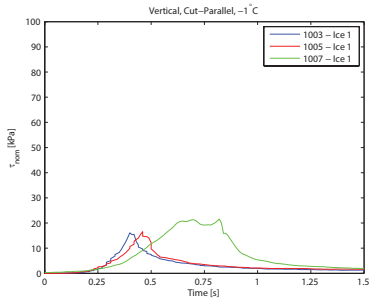
Vertical, Cut–Parallel, –1 °C
1003 – Ice 1
1005 – Ice 1
1007 – Ice 1
τnom [kPa]
Time [s]

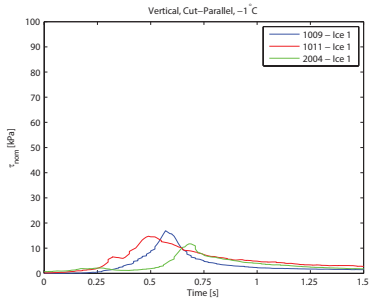
Vertical, Cut–Parallel, –1 °C
1009 – Ice 1
1011 – Ice 1
2004 – Ice 1
τnom [kPa]
Time [s]

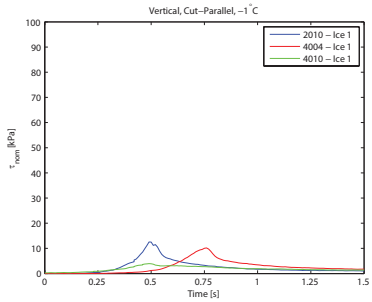
Vertical, Cut–Parallel, –1 °C
2010 – Ice 1
4004 – Ice 1
4010 – Ice 1
τnom [kPa]
Time [s]

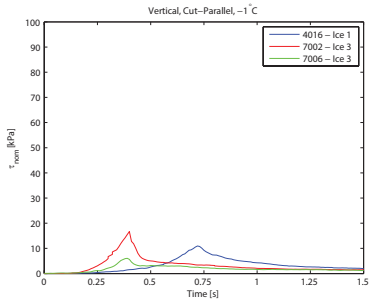
Vertical, Cut–Parallel, –1 °C
4016 – Ice 1
7002 – Ice 3
7006 – Ice 3
τnom [kPa]
Time [s]

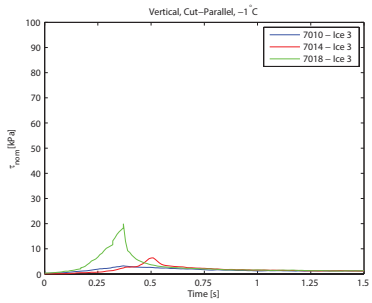
Vertical, Cut–Parallel, –1°C
7010 – Ice 3
7014 – Ice 3
7018 – Ice 3
τnom [kPa]
Time [s]

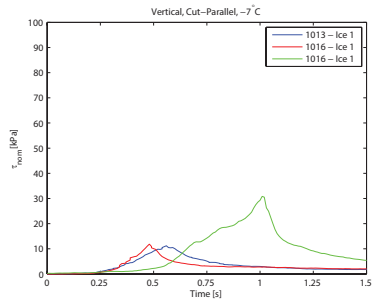
Vertical, Cut–Parallel, –7°C
1013 – Ice 1
1016 – Ice 1
1016 – Ice 1
τnom [kPa]
Time [s]

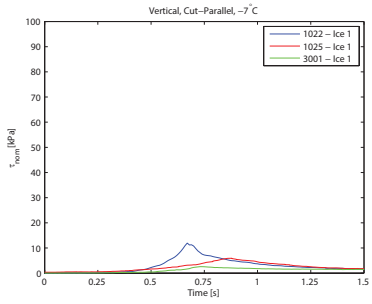
Vertical, Cut–Parallel, –7°C
1022 – Ice 1
1025 – Ice 1
3001 – Ice 1
τnom [kPa]
Time [s]

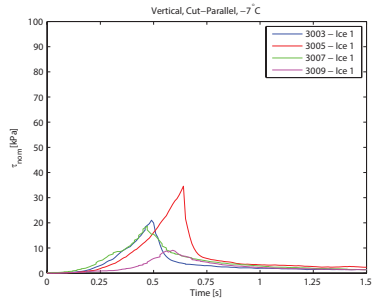
Vertical, Cut–Parallel, –7°C
3003 – Ice 1
3005 – Ice 1
3007 – Ice 1
3009 – Ice 1
τnom [kPa]
Time [s]

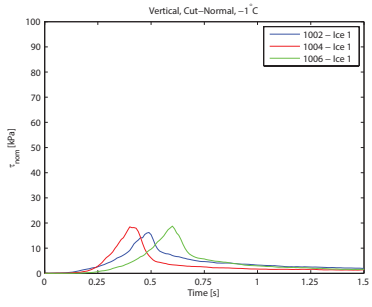
Vertical, Cut–Normal, –1°C
1002 – Ice 1
1004 – Ice 1
1006 – Ice 1
τnom [kPa]
Time [s]

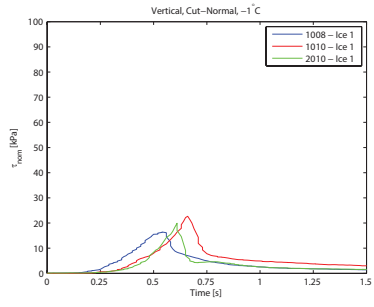
Vertical, Cut–Normal, –1°C
1008 – Ice 1
1010 – Ice 1
2010 – Ice 1
τnom [kPa]
Time [s]

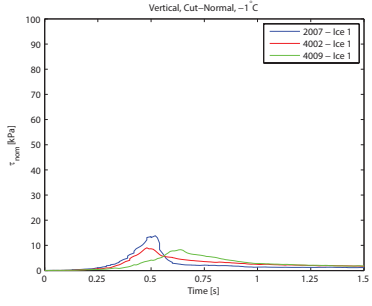
Vertical, Cut–Normal, –1°C
2007 – Ice 1
4002 – Ice 1
4009 – Ice 1
τnom [kPa]
Time [s]

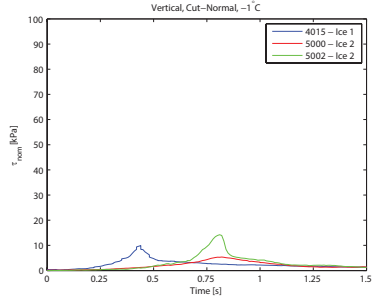
Vertical, Cut–Normal, –1°C
4015 – Ice 1
5000 – Ice 2
5002 – Ice 2
τnom [kPa]
Time [s]

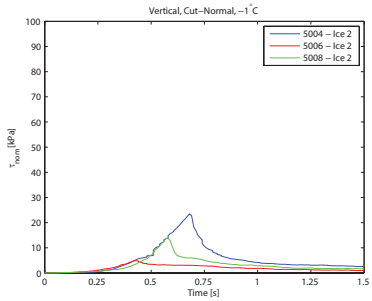
Vertical, Cut–Normal, –1°C
5004 – Ice 2
5006 – Ice 2
5008 – Ice 2
τnorm [kPa]
Time [s]

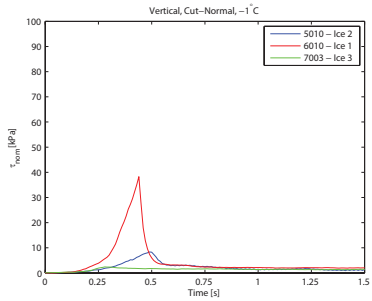
Vertical, Cut–Normal, –1°C
5010 – Ice 2
6010 – Ice 1
7003 – Ice 3
τnorm [kPa]
Time [s]

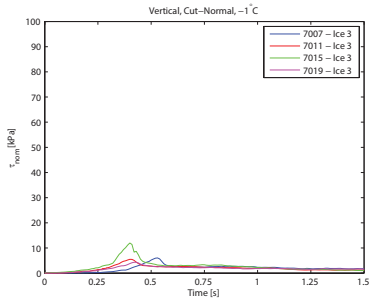
Vertical, Cut–Normal, –1°C
7007 – Ice 3
7011 – Ice 3
7015 – Ice 3
7019 – Ice 3
τnorm [kPa]
Time [s]

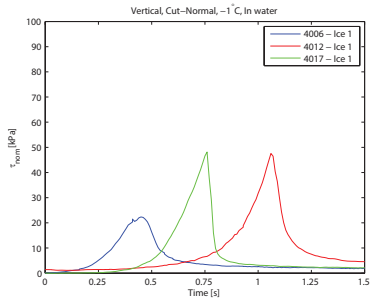
Vertical, Cut–Normal, –1°C, In water
4006 – Ice 1
4012 – Ice 1
4017 – Ice 1
τnorm [kPa]
Time [s]

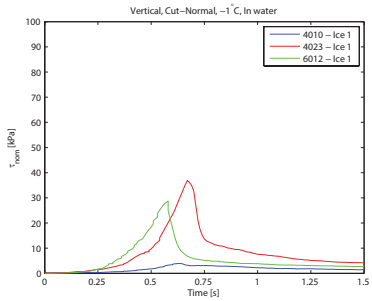
Vertical, Cut–Normal, –1°C, In water
4010 – Ice 1
4023 – Ice 1
6012 – Ice 1
τnorm [kPa]
Time [s]

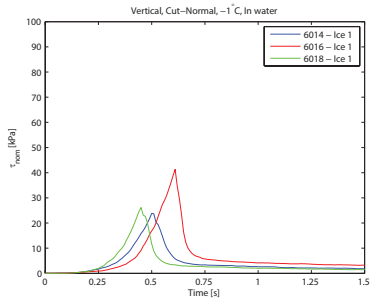
Vertical, Cut–Normal, –1°C, In water
6014 – Ice 1
6016 – Ice 1
6018 – Ice 1
τnorm [kPa]
Time [s]

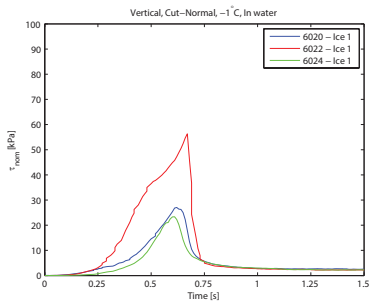
Vertical, Cut–Normal, –1°C, In water
6020 – Ice 1
6022 – Ice 1
6024 – Ice 1
τnorm [kPa]
Time [s]

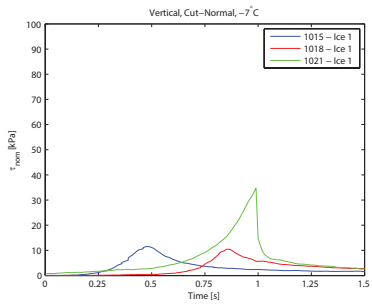
Vertical, Cut–Normal, –7°C
1015 – Ice 1
1018 – Ice 1
1021 – Ice 1
τnorm [kPa]
Time [s]

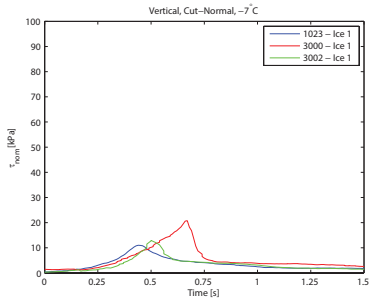
Vertical, Cut–Normal, –7°C
1023 – Ice 1
3000 – Ice 1
3002 – Ice 1
τnom [kPa]
Time [s]

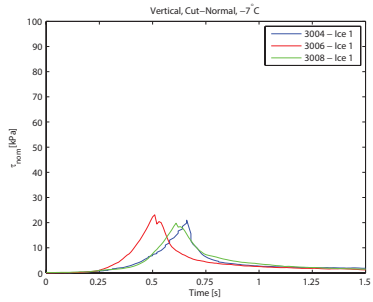
Vertical, Cut–Normal, –7°C
3004 – Ice 1
3006 – Ice 1
3008 – Ice 1
τnom [kPa]
Time [s]

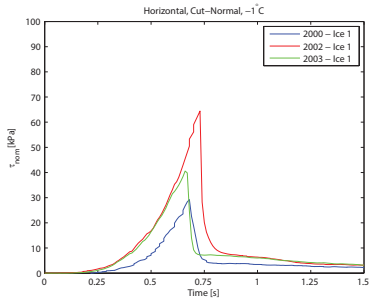
Horizontal, Cut–Normal, –1°C
2000 – Ice 1
2002 – Ice 1
2003 – Ice 1
τnom [kPa]
Time [s]

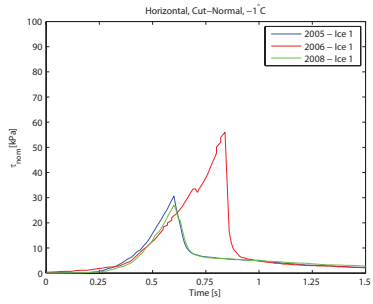
Horizontal, Cut–Normal, –1°C
2005 – Ice 1
2006 – Ice 1
2008 – Ice 1
τnom [kPa]
Time [s]

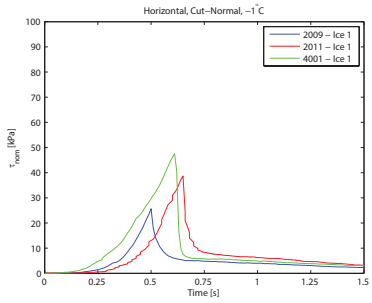
Horizontal, Cut–Normal, –1°C
2009 – Ice 1
2011 – Ice 1
4001 – Ice 1
τnom [kPa]
Time [s]

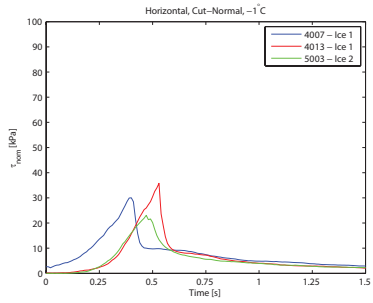
Horizontal, Cut–Normal, –1°C
4007 – Ice 1
4013 – Ice 1
5003 – Ice 2
τnom [kPa]
Time [s]

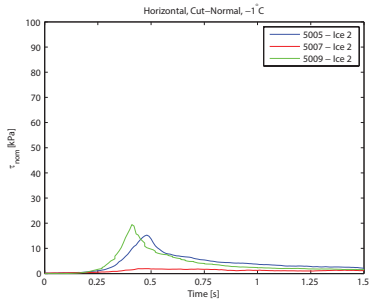
Horizontal, Cut–Normal, –1°C
5005 – Ice 2
5007 – Ice 2
5009 – Ice 2
τnom [kPa]
Time [s]

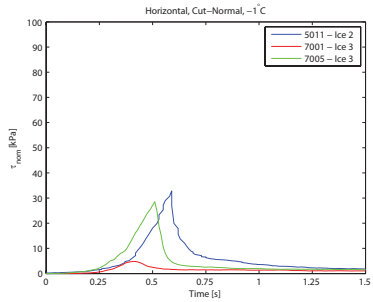
Horizontal, Cut–Normal, –1°C
5011 – Ice 2
7001 – Ice 3
7005 – Ice 3
τnom [kPa]
Time [s]

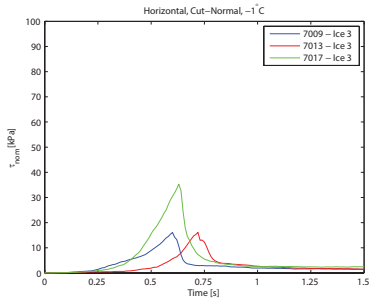
Horizontal, Cut–Normal, –1°C
7009 – Ice 3
7013 – Ice 3
7017 – Ice 3
τnorm [kPa]
Time [s]

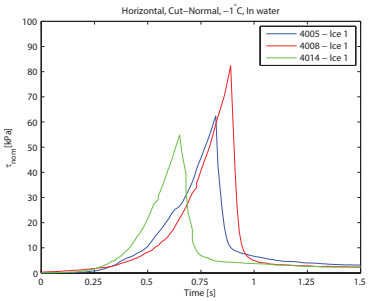
Horizontal, Cut–Normal, –1°C, In water
4005 – Ice 1
4008 – Ice 1
4014 – Ice 1
τnorm [kPa]
Time [s]

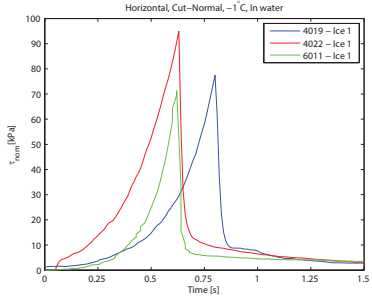
Horizontal, Cut–Normal, –1°C, In water
4019 – Ice 1
4022 – Ice 1
6011 – Ice 1
τnorm [kPa]
Time [s]

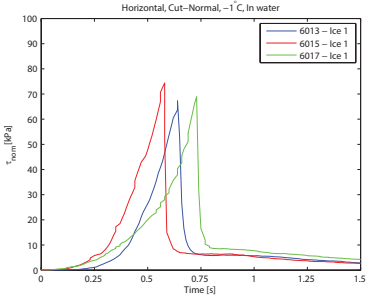
Horizontal, Cut–Normal, –1°C, In water
6013 – Ice 1
6015 – Ice 1
6017 – Ice 1
τnorm [kPa]
Time [s]

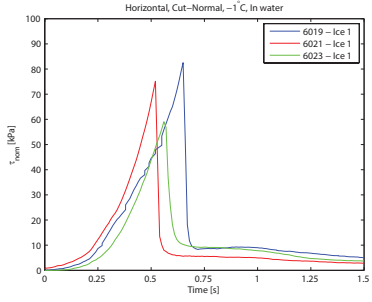
Horizontal, Cut–Normal, –1°C, In water
6019 – Ice 1
6021 – Ice 1
6023 – Ice 1
τnorm [kPa]
Time [s]

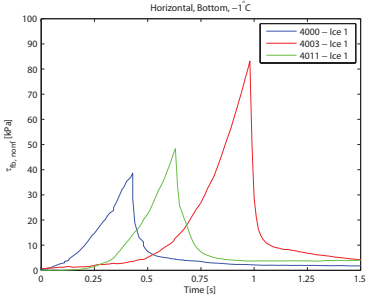
Horizontal, Bottom, –1°C
4000 – Ice 1
4003 – Ice 1
4011 – Ice 1
τfp, norm [kPa]
Time [s]

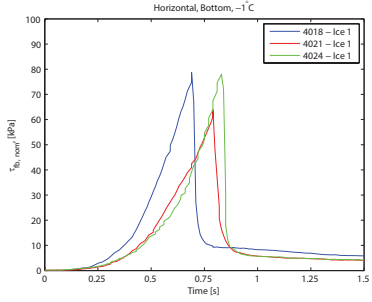
Horizontal, Bottom, –1°C
4018 – Ice 1
4021 – Ice 1
4024 – Ice 1
τfp, norm [kPa]
Time [s]

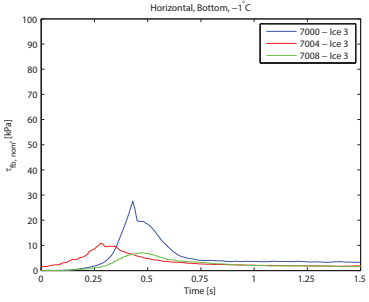
Horizontal, Bottom, –1°C
7000 – Ice 3
7004 – Ice 3
7008 – Ice 3
τfp, norm [kPa]
Time [s]

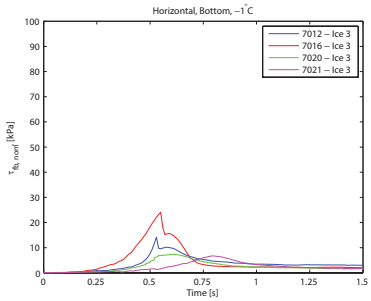
Horizontal, Bottom, –1°C
7012 – Ice 3
7016 – Ice 3
7020 – Ice 3
7021 – Ice 3
τ fit, norm [kPa]
Time [s]

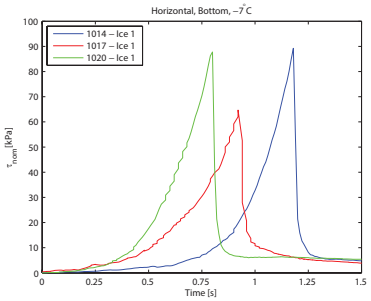
Horizontal, Bottom, –7°C
1014 – Ice 1
1017 – Ice 1
1020 – Ice 1
τ norm [kPa]
Time [s]

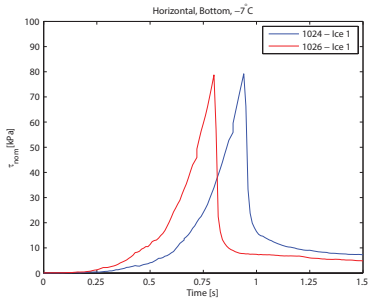
Horizontal, Bottom, –7°C
1024 – Ice 1
1026 – Ice 1
τ norm [kPa]
Time [s]

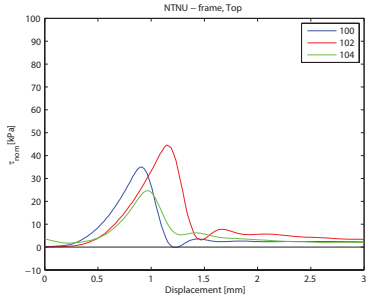
NTNU – frame, Top
100
102
104
τ_{nom} [kPa]
Displacement [mm]

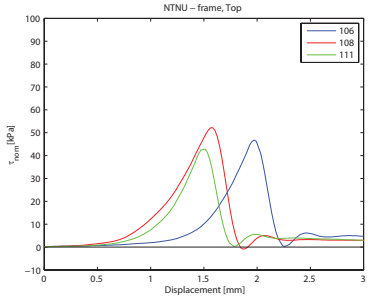
NTNU – frame, Top
106
108
111
τ_{nom} [kPa]
Displacement [mm]

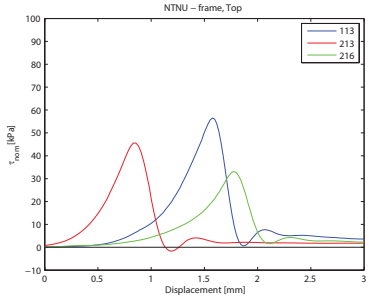
NTNU – frame, Top
113
213
216
τ_{nom} [kPa]
Displacement [mm]

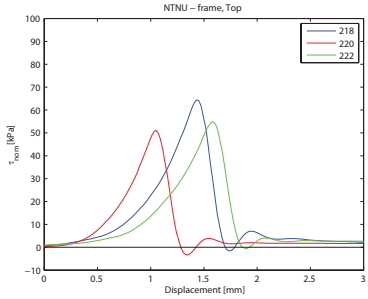
NTNU – frame, Top
218
220
222
τ_{nom} [kPa]
Displacement [mm]

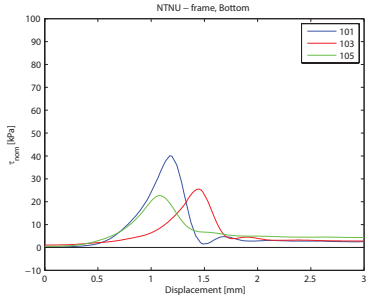
NTNU – frame, Bottom
101
103
105
τ_{nom} [kPa]
Displacement [mm]

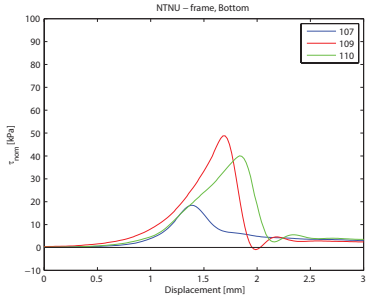
NTNU – frame, Bottom
107
109
110
τ_{nom} [kPa]
Displacement [mm]

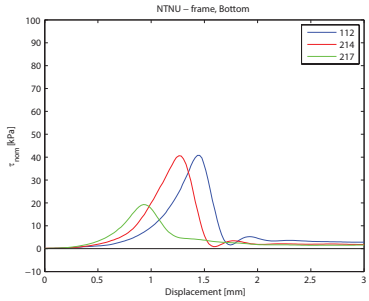
NTNU – frame, Bottom
112
214
217
τ_{nom} [kPa]
Displacement [mm]

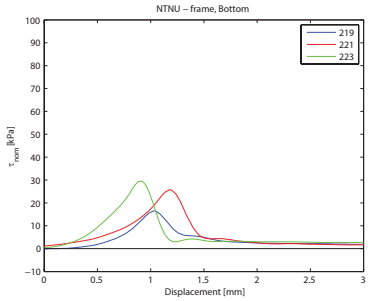
NTNU – frame, Bottom
219
221
223
τ_{nom} [kPa]
Displacement [mm]

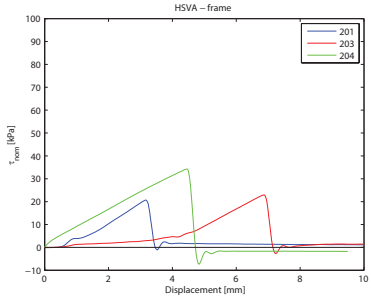
HSVA – frame
201
203
204
τnom [kPa]
Displacement [mm]

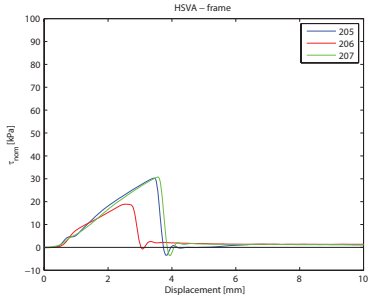
HSVA – frame
205
206
207
τnom [kPa]
Displacement [mm]

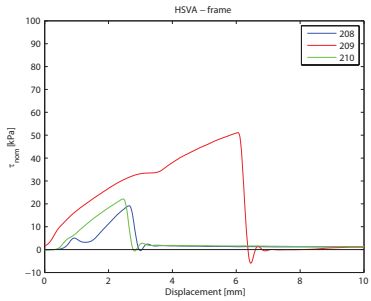
HSVA – frame
208
209
210
τnom [kPa]
Displacement [mm]

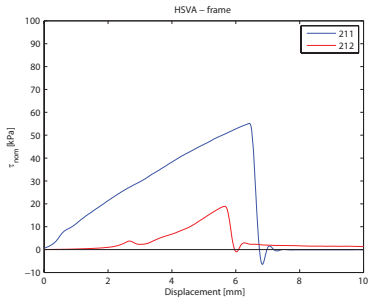
HSVA – frame
211
212
τnom [kPa]
Displacement [mm]

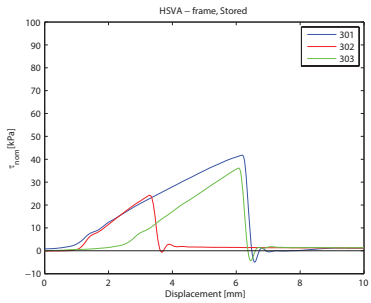
HSVA – frame, Stored
301
302
303
τnom [kPa]
Displacement [mm]

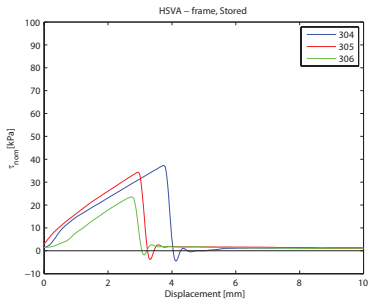
HSVA – frame, Stored
304
305
306
τnom [kPa]
Displacement [mm]

Appendix E

Test frame drawings

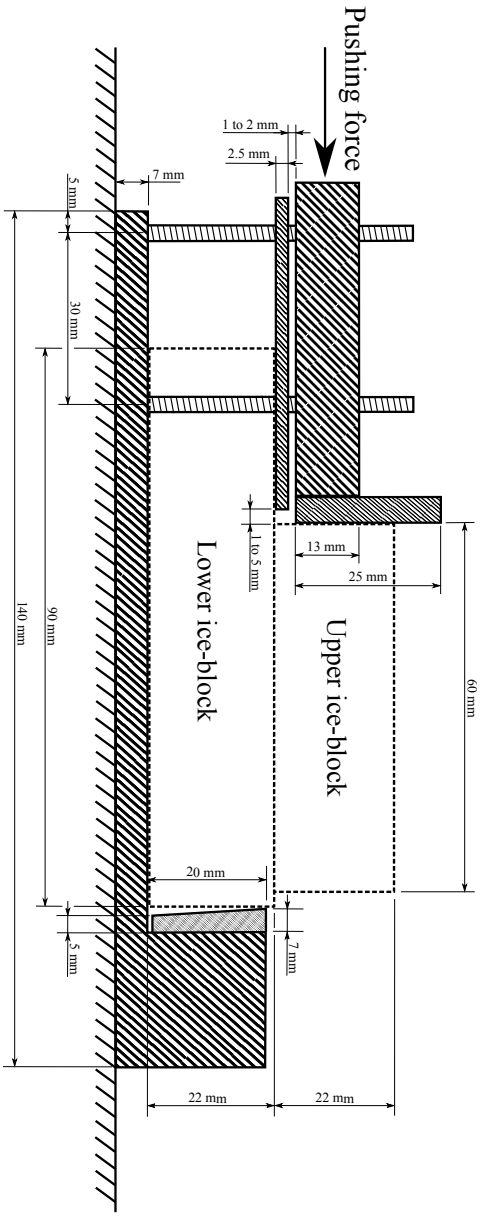

Figure E.1: Principle cross-sectional drawing of the NTNU-frame (not in scale).

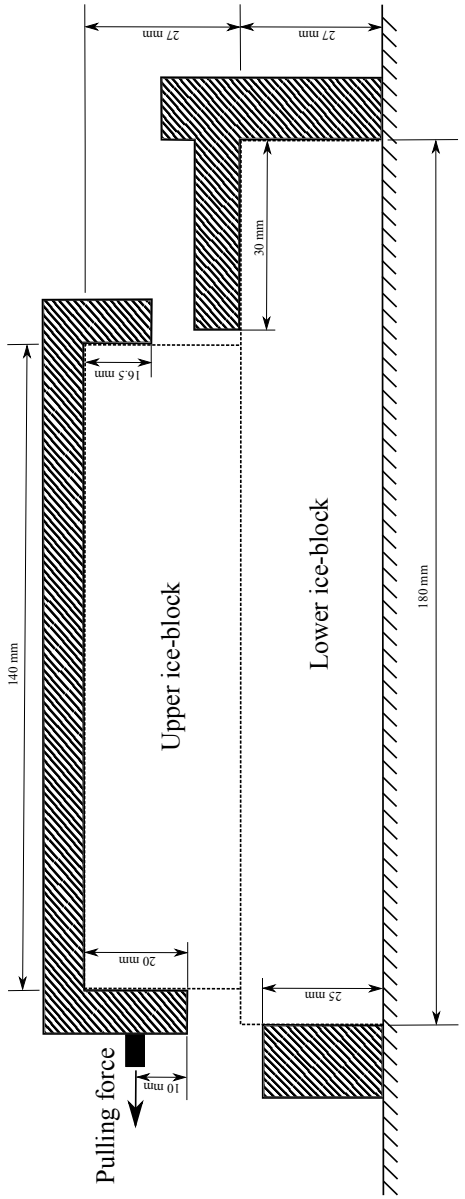

Figure E.2: Principle cross-sectional drawing of the HSVA-frame (not in scale).